



<https://theses.gla.ac.uk/>

Theses Digitisation:

<https://www.gla.ac.uk/myglasgow/research/enlighten/theses/digitisation/>

This is a digitised version of the original print thesis.

Copyright and moral rights for this work are retained by the author

A copy can be downloaded for personal non-commercial research or study,
without prior permission or charge

This work cannot be reproduced or quoted extensively from without first
obtaining permission in writing from the author

The content must not be changed in any way or sold commercially in any
format or medium without the formal permission of the author

When referring to this work, full bibliographic details including the author,
title, awarding institution and date of the thesis must be given

Enlighten: Theses

<https://theses.gla.ac.uk/>
research-enlighten@glasgow.ac.uk

MECHANISMS FOR SOLAR FLARES

by

R. M. Green

T H E S I S

submitted to the

UNIVERSITY of GLASGOW

for the degree of

Ph.D.

Department of Astronomy,
The University of Glasgow,
Glasgow, W.2.

February 1965.

ProQuest Number: 10647255

All rights reserved

INFORMATION TO ALL USERS

The quality of this reproduction is dependent upon the quality of the copy submitted.

In the unlikely event that the author did not send a complete manuscript and there are missing pages, these will be noted. Also, if material had to be removed, a note will indicate the deletion.



ProQuest 10647255

Published by ProQuest LLC (2017). Copyright of the Dissertation is held by the Author.

All rights reserved.

This work is protected against unauthorized copying under Title 17, United States Code
Microform Edition © ProQuest LLC.

ProQuest LLC.
789 East Eisenhower Parkway
P.O. Box 1346
Ann Arbor, MI 48106 – 1346

PREFACE

The first chapter of the present thesis gives a detailed account of the solar flare phenomenon from an observational standpoint. In chapter 2 early magnetic theories of flare origin are discussed.

The original work in the thesis is contained in chapters 3 to 7, in which two modes of field annihilation appropriate to the current sheet mechanism originally proposed by Sweet are studied in quantitative detail. The first of these modes is referred to as Parker's compressible mode; but the treatment given in chapters 4 and 7 is an independent one, developed prior to Parker's publication, and differs considerably from Parker's treatment in both its method and its conclusions. The second mode, which is described in chapter 6, arises from the fact that the treatment of chapter 4 indicates that Parker's mode is not definitive.

In chapters 8-10 a detailed account and criticism is given of current flare mechanisms, and in the final chapter some conclusions are stated.

Part of the work in this thesis was reported at the I.A.U. Symposium No 22 on Solar and Stellar Magnetic Fields in 1963, and will be published in the Proceedings of that Symposium.

The work described in this thesis was carried out while the author was a research student and later on the staff of the Department of Astronomy, Glasgow University. It is a great pleasure to acknowledge the kind encouragement, guidance and supervision received from Professor P.A. Sweet throughout the period of the work.

C O N T E N T S

| | | page |
|------------|---|------|
| CHAPTER 1. | THE PHENOMENON. | 1 |
| | (i) Optical | 2 |
| | (ii) Radio | 30 |
| | (iii) Geophysical | 45 |
| CHAPTER 2. | THEORIES OF ORIGIN | 57 |
| | (i) Introduction | 57 |
| | (ii) Classical Theories of Solar Flares | 61 |
| | (iii) Subsequent Developments | 81 |
| CHAPTER 3. | SINGULAR MAGNETOHYDROSTATIC CONFIGURATIONS | 88 |
| | (i) A Simple Two-Dimensional Model | 88 |
| | (ii) Determination of the Sheet Current Induced by Displacements of a Perfectly Conducting Medium. | 93 |
| CHAPTER 4. | QUASI-STEADY MAGNETOHYDRODYNAMICS AT NEUTRAL LINES | 102 |
| | (i) Order of Magnitude Considerations | 102 |
| | (ii) Hydromagnetic Equations | 109 |
| | (iii) Incompressible Mode | 114 |
| | (iv) Parker's Compressible Mode | 127 |

| | page |
|--|------|
| CHAPTER 5. DISCUSSION OF THE SOLUTION FOR THE COMPRESSIBLE MODE | 147 |
| (i) Solution for Q on the ξ -Axis. | 147 |
| (ii) Determination of the Minimum Value of Γ_0 . | 150 |
| (iii) Application to the Idealised Model. | 153 |
| CHAPTER 6. POSSIBLE ENHANCEMENT OF PARKER'S COMPRESSIBLE MODE | 161 |
| (i) General Description of a Possible Faster Mode. | 161 |
| (ii) Solutions on the ξ -Axis | 171 |
| CHAPTER 7. THE PARKER MODES UNDER SOLAR CONDITIONS | 178 |
| (i) Time-Scales | 178 |
| (ii) Effects of Ambipolar Diffusion | 186 |
| (iii) The Effects of a z-Field | 193 |
| CHAPTER 8. THE SEVERNY-WENTZEL MECHANISM | 197 |
| CHAPTER 9. PETSCHER'S MECHANISM | 210 |
| CHAPTER 10. GENERAL REQUIREMENTS OF A FLARE THEORY | 222 |
| (i) Introduction | 223 |
| (ii) The Role of Neutral Points and the Acceleration of Charged Particles. | 226 |
| (iii) The Gold and Hoyle Storage Mechanism | 232 |

| | page |
|---|------|
| CHAPTER 11. SUMMARY AND CONCLUSIONS | 238 |
| REFERENCES | 248 |
| APPENDIX 5-1. Solution for $g(\xi)$. | 256 |
| APPENDIX 5-2 The Numerical Solution of Equations (5-1-5) and (5-1-6) | 269 |
| APPENDIX 7-1 Data for Figure (7-1). | 272 |
| APPENDIX 9-1 Data for Figure (9-3) | 273 |

CHAPTER I THE PHENOMENON

The purpose of this introductory chapter is to outline the observational features of solar flares. This will provide a framework for the later discussion of flare theories. Observational investigations have followed two distinct lines of approach; on the one hand, statistical analyses of extensive samples of flare-patrol data have attempted to establish associations between the different processes involved in the complete flare phenomenon; on the other hand, much more detailed investigations have been made of particular events. On account of the apparent individuality of solar flares much of the statistical work appears inconclusive. It is likely, therefore, that the determination of the physical processes involved will depend primarily on the greater detail provided by the second type of observation. For this reason, the present discussion will concentrate mainly on investigations that have been made of individual flares. To this extent the discussion will be incomplete; it will be further incomplete, since the volume of reported observational research enforces an eclectic approach. Nonetheless it is hoped to cover the observational features that have the most direct bearing on current flare theories.

Like Gaul, the discussion is divided into three parts. In three sections, the optical, radio, and geophysical aspects of the phenomenon are separately discussed. The meaning of the first two of these headings is clear. Under the third heading it will be convenient to include, in addition to the discussion of ionospheric and geomagnetic disturbances, a description of other flare features which are not covered by the previous headings. Such features, which include the emission of solar ultraviolet, cosmic, and X-radiation, are important as the direct causes of the geophysical effects associated with flares.

(1) Optical

Due to the world wide coverage of flare patrols, the majority of flare events are observed. During the I.G.Y. the sun was under effective observation for more than 90% of the time⁽¹⁾. However, the data collected on the individual events observed is of a largely qualitative nature, and is frequently confined to an estimate of flare importance and duration.

The importance of a solar flare event is assigned primarily on the basis of flare area at the time of maximum intensity. The lower limit for a solar flare,

importance 1, is set at 100 millionths of the solar hemisphere⁽²⁾. Flare-like brightenings in $H\alpha$ below this limit are classified as subflares, though this distinction is arbitrary. In fact, flare areas form a continuous sequence, extending from the limit of optical resolution up to areas of several thousand millionths of the solar hemisphere. Before the importance of a flare can be assigned, the measured area must be corrected for fore-shortening. As a first approximation a simple secant law gives good results, for large flares at least, up to comparatively large central distances⁽³⁾. This indicates that the extension in height of such flares is small in comparison with their horizontal dimensions. Flare importance is the most completely reported observational parameter, and often the only one in flare-patrol data. The measure of flare importance, whatever its value as a neat descriptive parameter for use in statistical classification, can yield no physical insight into the flare process. For this, detailed spectroscopic investigations of particular events are required. On the other hand, flare patrols that are photometrically standardized allow quantitative investigations of light-curves and of the development of flare areas⁽⁴⁾. Further the cinematograph

technique, using high time resolution, has made possible the discovery of the fast, shock-like phenomena, discussed by Athay and Moreton⁽⁵⁾.

The association of solar flares with sun-spots has long been known. In 1939 Giovanelli⁽⁶⁾ investigated statistically the relationship of solar flares to the size, type, and development of their associated spot group. His results showed that flares most frequently occur in the magnetically complex $\beta\gamma$ and γ type of spot group. Further, he found that flare occurrence is most likely when the spot group is increasing in size. More recently, Howard⁽⁷⁾ has pointed out that Giovanelli made no attempt to treat flares of different importance classes separately. Howard suggests that a decrease in size, or a rapid ageing of the spot group, may be a characteristic of major cosmic ray flares, a characteristic not shared by the more normal flare of lesser importance. While observational evidence in support of Howard's contention is, of necessity, slight, measurement of the sun-spot areas for the few cosmic-ray flares, for which Mount Wilson direct photographs were available, did show a consistent decrease.

Two important features of solar flares that must be accounted for in a complete theory are the rate of

development and the duration of the event. The two time-scales are quite different. The flare first appears as a slow brightening, which is followed by the very sharp rise of the flash phase. Ellison estimated the time-scale of the flash phase as no more than two to three minutes⁽⁸⁾. The $H\alpha$ central intensity and line width increase together at this stage, reaching maximum values of up to three times the continuum, and up to 20 Å respectively. After these maximum values have been attained, however, the line width decreases more rapidly than the central intensity (Ellison⁽⁹⁾, Smith⁽¹⁰⁾). The development curve of $H\alpha$ line width is, therefore, distinctly more peaked than that for the central intensity of the line. Indeed Ellison⁽¹¹⁾ has remarked that the duration of maximum line width is probably only momentary, and is certainly less than 30 seconds; he laid great stress on this flash phase and considered it quite fundamental to the whole flare process.

An extensive programme of flare photometry has been carried out by Dodson, Hedeman, and McMath⁽⁴⁾ at the McMath-Hulbert Observatory. In the course of this programme photometric light curves for 194 flares and subflares were obtained. From an examination of these, it was claimed that flares exhibit three distinct preferred rates of rise, corresponding to an increase in

brightness of one magnitude in 4-5 minutes, in 10-15 minutes, and in 30-45 minutes respectively. The first and fastest of these rates of rise was found to be much the most frequent. This rate of rise clearly corresponds to the time-scale described by Ellison as the flash phase. Nonetheless, Dodson et al found that some very large and bright flares reached their maximum intensity at the second and considerably slower rate. The third and slowest rate, however, was found to be relatively rare. While Dodson's results are not incompatible with the very short rise time found by Ellison, it is perhaps important to realise the existence of flares whose rise to maximum is not particularly catastrophic.

The total duration of a flare is determined mainly by the post-maximum decay. In the same investigation, Dodson et al found a single preferred rate of decay, of one magnitude in a period of $1\frac{1}{2}$ to 2 hours. Many flares, however, decay more rapidly. In all cases, however, the decay time of a flare is far greater than the time required to reach maximum intensity. Due to these slower rates of decay, the total duration of a flare can be many hours. The duration is found to increase with flare-area and importance class. In particular, a large 3^+ cosmic-ray flare can have a duration of up to eight

hours⁽¹¹⁾. Smith⁽¹²⁾, from an examination of 41 class 3 flares observed during the I.G.Y., finds a mean duration of nearly $2\frac{1}{2}$ hours, though the distribution is noticeably skew. Severny and Shaposhnikova⁽¹³⁾, however, have claimed that flare durations as normally reported are subject to considerable observational uncertainty. They redefined the duration of a flare as the time interval during which the flare was at 50% of its maximum intensity. With this revised definition they claim to have found a closer correlation between flare-area and duration. Further the durations obtained are systematically reduced. Their sample of data, however, was of necessity small, since they had only 22 flares for which the necessary light curves were available. In Smith's complete sample of I.G.Y. flares, on the other hand, more than 4000 events were covered. It is clear that a detailed and extensive analysis of flare-patrol data of photometrically standardized films will be necessary to determine any close relationship between flare-area and life-time.

The determination of the physical conditions within the flare region itself requires a detailed spectroscopic investigation of individual events. Flare emission spectra can be studied in the Balmer lines of hydrogen, the H- and K-lines of ionized calcium, the helium D₃ line, and in addition a large number of metal lines, which can

also appear in emission. Most of the effort, however, has been concentrated on $H\alpha$, and much of the present discussion concerns this particular line.

At the maximum phase of a disc flare the $H\alpha$ profile is usually asymmetrical, a fact first discovered by Waldmeier⁽¹⁴⁾. The red emission wing is normally the stronger and the more extended. This asymmetry has been interpreted as a diffuse absorption feature due to a cloud of hydrogen atoms ejected from the flare region (Ellison⁽¹⁵⁾, Kahn⁽¹⁶⁾). A separate investigation was undertaken by Svestka^(17,18,19), who came to similar, though not identical, conclusions. Svestka found that although at the time of maximum intensity the asymmetry is usually positive, as found by Waldmeier and Ellison, in the post-maximum period a negative asymmetry can develop. This is most naturally interpreted as being due to the absorbing material falling back into the flare region. Svestka found that the velocities involved were certainly less than 300 km./sec. It must be stressed that large velocities do not apply to the flare region itself. A disc flare shows virtually no transverse motion, and the centre of the $H\alpha$ profile is not significantly shifted. Thus the velocity of the absorbing cloud is indicated by an asymmetry, and not by a shift of the line centre. The absorption features

corresponding to surges and similar structures which accompany flares, on the other hand, often show up with large Doppler shifts. The Doppler shifts of the flare emission region itself, however, are small, and the transverse motions are only of the order of two kilometres per second⁽²⁰⁾.

The interpretation of the large widths of $H\alpha$ emission observed in solar flares is at present uncertain. An explanation of thermal broadening must be rejected, since it would require a temperature of the order of 10^6 ° K. Ellison and Hoyle⁽²¹⁾, therefore suggested that the widths are due to Stark broadening. On the basis of a study of reported widths (often visually estimated) of 610 flares, Goldberg, Dodson, and Müller⁽²²⁾ argued that the observed line widths could be interpreted in terms of radiation damping. Conclusions based on such a crude statistical sample must be uncertain, however; serious attempts at the interpretation of flare emission broadening must be founded on profile determinations in well-observed events. Some investigations along these lines will now be described in some detail.

It is customary to proceed as follows: let $I(\lambda)$ be the observed intensity, and $I_0(\lambda)$ be the intensity of

the photosphere. Then the emergent intensity can be written as

$$I(\lambda) = I_0(\lambda) e^{-\tau} + \bar{S}(1 - e^{-\tau}) \quad (1-1)$$

where τ is the total optical thickness of the flare region, and \bar{S} is a mean source function. \bar{S} is given by

$$\bar{S} = \frac{1}{1 - e^{-\tau}} \int_0^{\tau} S e^{-\tau'} d\tau' \quad (1-2)$$

In general both τ and \bar{S} are functions of λ . Most investigations have been concerned with the interpretation of the far wings of the profile. For $\tau \ll 1$ it is assumed that \bar{S} is independent of wavelength. Equation (1-1) can then be reduced to the form

$$\tau = \frac{I(\lambda) - I_0}{\bar{S} - I_0} \quad (1-3)$$

where we are justified (in the wings) in replacing $I_0(\lambda)$ by a constant I_0 , equal to the intensity of the photospheric continuum. Under these assumptions it is seen that τ is proportional to $(I(\lambda) - I_0)$ which is a directly observed quantity. For pure thermal broadening $\log \tau$ will vary linearly with $(\Delta\lambda)^2$, where $\Delta\lambda$ is the distance from the line centre. For broadening due to radiation damping or the Stark effect, on the other hand, $\log \tau$ will vary linearly with $\log \Delta\lambda$ with slopes equal to -2 and -2.5 respectively. The simplifying assumptions involved in equation (1-3), therefore, allow

a ready comparison of such physical interpretations of the line widths with the observed profiles. In general the resulting fit is either unsatisfactory or ambiguous.

Jefferies, Smith and Smith⁽²³⁾ made a detailed investigation of the flare of September 18, 1957. Using the Universal spectrograph at Sacramento Peak⁽²⁴⁾, they were able to cover the spectral region 3900-7200 Å in a single exposure. Simultaneous profiles of different lines were thus obtained. Jefferies and his colleagues investigated the profiles of the first four lines of the Balmer series and of those helium lines that appeared in emission. Their findings were inconclusive. The Balmer profiles were not inconsistent with an interpretation of Stark broadening. However, an equally good fit corresponded to a linear relationship between $\log \tau$ and $\Delta \lambda$. This was interpreted as widening due to macroscopic motions within the flare region with a non-Maxwellian velocity distribution of the form

$$f(v) = B v e^{-v/v_0} \quad (1-4)$$

Here v_0 is a characteristic velocity. The values of v_0 found for the Balmer lines were of the order of 300 km./sec.

From a study of three flares Kazachevskaya and Severny⁽²⁵⁾ found that, except for the central cores,

the profiles of the first five Balmer lines could be satisfactorily explained on a Stark hypothesis. In a series of later papers, however, this estimate was revised to some extent.

Severny had reported extensive spectroscopic studies of fine-structure emission⁽²⁶⁾, which he referred to as continuous grains and moustaches. The size of these features is of the order of $0''.5$, so they can only be studied under conditions of excellent seeing. McMath, Mohler and Dodson⁽²⁷⁾ have pointed out that the moustaches are the same features as were studied by Ellerman⁽²⁸⁾, who called them 'solar hydrogen bombs'. These investigators further showed that the moustaches are the spectroscopic equivalent of the 'petits points' studied by Lyot⁽²⁹⁾ with a wide-band $H\alpha$ filter ($> 1 \text{ \AA}$). The moustaches are simply very narrow emission wings, extending up to 15 \AA on either side of lines of the Balmer series and some other Fraunhofer lines. As they are optically thin, comparatively low-level phenomena, they fade out near the line centre. According to Severny⁽²⁶⁾, their violet wings are in general brighter and broader than their red wings; occasionally only one wing of the moustache appears. Since the moustaches have the same extension on metal lines (CaII, Mg, and

some Fe lines) as on the Balmer series, Severny concludes that the broadening must be due to macroscopic motions (turbulence).

In another paper⁽³⁰⁾ Severny reported that, in large flares, under conditions of very good seeing, the wide emission wings could be resolved into a cluster of moustaches. In a later publication⁽³¹⁾ Severny suggests that the asymmetry of flare emission lines, originally reported by Ellison⁽¹⁵⁾, may be connected with the appearance of one-sided moustaches, which will in general be unresolved. It seems unlikely, however, that all flare asymmetry can be explained in this way. For Severny's own work^(26,30) shows that the asymmetry in the moustaches should be in a sense opposite to that discussed by Ellison.

In the same paper⁽³¹⁾ Severny has remarked that the position of the central core of the line emission does not always coincide with that of the far wings. This suggests different levels, even regions, of origin. Severny argued, therefore, that the profiles for flares of class 2 or less, which in general do not possess very wide emission wings, are satisfactorily accounted for on a Stark hypothesis⁽²⁵⁾. This same explanation is applied to the more central parts of the profiles occurring in larger flares. On the other hand, when equation (1-3) is

applied to the far wings of the emission profiles of these latter flares, the most satisfactory agreement is found by assuming a linear relationship between $\log \tau$ and $(\Delta\lambda)^2$. The far emission wings are interpreted, therefore, in terms of Doppler broadening due to a Maxwellian distribution of velocities. The velocities are found to be of the order of 80 - 250 km./sec. The same velocities apply throughout the Balmer series. Although the velocity distribution is apparently Maxwellian, the Doppler broadening cannot be thermal in origin, but rather is due to macroscopic motions. This is shown by the fact that the widths of the H- and K-lines of CaII yield velocities of the same order as found for the Balmer series. In this way, Severny finds a place for both the Stark effect and macroscopic motions in his interpretation of flare spectra.

A Stark interpretation can be tested by comparing the relative widths of lines of the Balmer series. Suemoto and Hiei⁽³²⁾ have investigated two disc flares in this way. In their investigation it was necessary to study higher members of the Balmer series, for which the effects of self-absorption in the line centre were not serious. Suemoto and Hiei found that, whereas the half-widths of lines in the series decreased from $H\alpha$

down to H_9 , thereafter they increased at a slow rate up to H_{14} , which was the last line observed. This gradual increase in width could be satisfactorily explained on the basis of the Stark effect, since the Stark splitting of the energy levels increases with increasing quantum number. A similar investigation has been carried out by Hirayama⁽³³⁾, who obtained essentially the same results from a study of two limb flares.

From the discussion above, it is clear that no single interpretation of flare emission profiles is entirely satisfactory. Nonetheless, under differing circumstances, a place can be found for interpretations in terms of both the Stark effect and macroscopic motions. Severny⁽³⁴⁾ has put forward an interesting suggestion that the shape of the line profile in a flare and the predominant broadening mechanism depend critically on the orientation of the magnetic field in the flare region to the line of sight. Severny has argued that the magnetic pinch effect is the mechanism responsible for flare generation, and that material will be ejected at high velocity along the magnetic field lines. If, then, the flare magnetic field configuration is such that the line of sight is along the axis of the pinch then the macroscopic motions

should be primarily responsible for the width of the emission line. If, however, the line of sight is across this axis, then the profile will be predominantly Stark-broadened. Support was found for this interpretation in laboratory experiments at the Crimean Astrophysical Observatory. This suggestion of Severny's forms at present the only attempt to synthesize otherwise conflicting interpretations of flare emission profiles.

Once the broadening mechanism has been determined, an estimate can be made of the physical conditions within the flare. This is done by assigning a value to the mean source function \bar{S} , defined in equation (1-2). It is not intended to discuss these estimates in detail. They have been collected in tabular form by Smith and Smith in⁽³⁵⁾. The estimates of different investigators vary considerably; typical values are given in equation (1-5);

$$\begin{aligned}
 N_e &= 10^{13} \text{ cm}^{-3} \\
 N_2 &= 10^{16} \text{ cm}^{-2} \\
 T_e &= 1 \text{ to } 1.5 \cdot 10^4 \text{ }^\circ \text{K.}
 \end{aligned}
 \tag{1-5}$$

In these equations N_e , N_2 and T_e denote the electron density, the number of hydrogen atoms per unit cross-section in the second quantum state, and the electron temperature respectively.

The total energy involved in a flare event has been estimated in a number of ways. From a sequence of $H\alpha$ spectroheliograms, Billings and Roberts⁽³⁶⁾ determined the isophotes of central $H\alpha$ emission for a class 2 flare. Estimating the effective line-width, it was then possible to determine the total energy of the line emission. A maximum rate of emission of 10^{27} ergs/sec. was found. The total energy appearing in $H\alpha$ was estimated at $3 \cdot 10^{30}$ ergs. These estimates appear larger than those of most other investigators. The reason is that the photometric method systematically includes faint outlying areas that the visual observer would describe as bright plage.

Earlier Ellison⁽⁹⁾ had investigated the $H\alpha$ profiles of five flares, mostly of importance 3 or 3⁺. The equivalent widths of $H\alpha$ were measured in a central position of each flare; the total flare area was measured separately. Then, on the assumption that the line profile was the same throughout the flare area, the total rate of $H\alpha$ emission was calculated. The rates obtained varied from $1.7 \cdot 10^{26}$ to $1.1 \cdot 10^{27}$ ergs/sec. Ellison remarked that, on account of the assumptions involved, these values should be considered as upper limits. More recently Ellison⁽¹¹⁾ has used these

determinations of $H\alpha$ emission to estimate the total flare energy. He included in his estimate not only the emission in $H\alpha$ and the other Balmer lines, but also the emission in lines of other elements in the visible spectrum. These lines have been catalogued by Severny, Steshenko, and Khoklova⁽³⁷⁾ for the flare of August 17, 1959. They include over 400 metal lines, notably Fe and Fe^+ , which appear faintly in emission or have their absorption profiles partly filled in. Ellison's final estimate for the total energy radiated in visible line emission in a 3^+ flare was $5 \cdot 10^{31}$ ergs.

Parker⁽³⁸⁾ has given estimates for the total radiation of the 3^+ flare of February 23, 1956. Parker based his estimates on a report of this flare by Notuki, Hatanaka and Unno⁽³⁹⁾, who found a central intensity in $H\alpha$ of about three times the continuum, and a maximum width of more than 18 Å, the extent of the line shifter of their spectrohelioscope. From this data Parker estimates a rate of emission at flare maximum of $6 \cdot 10^{28}$ ergs/sec., which seems extraordinarily high. This flare was also observed in white light, and in the same paper Parker estimated the contribution of the flare continuum. For the total visible energy radiated by this quite exceptional flare, Parker obtained a value of $2 \cdot 10^{32}$ ergs.

There is general agreement, then, that the energy expended in a 3^+ flare is of the order of 10^{32} ergs. The volume of even the largest flares does not greatly exceed 10^{29} cm^3 . If, therefore, the energy of the eruption is stored in situ, an energy density of 10^3 ergs cm^{-3} is required. It has frequently been pointed out, e.g. Parker⁽³⁸⁾, Gold and Hoyle⁽⁴⁰⁾, that such an energy density is far in excess of the thermal energy density of the chromosphere, which is no more than a few ergs per cm^3 . Indeed the total thermal energy content of the whole chromosphere and corona would be insufficient to supply an event as large as that of February 23, 1956. If the energy of the flare is stored in situ - and, since no inflow of material is observed, and no change has ever been reported in the photosphere below the flare, this is a reasonable assumption - the only possible storage mechanism is the chromospheric magnetic field. The energy density derived above would require a magnetic field of a few hundred gauss. The energy density that has been derived here is probably a lower limit, since the energy may be dissipated in a smaller volume than we have allowed. There is some indication of this in the fact that in its initial stages the flare appears to have a

filamentary structure, which later diffuses in the post-maximum phase. Further evidence of fine structure is provided by Severny's spectroscopic observations to which reference has already been made⁽³⁰⁾, and by the work of Suemoto and Hiei⁽³²⁾.

If a flare is to be interpreted as a dissipation of magnetic energy, it is clear that observations of magnetic field changes in flare regions will be of crucial importance. Severny⁽³¹⁾ has reported that (i) flares tend first to appear at 'neutral points' of the magnetic field; (ii) a considerable field gradient at the neutral point is necessary for the appearance of a flare; (iii) the magnetic field is considerably altered during the flare, which leads to a redistribution and, in some cases, to almost a destruction of the field near the neutral point. These conclusions have been severely criticized, mainly due to Severny's identification of the neutral points. The observations were made in the magnetically sensitive line $\lambda 4886$ Fe. The measurements refer only to the field's longitudinal component. Severny plotted isogauss contours of this longitudinal field; and from the shape of these contours he designated several points on the contour of zero longitudinal

field as 'neutral points'. While it is trivially obvious that any real neutral point must lie on this particular contour, it is difficult to see how such neutral points, if they exist, can be identified from knowledge of a single component of the field. In spite of this objection, Severny's observations certainly suggest that flares begin on the apparent neutral line (of longitudinal field), and that flares result in a simplification of the magnetic field.

Severny's claims have not been entirely confirmed by other observers. Bruzek⁽⁴¹⁾ reported that flares do indeed tend to start near the apparent neutral lines. He suggested, however, that since they frequently recur in the same location, it is unlikely that the field can be significantly altered by the eruption. Howard and Babcock⁽⁴²⁾ made scans of a flare region with the Mount Wilson magnetograph during the progress of a 3^+ cosmic-ray flare. They found that the magnetic field pattern remained essentially unchanged throughout the entire development of the flare. Similar observations were undertaken by Michard, Mouradain, and Semel⁽⁴³⁾ who measured the magnetic field during the course of a flare of importance 1^+ . Though changes in the magnetic field were observed, they did not coincide with the

occurrence of the flare and seemed unconnected with it.

Evans⁽⁴⁴⁾, on the other hand, reported a sharp change in his measurement of the magnetic field during a 1^+ flare. Coincident with the flare's rise to peak intensity, there was a sharp decrease in field strength of 16%. This was followed by an even sharper recovery in the flare's post-maximum phase.

On the question of whether magnetic field changes are observed which can be connected with flares, the evidence is, therefore, conflicting. Part of this conflict may have been resolved by recent work of Howard and Severny⁽⁴⁵⁾. Most of the observations described in the last two paragraphs refer to close examinations of the magnetic field at the site of the flare's inception. Howard and Severny, on the other hand, examined scans of the magnetic field of the whole of the associated spot group. These scans were taken at the Crimean Astrophysical Observatory and covered a period of four days. The flare in question was the 3^+ cosmic-ray flare of July 16, 1959, the flare studied by Howard and Babcock⁽⁴²⁾. But, whereas the Mount Wilson scans were limited to measurements of fields less than 40 gauss, the Crimean investigation had no such restriction and outlined more completely the general

structure of the sun-spot field. The Crimean workers were unable to scan the sun at the actual time of the flare, viz. 21.14 U.T., July 16 to 00.30 U.T., July 17. However, by comparing two scans, taken at times straddling the flare, Howard and Severny determined that considerable changes in the structure and gradients of the spot group's magnetic field took place between 15.00 U.T., July 16 and 06.00 U.T., July 17. It was estimated that between these times there was a decrease in energy of nearly $4 \cdot 10^{32}$ ergs in the longitudinal field.

It must be emphasised that observations of solar magnetic fields are made by measuring the Zeeman effect in low-level lines. The fields measured refer, therefore, to photospheric levels, and never to flare altitudes. Magnetic changes taking place in the flare region itself and, therefore, at chromospheric levels, are quite unobservable. Further the changes observed in the magnetic field at the position on the solar disc where the flare occurs may be quite unconnected with the flare itself. If, however, a flare results from a dissipation of magnetic energy, then this energy must be drawn from the magnetic field of the associated spot group. It is to be expected, therefore, that observations of the type

undertaken by Howard and Severny should still reveal a reduction in the total magnetic energy of the spot group in connection with flares. Clearly, however, unequivocal identification of such large-scale changes with particular flares can only be expected in the case of very large events, like that of July 16, 1959. The connection of the field changes, observed in Severny's early work, with particular flares is, then, probably open to some doubt. On the other hand, the second main result of Severny's original work has been generally confirmed, namely the first appearance of flares on the longitudinal neutral line. This result coincides well with an observation of Ellison et al.⁽⁴⁶⁾ that in a complex sunspot group flares tend to align themselves along the dividing line of spots of opposite polarity.

The only observations of transverse magnetic fields on the sun have been undertaken much more recently by Severny⁽⁴⁷⁾. Though such observations are still to some extent exploratory, they have already yielded several interesting results. The configurations of the transverse fields of spot-groups are found to be of a very complicated form and, in general, cannot be understood in simple dipole terms. The most important of

the peculiarities of the field are the points at which the gradients of the field are so sharp that Severny refers to a 'coexistence' of fields in different directions at these points. Severny reports that it is at these points, rather than at the neutral points of the transverse field, that flares seem to occur. However, once again it must be remembered that these observations refer to fields at photospheric levels, and it can only be deduced that flares tend to start at such points of magnetic complication if it is assumed that the photospheric field gives a real indication of the form of the field in the chromosphere. Finally, it may be of interest to note that Gopasuk et al⁽⁴⁸⁾ have found that it is possible to predict the occurrence of flares from the form of the magnetic field, taking account of both the transverse and the longitudinal measurements. In conclusion, it appears that a correlation of flares with certain field configurations, judged subjectively, is established, but that quantitative changes in the field energy, in conjunction with flares, can only be determined in exceptional cases.

At present chromospheric fields, and, therefore, fields in the actual flare regions cannot readily be measured. Zirin and Severny⁽⁴⁹⁾ have, however,

succeeded in making longitudinal measurements in $H\beta$. Their investigations refer mainly to prominences. An observation by Ellison, McKenna and Reid⁽⁵⁰⁾ may give an indication of magnetic field changes in the chromosphere coincident with great flares. These workers reported two new features; studying Cape heliograph films for the class 3 flare of April 1, 1960, they found that shortly after flare maximum an 'expanding halo' seemed to develop round the flare filaments. This feature was later named the flare nimbus. Within the nimbus the chromospheric striation pattern became blurred and was replaced by the coarse mottling typical of the quiet chromosphere. Conditions of good seeing are required to observe the striation pattern - the variations in this pattern are, therefore, less frequently observed than the associated flare nimbus. Later a number of observations of these two features were reported by the Dunsink workers^(51,52,20), and by Smith and Borton⁽⁵³⁾ at Sacramento Peak. The latter considered the two features closely connected and refer to an 'obscuration of the striation pattern'. They interpreted the phenomenon as the result of an expanding cloud of absorbing material ejected by the flare. They pointed to evidence for such clouds in the asymmetry of the $H\alpha$

profile, already discussed on page 8.

The two features described above have been observed only in conjunction with large flare events, usually accompanied by Type IV radio bursts and cosmic ray effects. Like the Sacramento Peak workers, Ellison McKenna and Reid⁽⁵¹⁾ at first interpreted the nimbus as a uniform absorption cloud, which partially obscured the striation pattern below. They suggested, however, that the nimbus was not due to an expanding cloud of hydrogen atoms, since this could be expected to be conspicuous due to Doppler shifts and irregularities in density, which were not observed. Instead they proposed that the cloud was the optical counterpart of the relativistic electrons, proposed by Boischot and Denisse⁽⁵⁴⁾, to explain the Type IV emission. It was suggested that the increased absorption was due to the excitation of neutral hydrogen by collisions with the relativistic electrons at the chromospheric reflection points of the magnetic field. The mechanism was not examined in any detail.

In a later paper, however, Ellison⁽¹¹⁾ remarked that subsequent photometric work by Reid had shown that the main effect responsible for the nimbus was a reduction in the brighter elements of the striation pattern, rather than any uniform absorption. Work by

Stepanov⁽⁵⁵⁾ has indicated that weak chromospheric magnetic fields are responsible for the alignment and increased luminosity of the $H\alpha$ mottling that makes up the striation pattern. Ellison, therefore, concluded that it is the destruction of these magnetic fields that results in the disappearance of the striation pattern and the associated phenomenon of the flare nimbus.

These observations of changes in the chromospheric striation pattern form the only indication of magnetic field changes in the chromosphere in association with flares. This evidence is at best circumstantial. Even so, these observations do indicate important chromospheric effects. Many other atmospheric phenomena can accompany solar flares, notably surges, prominence activations, and loop prominences. All these features are quite distinct from the chromospheric flare itself, and a detailed discussion is not attempted here. On the disc they appear in absorption, frequently with large Doppler shifts, which are noticeably absent in the emission of the flare region itself. On the whole, however, surges and related phenomena are more easily studied at the limb, where they appear in emission. Indeed, at the limb, it is possible to mistake such forms of flare associated activity with the flare

emission itself. For this reason, in the previous discussion attention has been confined in the main to disc-flares, since in such an event the recognition of a flare is unambiguous.

The present discussion of the optical phenomenon will be completed with an account of what have become known as 'homologous flares'. It has long been recognised that certain flares in the same active region tend to show close similarities. For example, Dodson and Hedeman⁽⁵⁶⁾ found that over a period of a few days "flares have appeared not in approximately, but apparently in exactly the same small portion of the solar disk". Ellison, McKenna and Reid⁽⁵⁷⁾ found three flares that not only occurred in the same position relative to their sunspot group, but further had similar shapes and similar forms of associated activity. For example, a region of plage, which had no visible connection with the flare, being 20° distant in longitude, brightened simultaneously and in phase with the flare on all three occasions. Hansen and Gordon⁽⁵⁸⁾ investigated five limb events of October 13, 1958. There must be some doubt as to whether these features, which were photographed on flare patrol films, were themselves flares or forms of associated activity. Certainly,

however, the features were connected with flares, since each was associated with SCNA. These five limb events all showed very striking similarity of form and development, and are probably at present the best example of homologous flare activity.

The phenomenon of homologous flares is an important one and should be considered in flare theories. As Parker⁽⁵⁹⁾ has put it, the observations suggest that "succeeding flares follow some blueprint", characteristic of their site, and that this blueprint is not destroyed by individual events.

(ii) Radio

In the discussion up to this point it has been tacitly assumed that the $H\alpha$ observations reveal a fundamental aspect of the flare process, and that the seat of the eruption lies in the chromosphere, within the area of $H\alpha$ emission. Other observational methods, however, reveal different aspects of the flare phenomenon, which may be no less fundamental. For example, the radio observations, which refer mainly to coronal levels, provide a different insight into the flare sequence. Further they present some evidence, admittedly slight, that the seat of the flare instability is situated not in the chromosphere, but at some coronal height.

A discussion of the radio data and its interpretation is now given.

Solar radio bursts have been more extensively studied at metre wavelengths than in the decimetre and microwave region. At the longer wavelengths, considerable insight into the physical processes involved has been obtained by the technique of dynamic spectroscopy developed by Wild and his associates (Wild and McCready⁽⁶⁰⁾). Metre-wave bursts have, by this technique, been successfully classified into five distinct spectral types. Of these, Type I has only a very loose association with the flare process and need be discussed no further. All the remaining types, however, are closely connected with solar flares.

Type III (fast-drift bursts) are much the most common of flare-associated radio bursts. They are characterized by an instantaneous band-width of about 30 Mc/s which drifts rapidly from high to low frequencies. In view of the comparatively narrow bandwidth and the high frequency drift, it is generally accepted that Type III bursts originate in plasma oscillations at high coronal levels, excited by an outward moving disturbance. This interpretation has been confirmed by Wild, Sheridan and Neylan⁽⁶¹⁾.

Their observations of Type III bursts associated with limb flares were made with a swept-frequency interferometer. A systematic variation in the position of the source with frequency was found. Both the plasma hypothesis and these interferometric measurements indicate outward velocities of up to half the velocity of light. The plasma oscillations are believed, therefore, to be excited by relativistic electrons ejected from the flare region.

Type III bursts tend to occur in groups with quasi-periodic spacing, the whole event lasting a few minutes. Giovanelli⁽⁶²⁾ has shown that such groups of Type III bursts occur simultaneously with the $H\alpha$ flash phase. The complete radio event is conveniently divided into two distinct phases. The first radio phase (phase 1) is coincident with the flash phase and consists at metre wavelengths of a group of Type III bursts, followed in the most complete form of the event by Type V continuum. This Type V burst is best understood as synchrotron radiation emitted by the electrons that are responsible for the Type III plasma radiation. The later phase of the radio flare (phase 2 in the present nomenclature) is only observed in the larger events. In the case of small flares (class 1, 1⁻),

phase 1, described above, represents the complete radio accompaniment of the eruption. When both phases are present there is generally a delay of some ten minutes separating the two phases. Phase 2 begins with a Type II burst of about 15 minutes duration. In many cases this is the complete second phase. More rarely the Type II burst is followed by an intense burst of Type IV continuum.

The Type II burst has characteristically a very narrow bandwidth, often only a few Mc/s. Its spectrum shows a slow systematic drift, of the order of 1 Mc/s per second, from high to low frequencies. Further its spectral characteristics are frequently reflected in the emission of the second harmonic. The narrow bandwidth suggests that plasma radiation is being observed, and the frequency drift must be interpreted as an outward movement of the initiating disturbance. This interpretation has been verified by Weiss⁽⁶³⁾, who made observations similar to those of Wild, Sheridan and Neylan⁽⁶¹⁾. The interferometric measurements of position, however, require electron densities greater by a factor of 10 than those normally accepted for the quiet corona. In fact, the required densities are typical of those deduced optically by Newkirk⁽⁶⁴⁾ for

coronal streamers. It has been inferred, therefore, that the disturbances responsible for Type II (and Type III) bursts travel outwards along coronal streamers. The radial velocities required to account for the frequency drifts in Type II bursts are of the order of 1000-1500 km/sec. (Maxwell and Thompson⁽⁶⁵⁾). Such speeds are comparable with the high velocity $H\alpha$ phenomena, discovered by Athay and Moreton⁽⁵⁾.

In view of these observational features, it is natural to interpret the Type II burst as plasma radiation excited by the passage of a hydromagnetic shock through the corona. Further, as already mentioned, in the complete flare event a Type II burst follows the Type III event by about ten minutes. It is possible, therefore, to assume a common origin for the disturbances responsible for the two types of burst, a common origin presumably at the site of the instability that initiates the $H\alpha$ flash phase. Under this assumption, Wild, Murray and Rowe⁽⁶⁶⁾ have attempted to determine the height of this instability in the solar atmosphere. The following method was used. A height-time diagram was drawn up for a compound Type III - Type II event. An extrapolation was then made back in time to the point of intersection of the quasi-linear tracks of the two bursts in this diagram.

This point indicated a time corresponding to the beginning of the flash phase (or of the Type III event), and a height in the solar atmosphere of 50,000 km. Such a height is well above the region of H α flare emission, and the method would, therefore, suggest that the seat of the flare is not in the visible flare region. The H α flare would then be a secondary phenomenon. The extrapolation involved, however, is a very large one and must be subject to considerable error. The evidence must not, therefore, be regarded as conclusive.

In about 20% of cases the Type II burst is followed by Type IV continuum. In general, Type IV bursts are restricted to the most energetic flare events. The term 'Type IV' is used here in what is now its accepted sense - though perhaps this is not strictly accurate. A Type IV burst is taken to mean any prolonged intense continuous radiation that follows a flare. The term was originally used by Boischoat⁽⁶⁷⁾ to describe a particular kind of flare continuum at metre wavelengths, namely that from an outward moving source high in the corona. This burst will be denoted here by Type IVm_a. From interferometric measurements, Boischoat found velocities of the order of 1000 km/sec. He interpreted the Type IVm_a radiation, therefore, as synchrotron

radiation from electrons trapped in magnetic fields behind the shock front responsible for the Type II burst. The motion of the source is a fundamental feature of the type of radiation described by Boischoy.

This type of radiation represents only part of the post-flare continuum event. The continuum storm following a flare can last for many hours or even several days. The Type IVm_a burst, however, seldom lasts longer than 1-2 hours. The mechanisms responsible for the complete Type IV radio outburst are not clearly understood. Still, a second component, Type IVm_b, is now generally recognised at metre wavelengths. Unlike Boischoy's Type IV, the source of this long-lived second component is found to be stationary. Further, interferometric measures of the heights of emission are not inconsistent with a plasma, rather than a synchrotron, hypothesis. There is no general agreement, however, on the mechanism involved. Takekura⁽⁶⁸⁾, for example, has suggested a synchrotron mechanism to explain both Type IVm_a and Type IVm_b, though certain rather restrictive assumptions are required in the latter case. Denisse⁽⁶⁹⁾, on the other hand, has developed a mechanism suggesting that the emission is due to plasma radiation initiated by magnetically trapped high-energy electrons.

Of the flare associated bursts at metre wavelengths, the Type IV event is perhaps the least completely understood. Moreover, the stationary Type IV_m resembles closely the continuum part of Type I storms; and it is not clear what distinctions there are, if any, between these two types of burst. Type IV continuum is by far the rarest of metre-wave bursts and is an indication of a very large and energetic event. Of all flare phenomena, this type is found to have the closest correlation with the more pronounced geophysical effects of solar flares.

Microwave bursts, unlike their metre counterparts, have been but slightly explored. The techniques of dynamic spectra, so effective at longer wavelengths, have only recently been extended beyond the metre-wave region. The technique was applied to parts of the microwave region by Maxwell, Swarup and Thompson⁽⁷⁰⁾, and by Haddock⁽⁷¹⁾. Dynamic spectra have also been obtained in the decimetre region (500-950 Mc/s) by Young, Spencer, Moreton and Roberts⁽⁷²⁾. These latter studies revealed two distinctive spectral features, namely fast-drift bursts and intermediate-drift bursts. The fast-drift bursts appear in groups, and are similar to metre Type III. In general, however, they do not appear at the

same time as the metre bursts, and cannot be regarded as high frequency extensions of the latter. Kundu, Roberts, Spencer and Kuiper⁽⁷³⁾ have shown, by comparing metre and decimetre dynamic spectra, that, even when decimetre fast-drift bursts and Type III bursts occur at the same time, they must be regarded as distinct phenomena. The intermediate-drift bursts have recently been studied by Thompson and Maxwell⁽⁷⁴⁾. They find that these bursts are rare outside the major events that exhibit Type IV continuum. It may be that these bursts, which, on a plasma hypothesis, require source motions of 100-4000 km/sec, are best interpreted as a fine structure in the decimetre Type IV continuum.

Dynamic spectra taken in the microwave region do not show the spectral fine structure found at lower frequencies. According to Kundu and Haddock⁽⁷⁵⁾ the spectra of microwave bursts show only broad-band continuum. Further, since single frequency records taken at cm-wavelengths show the microwave bursts as smooth uncomplicated features, it is reasonable to attempt a classification of microwave bursts from their appearance on these single frequency records. Several such classifications have been made and are at present in use. Here a classification adapted from Wild, Smerd, and Weiss⁽⁷⁶⁾ is followed.

The first type distinguished by Wild et al⁽⁷⁶⁾ is the "gradual burst", which Covington⁽⁷⁷⁾ called the gradual rise and fall (GRF). This type of burst has a typical time-scale of one hour, and Covington's nomenclature describes appropriately the form of its intensity variation. From measurements by Kundu⁽⁷⁸⁾ of the source size, a brightness temperature of 10^6 ° K is deduced. It is likely, therefore, that this type of burst originates in thermal emission in the high chromosphere.

The second type of burst discussed by Wild et al⁽⁷⁶⁾ is the "impulsive burst". This is the most common type of microwave activity, and has a typical lifetime of about 5 minutes. In a flare, the impulsive burst tends to coincide with the Type III bursts at metre wavelengths. It is, therefore, a phase 1 phenomenon. For this reason, the impulsive burst has been referred to as the microwave early burst (MEB), a term which will be used here. It must be stressed that dynamic spectra, taken in the microwave region^(75,73), do make it clear that the Type III bursts and the MEB are distinct phenomena. The microwave spectrum of the latter is continuous. Kundu⁽⁷⁸⁾ has found characteristic MEB source sizes of $1.0'$ - $1.6'$. These sizes imply brightness temperatures in the range 10^7 - 10^9 ° K, and, therefore, a non-thermal

origin for the radiation. The mechanisms of synchrotron radiation and bremsstrahlung have both been proposed, and it is possible that each is present to some extent. Hachenburg and Wallis (79) and Takakura (80) have established the spectral distribution of the MEB by comparing records taken at different frequencies. It was found that, while these bursts extend up to the highest frequencies observed, there is a rather sharp low-frequency cut-off at about 1000 Mc/s. This indicates that the source of the MEB is restricted to regions of chromospheric density.

The final distinctive type of microwave burst recognised by Wild et al (76) is the Type IV_{μ} . Like the Type IV_m burst, the microwave equivalent is characterized by broad-band continuum emission, and is a phase 2 phenomenon. Type IV microwave bursts, however, though rare in comparison with the MEB, are rather more common than their metric counterparts. They can occur with quite low intensities, and only the more intense Type IV_{μ} burst is accompanied by Type IV metre radiation. While it is certainly thought that Type IV_{μ} must be recognised as a distinct phenomenon from Type IV_m , it is not clear at present whether this microwave Type IV contains more than one component. The mode of polarisation reverses

between cm and dm wavelengths, but this can be explained without invoking distinct mechanisms. Takakura⁽⁸⁰⁾ has suggested that Type IV μ originates in synchrotron radiation due to electrons accelerated by the Fermi mechanism.

In the most complete form of the radio flare, the first radio evidence is a slow increase of intensity in the microwave region, a GRF burst. This burst appears before the H α flash phase, but not necessarily before the first slow brightening in H α . While such early H α brightenings may be recognised on flare patrol films after the event, however, they hardly give a clear indication of an incipient flare at the time. In this sense, the GRF is the first indication of a flare.

The explosive phase of the flare sets in later with the H α flash, which coincides with phase 1 of the radio flare. At the site of the flare instability, pulses of high velocity electrons are accelerated, and these are responsible for the Type III - Type V radiation. There is no evidence that protons are accelerated with these electrons. And the occurrence of Type III bursts in quite small events seems to preclude proton acceleration. Wild⁽⁸¹⁾ has suggested, therefore, that the Type III electrons are runaway electrons accelerated

in the initial explosion. De Jager⁽⁸²⁾ has further supposed that the Type III electrons are also responsible for the MEB. Kundu⁽⁸³⁾, and Anderson and Winckler⁽⁸⁴⁾ have shown that the MEB is precisely coincident with bursts of high-energy X-rays (1-100 KeV). Further, the profiles of the two bursts show decided similarity.

It has been suggested by de Jager, therefore, that the primary flare explosion takes place at a certain low height in the corona. Here pulses of electrons are accelerated. In moving outwards through the corona these electrons cause the Type III metre bursts. On the other hand, in moving downwards they encounter increased densities and magnetic fields at chromospheric levels. Here they are capable of generating the X-ray burst by the bremsstrahlung mechanism, and the MEB either by the same mechanism or by synchrotron emission. Wild et al,⁽⁷⁶⁾ on applying the theory of Ginzburg and Zheleznyakov⁽⁸⁵⁾ to a large group of Type III bursts, have found that 10^{35} electrons require to be emitted with energies of the order of 100 KeV. Thus the pulses of electrons, required for phase 1, need a total energy supply of 10^{28} ergs.

Wild⁽⁸⁶⁾ has given a qualitative picture of the possible interrelation of the various features of the

radio event. The following summary includes many points from this model. In the majority of flares phase 1 is the complete radio event; in larger events, however, phase 2 follows at an interval of about ten minutes at metre wavelengths, and almost at once in the microwave region. The general features of phase 2 may be interpreted as follows:- A hydromagnetic shock emanates from the explosion responsible for the $H\alpha$ flash and the radio phase 1. This shock moves outwards with a velocity of about 1000 km/sec. On reaching the corona the shock initiates the plasma oscillations responsible for the Type II burst. Behind the shock front a cloud of solar plasma is moving outwards dragging with it its associated magnetic field. Within this region electrons and probably protons are accelerated by the Fermi mechanism. The synchrotron emission of the former is responsible for the Type IV_m burst. The protons, on the other hand, having greater magnetic rigidity, can escape and are recognised at the earth in rare cases as cosmic rays.

There is another possibility, however. The cosmic-ray protons may be accelerated at lower levels, perhaps in the flare region itself. In this case the Type IV_μ burst will be due to synchrotron radiation from electrons accelerated by the same process.

It has already been mentioned that Denisse⁽⁶⁹⁾ suggested a plasma interpretation for the Type IVm_b burst. On this view, the stationary Type IVm is caused by plasma excitation by electrons being 'dumped' from weakening magnetic traps that have been carried far out into the corona behind the Type II shock front.

To account for the Type IVm_a radiation, Boischoat and Denisse⁽⁶⁷⁾ postulated 10^{32} - 10^{33} electrons with energies of the order of 3 MeV spiralling in a field of one gauss. The total kinetic energy of the electron cloud would then be of the order of 10^{27} ergs. It is clear, therefore, that the energies required to initiate the Type IV continuum storm, or indeed any of the radio bursts that accompany flares, fall far short of the total flare energy emitted in the optical region.

Type IV bursts at all frequencies have close correlations with the geophysical effects of flares, including cosmic-ray events and geomagnetic storms. Comment on this important point, however, must be deferred until later in the next section when the relevant geophysical data will have been discussed.

(iii) Geophysical

For a flare to have any geophysical effect at all, it must be a comparatively large event. Only quite exceptional flares produce the whole range of geophysical effects - namely cosmic-ray increases, ionospheric disturbances and magnetic storms. Cosmic ray events, in particular, are rare. Before the event of February 23, 1956, only four cases had been recorded of flare-associated, cosmic-ray, ground level effects (GLE). Since that date, however, improved methods of detection and balloon or rocket-borne experiments have greatly increased the sensitivity of detection of such events.

The association of the sudden ionospheric disturbance (SID) with flares was first recognised by Dellinger⁽⁸⁷⁾, who found that a solar flare could produce a short-wave fadeout (SWF). Originally it was thought that SWF was caused by increased D layer ionization resulting from an increase in $L\alpha$ emission. For it was realised, correctly, that solar $L\alpha$ radiation was responsible for the normal D layer. A review of all SID phenomena by Friedman and Chubb⁽⁸⁸⁾, however, showed that the great decrease in the height of the D layer, as evidenced by the sudden phase anomaly (SPA) of VLF transmissions, required an impossibly large increase in

$H\alpha$ emission, in fact 10^5 times the quiet sun. It is now realised that the ionization responsible for the SID is caused by X-ray emission in the spectral region of 1 - 2 A. This interpretation was verified by the earliest rocket experiments, reported by Byram, Chubb and Friedman⁽⁸⁹⁾, who found large changes in the soft X-ray intensity, but no detectable change in $H\alpha$, at the time of flares.

X-ray quanta of energies greater than 20 KeV (0.6 A) penetrate the atmosphere to levels accessible to balloon observations. The less energetic part of the flare X-ray spectrum must, however, be studied by rocket or satellite observations. A detailed review of satellite X-ray measurements has been given recently by Friedman⁽⁹⁰⁾. From these satellite observations it is clear that the X-radiation must be separated into more than one component. For example, the results from the solar radiation satellite SRIII indicate that, whereas X-rays in the region 2 - 8 A showed transient variation similar to the $H\alpha$ flare, X-rays in the region 8 - 15 A could continue at an enhanced level long after the optical flare had disappeared. The longer wavelength phenomenon is probably due to enhanced emission

in the corona, possibly line emission - a sort of slowly varying component.

The X-ray emission in the 2 - 8 A region, however, is very closely associated with the flare itself, and correlates well with SID. It can be interpreted as thermal continuum. Beyond 20 KeV, on the other hand, the radiation is better fitted to non-thermal bremsstrahlung (Kawabata⁽⁹¹⁾). The high energy electrons responsible for this X-radiation are assumed to initiate the Type III bursts (de Jager⁽⁸²⁾), and the MEB (Kundu⁽⁸³⁾). Solar X-ray spectroscopy is still at an early stage, and observations till now have been limited by lack of spectral resolution. The interpretations mentioned above must, therefore, be regarded as tentative.

Kreplin, Chubb and Friedman⁽⁹²⁾ have described results obtained from the satellite SRI. This satellite, besides investigating solar X-rays in the spectral region 2 - 8 A, also monitored solar $L\alpha$ radiation. The accuracy of the $L\alpha$ measurements was not sufficient to detect any certain change in the sun's total $L\alpha$ flux. An upper limit of 11% was, however, set for any enhancement of $L\alpha$ above the level of the quiet sun. Using ultra-violet flux data of Detwiler, Garrett, Parcell and

Tousey⁽⁹³⁾, it is seen that this upper limit corresponds to a total rate of emission of approximately $2 \cdot 10^{27}$ ergs/sec. If, however, the $L\alpha$ radiation corresponding to this upper limit were confined to an area of the size of the visible flare, then an increase by a factor of a thousand would be required. While the extent of $L\alpha$ emission in flares is still very uncertain, it does seem that this radiation is not in any sense a predominant feature of the flare event.

Large flares are sometimes followed by the sudden commencement of a magnetic storm. The delay between the flare and the sudden commencement depends on the size of the storm, and lies between 1-2 days. It is inferred, therefore, that a cloud of solar plasma is blown out at the time of the flare, and from the travel time a velocity of 1000-2000 km/sec is deduced. In view of these figures, it is tempting to identify the Type II radio burst with the plasma stream. Work by McLean⁽⁹⁴⁾ shows, however, that Type II bursts correlate well with sudden commencements if, and only if, they are accompanied by Type IV continuum. On the other hand, Parker⁽⁹⁵⁾ has suggested that the magnetic storm may not be due to an ejection of plasma at the explosive phase of the flare. He argues that the storm is caused by

an interplanetary blast wave generated by an expansion of the enhanced corona over a longer period of time. Further, Parker^(96,59) has calculated the kinetic energy of such a blast wave, assuming a volume of 0.1 a.u.^3 and a density of $30 \text{ particles/cm}^3$. His result gives a total energy of $2 \cdot 10^{32}$ ergs. Moreover, the density he uses is rather less than that deduced by Blackwell and Ingham⁽⁹⁷⁾ from zodiacal light observations. Unless, therefore, the blast wave is, for some reason, confined to a comparatively narrow sheet near the sun's equatorial plane, one must conclude that the energy involved in the plasma stream is at least as great as that emitted by the optical flare.

Solar cosmic-ray particles have only been detected at ground level in very rare events. Such detection is quite the most exceptional recognition of flare-associated phenomena. Since 1956, however, the use of particle counters and emulsions in balloons, or at still greater altitudes, in satellites, has greatly increased the detectability of lower energy solar cosmic-ray events. Further, these events can be detected indirectly by polar cap absorption (PCA) of cosmic radio noise in the VHF region. With this improved sensitivity of detection, it is now recognised that solar cosmic ray

bursts are not the rare phenomenon that the scarcity of GLE would indicate. Even so, any detection of cosmic ray effects is indicative of a large flare event. Thompson and Maxwell^(98,99), for example, have noted that both direct and indirect detection of low-energy solar cosmic rays are well correlated with Type IV radio outbursts.

To produce an observable effect at ground level, particle energies in excess of 1 BeV are required. The most famous event of this kind, that of February 23, 1956, was studied by Meyer, Parker and Simpson⁽¹⁰⁰⁾. They found that the total kinetic energy of particles above 2 BeV, emitted by the flare, was not less than $3 \cdot 10^{30}$ ergs. In a later paper, Parker⁽³⁸⁾ suggested that the particles are accelerated by the Fermi mechanism⁽¹⁰¹⁾ in the initial site of the flare. Assuming a magnetic field of 500 gauss, Parker argued that the fluid motions and magnetic inhomogeneities within the flare region would be sufficient to accelerate protons from thermal to relativistic velocities in about two minutes. A rather different non-statistical mechanism has been proposed by Severny and Shabanskii⁽¹⁰²⁾.

All estimates of the total energy of solar cosmic ray bursts are uncertain owing to lack of knowledge of

the low-energy spectrum. In the paper just referred to, Parker calculated the spectrum for his mechanism and found that the turnover occurred at an energy of 450 MeV. For higher energies, the spectrum was an inverse fifth power law. This is in agreement with observation. This result would suggest that the figure of $3 \cdot 10^{30}$ ergs, quoted above, is a fair estimate of the total energy of the cosmic ray burst. It should be noted, however, that there is no observational evidence to support the high energy turning point deduced by Parker.

In a recent review, Mollison and Webber⁽¹⁰³⁾ have tabulated data from satellite observations of 30 major cosmic ray events that have occurred since 1956. They calculated the integrated intensity of particles with energies in excess of 30 MeV and 100 MeV. From these values it is readily seen that for large, but not exceptional, events the total energy in excess of 30 MeV is of the same order as Parker's result. This suggests that Parker's figure for the flare of February 23, 1956, may well be an underestimate. Some authors - e.g. Stepanyan and Vladimirov⁽¹⁰⁴⁾ - have argued that the energies involved in the cosmic ray burst may be quite as large as the value usually quoted for the optical event, namely $2 \cdot 10^{32}$ ergs.

The correlation of cosmic-ray events with Type IV continuum has already been mentioned. Both at metre wavelengths and in the microwave region this radiation is generally interpreted as synchrotron radiation. It is probable that the electrons responsible for this are accelerated by the same Fermi process as the cosmic ray protons. The complete Type IV burst is not at present understood. It does appear, however, that there is synchrotron radiation being emitted from two quite separate regions. The Type IV_m_a burst is emitted from an outward moving, high in the corona. On the other hand, the Type IV_μ is emitted from comparatively dense regions of high magnetic field in the low corona or chromosphere. It is not clear which source should be identified as the cloud of accelerated counterparts of the cosmic ray protons. It could even be that cosmic ray acceleration takes place independently in each region. For similarities have been found between the time variations of cosmic ray intensity and the intensity of Type IV_m (Boischof and Warwick⁽¹⁰⁵⁾). Mallitson and Webber⁽¹⁰³⁾, on the other hand, have found that the strength of a cosmic ray event is related specifically to the intensity of the microwave burst.

The protons accelerated at the time of the flare will be confined in the solar magnetic field. In a typical cosmic ray event, therefore, the onset of PCA is delayed for several hours, the time required for the cosmic ray particles to diffuse from the solar magnetic trap (Stepanyan and Vladimirskii⁽¹⁰⁴⁾). In certain exceptional cases, however - particularly the large events in which a GLE is observed - the first particles reach the earth within minutes of the flash phase of the flare. To account for these very short onset times, special magnetic configurations must be specified in the earth-sun space. A number of authors - e.g. Gold⁽¹⁰⁶⁾ - have suggested that the solar magnetic field may become drawn out from an active region to form a magnetic bottle in interplanetary space, the feet of the magnetic field lines remaining anchored on the solar surface. The Forbush decrease in galactic cosmic radiation provides evidence for the existence of such field configurations at the earth. These configurations may be drawn out by the interplanetary blast wave responsible for geomagnetic storms, which indeed are often accompanied by Forbush decreases.

If a flare, situated in the active region at the neck of a magnetic bottle, accelerates cosmic ray particles, these particles may escape from the sun, but they will be initially confined to those regions of interplanetary space to which the field of the active region extends. In general, such magnetic configurations will not engulf the earth; then the protons must have time to diffuse from the magnetic bottle before they can produce any geophysical effect, usually PCA. In this way the onset times of several hours are again explained. In rare cases, however, the earth may be included in the field configuration, and in this event solar protons have direct access to the earth. The onset time should be simply the travel time, and the cosmic ray burst should follow the accelerating flare by only a few minutes. The exceptionally short onset times in some large events are, therefore, satisfactorily accounted for. Additional evidence in favour of this explanation is provided by the well-known east-west asymmetry of flares producing GLE, and by the shorter onset times found for cosmic ray bursts associated with flares in the western hemisphere.

Mallitson and Webber⁽¹⁰³⁾ have noted that the large cosmic ray events since 1956 have been restricted to flares in only a few active regions, each such region

tending to produce several flares with cosmic ray GLE. Ellison, McKenna and Reid⁽⁵²⁾ have studied one such active region in detail. A series of 3⁺ flares which occurred in this region have been referred to as the July 1961 event. The largest of these flares, that of July 12, was accompanied by intense Type IV radiation at both metre and microwave wavelengths. Despite the magnitude of this event no cosmic rays were detected at ground level, though the flare did give rise to PCA. Further, this flare was followed 24^h.9 later by a sudden commencement of geomagnetic activity, with a simultaneous Forbush decrease in cosmic radiation. On July 18 and July 20, two other flares occurred; though each was a 3⁺ event, the optical and radio data indicated that these events were smaller than that of July 12. In particular, the Type IV bursts were significantly less intense. Nonetheless each was followed within 35 minutes by a cosmic ray GLE. It is clear that these observational features can be satisfactorily explained on Gold's magnetic bottle hypothesis. It may be assumed that the flare of July 12 failed to produce a GLE due to the lack of a suitable interplanetary field configuration. The interplanetary blast wave of this event, however, set up such a configuration, and ground level detection of

cosmic rays was, therefore, possible for the later and smaller events.

This concludes the description of the observational features of solar flares. A number of points that might be important to flare theories have been omitted from the discussion. For example, no account has been taken of the possible increase in the relative abundance of Deuterium in active regions (Severny⁽¹⁰⁷⁾, Goldberg, Mohler and Müller⁽¹⁰⁸⁾). It is felt that the results of these measurements in $D\alpha$ can scarcely be considered conclusive. Such measurements are hampered by the proximity of $D\alpha$ to the hydrogen line, and more seriously by its coincidence with a variable telluric line of water vapour. Observationally, the question of nuclear reactions in flares must be left open.

In the next chapter a discussion of theory requirements will be attempted in the light of the observational data that have been discussed here.

(1) Introduction

The discussion of the previous chapter indicates that the complete flare event must be regarded as an aggregate of many diverse solar and geophysical features. The total event is seen to be far more complex than the $H\alpha$ phenomenon by which it was originally observed. The $H\alpha$ phenomenon is but one aspect of the flare, and not necessarily the predominant one. Many of the observational features and their interrelation are understood in a qualitative manner. The radio and geophysical data are perhaps better understood than the optical phenomena; at least, there is more general agreement on their interpretation.

Other aspects of the flare event are understood rather more completely, and quantitative theories have been developed that account for the essential features of the observations. For example, assuming the provision of 10^{35} electrons in the 100 KeV range, the mechanism of Ginzburg and Zheleznyakov⁽⁸⁵⁾ satisfactorily accounts for the brevity, bandwidth, frequency drift, and harmonic structure of Type III radio bursts. All flare associated features, whether understood at present in a qualitative or quantitative manner, require for their initiation an explosive primary event. The concern

of a theory of flare origin is the nature and the development of this primary event,

The fact that no photospheric change of any kind has ever been observed at the base of a solar flare has led to the belief that the source of flare energy is either chromospheric or coronal. On the other hand, Severny's discovery⁽³⁰⁾ of fine structure in the wings of flare emission, which he described as moustaches, must cast some doubt on this interpretation. For, if these particular moustaches are identified with Ellerman bombs, then they are low-level phenomena. This interpretation of the fine structure has not, however, been generally accepted.

If a chromospheric or coronal origin of flare energy is assumed, the insufficiency of thermal energy in these regions of the atmosphere requires that the energy source be magnetic. It is deduced, therefore, that the flare energy is drawn from the magnetic field in the general environs of the primary event. Most of the observed features of solar flares are regarded as secondary phenomena. The possible exception is the $H\alpha$ flare.

Certainly $H\alpha$ emission is virtually a sine qua non of any flare event. Again, estimates of the energy dissipated in this emission, $2 \cdot 10^{32}$ ergs in great flares,

are large, larger than the usual estimates for all other associated features. As has already been mentioned, however, some authors^(104,95) have suggested that the energy expended in cosmic ray showers and the interplanetary blast wave may be as large as that emitted in the chromospheric flare. The possibility exists, therefore, that the $H\alpha$ flare, like other associated features, is a secondary phenomenon, and that the primary event is unobserved.

Some arguments⁽⁷⁶⁾ have been advanced to suggest that the primary event is sited in the corona. These arguments are, however, based on a crude interpretation of the radio data, and involve a large extrapolation of doubtful accuracy. The evidence is not conclusive, therefore, and observations do not specify a site for the primary event. The physical conditions at this site are, in effect, quite unknown. They may correspond to chromospheric conditions or to conditions in the, probably disturbed, corona.

A theory of solar flares will generally concentrate on explaining the largest events. Such 3^+ flares involve energies of the order of $2 \cdot 10^{32}$ ergs. In a magnetic explanation, the source of energy must ultimately lie in the magnetic field of the associated

spot group. Sweet⁽¹⁰⁹⁾ estimated the energy of the potential field above the photosphere in a large spot group as $2 \cdot 10^{34}$ ergs, a figure a hundred times larger than required for a 3^+ flare. He pointed out, however, that as the potential field represents the configuration of minimum energy, this energy is not available to supply the flare. It is, therefore, the energy involved in distortions of the sunspot potential field at chromospheric heights that must provide the flare energy. Since at chromospheric and coronal levels, above active regions, the magnetic pressure far exceeds the gas pressure, any distortion of the sunspot field from potential form must be force-free.

Briefly, two main requirements of a complete magnetic flare theory may be stated as follows. Firstly, it must provide a stable process of storing energy up to $2 \cdot 10^{32}$ ergs in force-free fields at chromospheric or coronal levels. The ultimate source of this energy is probably in photospheric motions. At photospheric levels the gas pressure is in excess of, or at least of the same order as, the magnetic pressure, and gas motions will be able to distort the field. These motions of the feet of the magnetic field lines, anchored in the photosphere, will induce force-free

perturbations of the potential field at chromospheric levels. The existence and stability of such force-free configurations form, therefore, the first requirements of a complete flare theory.

The second main requirement of a flare theory is the appearance of an instability in the field configuration. The development of this instability must proceed at a rate commensurate with the time-scale of a flare. This time-scale is usually identified with the flash phase of the $H\alpha$ flare, and may, therefore, be taken as about 200 seconds. The total duration of the flare is of course far longer, and may be regarded as the time of relaxation to normal chromospheric conditions. Other interpretations have been offered of the decay phase of the flare, and these will be discussed later.

(ii) Classical Theories of Solar Flares

The first magnetic theory of solar flares was proposed by Giovanelli. Subsequently this theory was severely criticised by Cowling⁽¹¹⁰⁾ on very fundamental grounds. Nonetheless the detailed nature of the theory merits serious discussion. This discussion will provide a context for later developments, and the criticism will illustrate some of the difficulties with which such

theories must contend. Giovanelli⁽¹¹¹⁾ attempted to explain the sudden onset of a flare by a discharge mechanism due to runaway electrons. In separate papers^(112,113) he dealt with the discharge mechanism itself, and the field configurations responsible for its inception.

A detailed study⁽¹¹²⁾ was made of the behaviour of the conductivity of a highly ionized gas under the influence of an applied electric field. For small applied fields the electron energies are limited by elastic collisions with ions. The collisional cross-section for this type of collision decreases with increasing electron velocity. Under simple assumptions, and neglecting the velocity distribution of the electrons, Giovanelli computed a critical field strength E_c , above which applied fields would produce a discharge. For field strengths $E < E_c$, elastic collisions limit the electron energies. For fields $E > E_c$, however, these collisions are ineffective in limiting the electron velocities, and runaway electrons are produced. Under conditions of complete ionization the velocities of the runaway electrons are limited only by the extent of the electric field. On the other hand, if the gas is only partially ionized, the presence of neutral atoms may

place an effective upper limit on the electron velocities. Elastic collisions between electrons and neutral atoms will generally be unimportant, owing to the fact that the cross-section for this type of collision is small compared with that for collisions between electrons and ions. Inelastic collisions, however, may be important, effectively limiting the electron energies to values not far in excess of the excitation or ionization potentials. The presence of a magnetic field will also be effective in providing an upper limit to the electron energies.

As the applied electric field E is increased to the critical value E_c , there is, then, on Giovanelli's simplified theory a discontinuous increase in the electron drift velocity. This abrupt change can be interpreted as a change in the conductivity of the ionized gas. For hydrogen ions at a temperature of 5750° K, Giovanelli computed the critical field as

$$E_c = 5 \cdot 10^{-17} n_1 \text{ e.s.u.} \quad (2-1)$$

where n_1 is the ion density. If we take $n_1 \sim 10^{11} \text{ cm}^{-3}$, appropriate to the chromospheric levels of the optical flare, the electric field required to initiate a discharge is $5 \cdot 10^{-6} \text{ e.s.u.}$ or about $1.5 \cdot 10^{-3} \text{ volts/cm.}$

This, then, was Giovanelli's discharge mechanism. The second part of his theory involved finding a situation appropriate to the solar atmosphere that would provide an electric field of at least $1.5 \cdot 10^{-3}$ volts/cm to drive the discharge. Before outlining Giovanelli's investigations on this point, it will be convenient to state the electromagnetic equations involved; these will be required throughout the present chapter. They are simply Maxwell's equations and the conductivity equation, which, using Gaussian units, may be written as

$$\text{curl } \underline{H} = \frac{4\pi \underline{j}}{c} \quad (2-2)$$

$$\text{curl } \underline{E} = -\frac{1}{c} \frac{\partial \underline{H}}{\partial t} \quad (2-3)$$

$$\frac{\underline{j}}{\sigma} = \underline{E} + \frac{\underline{v} \wedge \underline{H}}{c} \quad (2-4)$$

As is usual, the displacement current had been neglected in equation (2-2), and, for the moment, the Hall current term has been omitted from the conductivity equation.

As mentioned earlier, Giovanelli⁽⁶⁾ has shown from a statistical analysis that flares tend to occur when the spot area is changing most rapidly. He attempted, therefore, to explain the electric fields required for

the discharge mechanism as fields induced by the development of the sunspot's magnetic field. Now the typical linear dimension, L say, of a sunspot is of the order of 10^9 cm. Further the observed time-scale of growth is about a week, $5 \cdot 10^5$ seconds. This indicates a velocity of propagation of the field, \underline{u} , where $|\underline{u}| \sim 2 \cdot 10^3$ cm/sec. If the magnetic field, \underline{H} , of the spot is taken to be 500 gauss at chromospheric levels, then an observer whose position is fixed relative to the solar surface will measure an electric field of 10^{-2} volts/cm. Such a field appears more than is required to initiate the discharge. However, the electric field available to drive currents is not $(\underline{u} \wedge \underline{H})/c$ as computed above, but the field measured by an observer moving with the fluid. That field is $(\underline{w} \wedge \underline{H})/c$, where \underline{w} is the fluid velocity relative to the field lines.

The field strength available to drive the discharge will only be of order 10^{-2} volts/cm, if $\underline{w} = \underline{u}$, that is if the fluid velocity is zero. Giovanelli⁽¹¹³⁾, therefore, considered the propagation of the sunspot field in a static atmosphere. From equations (2-2) to (2-4) the equation of magnetic diffusion is derived as

$$\frac{\partial \underline{H}}{\partial t} = \frac{c^2}{4 \pi \sigma} \nabla^2 \underline{H} \quad (2-5)$$

This equation yields a time-scale τ for the growth of the sunspot field, given by

$$\tau \sim 4 \pi \sigma L^2 / c^2 \quad (2-6)$$

In the chromosphere the conductivity σ is of order 10^{13} e.s.u.; hence, as first shown by Cowling⁽¹¹⁴⁾, the time-scale of propagation of the sunspot field in a static atmosphere is about 300 years.

Giovanelli noted, however, that the presence of a magnetic field decreased the conductivity in the direction perpendicular to the magnetic field; he concluded, therefore, that an increased rate of field propagation was possible. But the modified form of the conductivity is due to the inclusion of the Hall current term in the conductivity equation, (2-4). The diffusion equation, (2-5), then becomes

$$\frac{\partial \underline{H}}{\partial t} = \frac{c^2}{4 \pi \sigma} \nabla^2 \underline{H} - \frac{c}{4 \pi e} \text{curl} \left(\frac{1}{n} \text{curl} \underline{H} \wedge \underline{H} \right) \quad (2-7)$$

where n is the electron density. Consider a static isothermal atmosphere of fully ionized hydrogen. Then, under a conservative field of force, - with potential function Ω say - , the final term on the right hand side

of equation (2-7) will vanish identically. For, if M is the mass of the hydrogen ion, the equation of motion can be written as

$$(\text{curl } \underline{H} \wedge \underline{H})/n = 4\pi kT \text{ grad}(\log n) + 4\pi M \text{ grad } \Omega \quad (2-8).$$

The diffusion equation, therefore, reduces to (2-5), and the rate of field propagation is unaffected by the modified conductivity. In point of fact, the Hall current term can be neglected anyway in any quasi-steady chromospheric problem involving sunspot fields, since the gas pressure cannot sustain magnetic forces, and so $\underline{j} \wedge \underline{H} = 0$. The assumption of a static atmosphere is, therefore, not only artificial, as Giovanelli admitted, it is also wrong, since the process of static diffusion would involve magnetic forces that the chromospheric gas could not sustain. The sunspot field must be transported by material motions, and, in general, electric fields sufficient to drive Giovanelli's discharge will not be induced.

Cowling⁽¹¹⁰⁾ had two main criticisms of the discharge theory, as proposed by Giovanelli. The first criticism is similar to that just given, in that it questions the existence of the required electric fields. Cowling's argument may be put as follows. The total

energy of a flare is of order $2 \cdot 10^{32}$ ergs; a typical flare area is perhaps $4 \cdot 10^{19}$ cm², and the duration of a large flare may be $5 \cdot 10^3$ seconds, or $1\frac{1}{2}$ hours. From these values the rate of emission, I , may be estimated as $I \sim 10^9$ ergs cm⁻² sec⁻¹. Now, in a discharge theory, this rate of emission must be provided by Joule dissipation of magnetic energy. If ℓ is the thickness of the flare region, then the total rate of dissipation will be of order $j^2 \ell / \sigma$ per unit surface area.

In the solar atmosphere, the current density j is determined, not by any applied electric field, but by the magnetic field configuration. To order of magnitude, equation (2-2) gives $j \sim cH/4\pi\ell$, and the total rate of Joule heating will be $c^2 H^2 / 16\pi^2 \sigma \ell$. This must be equated to the observed rate of emission, to provide an equation for ℓ , viz

$$\ell \sim \frac{c^2 H^2}{16 \pi^2 \sigma I} \quad (2-9)$$

Substituting the values already given, - $I \sim 10^9$ ergs cm⁻² sec⁻¹, $\sigma \sim 10^{13}$ e.s.u., $H = 500$ gauss -, it is found that $\ell \sim 140$ cm. Cowling regarded this extreme thinness of the flare region as unacceptable. The important point is, however, that if the flare is interpreted as a discharge, this discharge must be very

thin in one direction, a feature not recognised in Giovanelli's theory.

Cowling's second criticism concerned the nature of the discharge itself. In Giovanelli's theory the discharge occurs due to the onset of runaway electrons, which is equivalent to a sudden increase in the conductivity of the gas. In this theory the electric field was treated as an applied field, and consequently the sudden increase in the conductivity resulted in a rapid increase in the current density, and therefore in the Joule dissipation, which was treated as σE^2 per unit volume. This point of view is, however, quite wrong in the context of solar problems. Here \underline{j} is determined by the magnetic field configuration through equation (2-2) and will be virtually unaffected by abrupt changes in the conductivity. The only immediate effect of a sudden change in the conductivity will be a reduction of the electric field, which is given by equation (2-4). This field is reduced, since it must provide effectively the same current for the larger conductivity. The Joule dissipation, which is always given by \underline{j}^2/σ , will clearly be reduced by any increase in the conductivity.

The onset of runaway electrons would, then, inhibit rather than enhance the energy dissipation. The sudden onset of a flare cannot, therefore, be accounted for by this type of discharge. If runaway electrons are important in the dissipation process at all, it is in limiting the rate of conversion of magnetic energy into heat within the flare region, rather than in providing a mechanism to account for the flare's explosive onset.

A rather different type of discharge theory was put forward by Dungey⁽¹¹⁵⁾. Here it is recognised that under solar conditions the current density is determined by the magnetic configuration. Cowling's first criticism is, therefore, satisfactorily met. Dungey's discharge, which he defines simply as a region of very high current density, is due to the severe distortion of the lines of magnetic force at the neutral point of the field. A current region is then formed that is very thin in one direction. Dungey's investigation is concerned with conditions at the neutral point that lead to the onset of such a discharge; the subsequent behaviour of the discharge was not considered. Although several points in his analysis are open to criticism, Dungey's work did give the first real insight into the

nature of discharges in the solar atmosphere and the relevance of neutral points.

The magnetic field near the neutral point was examined by Dungey under the approximation that the lines of force are frozen to the material. Under this approximation equations (2-2) to (2-4) can be reduced to a single equation to give

$$\frac{\partial \underline{H}}{\partial t} = (\underline{H} \cdot \text{grad}) \underline{v} - (\underline{v} \cdot \text{grad}) \underline{H} - (\text{div } \underline{v}) \underline{H} \quad (2-10)$$

In the equation of motion the pressure term is neglected to yield

$$\frac{\partial \underline{v}}{\partial t} = - (\underline{v} \cdot \text{grad}) \underline{v} + \frac{1}{4\pi\rho} \text{curl } \underline{H} \wedge \underline{H} \quad (2-11)$$

And, finally, there is the continuity equation

$$-\frac{\partial \rho}{\partial t} = \rho \text{div } \underline{v} + \underline{v} \cdot \text{grad } \rho \quad (2-12)$$

Next a frame of reference is chosen in which the neutral point is also a stagnation point. Then $\underline{v} = \underline{H} = 0$ at this point and all terms in equations (2-10) and (2-11) will vanish there. The neutral point is taken as origin of a Cartesian system with co-ordinates x_i , $i = 1-3$. At the origin the derivatives $\partial v_i / \partial x_j$ and $\partial H_i / \partial x_j$ are respectively denoted by v_{ij} , H_{ij} . Then, using the dummy suffix notation, the equation of continuity (2-12) becomes at the neutral point.

$$-\frac{\partial \rho}{\partial t} = \rho \nu_{kk} \quad (2-13)$$

Similarly, if equations (2-10) and (2-11) are differentiated partially with respect to each of the x_j in turn and then applied at the neutral point, a set of equations is derived, one for each of the v_{ij} and H_{ij} , that are similar in form to equation (2-13). In this way a set of simultaneous non-linear first-order ordinary differential equations is obtained in the v_{ij} , H_{ij} , and ρ . This set of equations can readily be solved, given only the necessary starting values.

Having set up these equations, Dungey considered the following example. Suppose that \underline{j} is zero at the neutral point, then a set of orthogonal principal axes can be chosen, so that all the H_{ij} vanish except the diagonal elements. This set of axes is taken as coordinate axes. Suppose, further, that initially there is no fluid velocity in the neighbourhood of the neutral point, then all the v_{ij} will be initially zero. Now a small perturbation is applied to a number of the velocity and field derivatives, and the differential equations referred to above are solved numerically. It was found that initially the perturbations grew exponentially, until the anti-symmetric terms in the matrix H_{ij} , which refer to the current density, became the same order as

the (initially non-zero) diagonal terms. Thereafter, all terms grew and became infinite after a finite time. It was concluded that the current density at the neutral point becomes infinite after a time not many times larger than $(4 \pi \rho)^{\frac{1}{2}} / H_{11}$, a typical Alfvén time of the system.

From this example, Dungey drew the conclusion that the magnetic field at a neutral point is unstable, and that an initial perturbation, however small, will grow to produce a discharge within a finite time. To examine this conclusion, it is intended to apply the well-known theorem that the potential field is the configuration of minimum energy. Consider a magnetic field configuration, with a neutral point, that is bounded by a surface Σ , on which the normal component of \underline{H} is specified. For this distribution of flux on Σ there is a unique potential field within Σ , which may be denoted by \underline{H}_0 , and which is supposed to possess a neutral point within Σ . Let W_0 be the energy of this field. Next let $\delta \underline{H}$ be any perturbation on this field, which retains the flux distribution on Σ , where forces are applied to hold the magnetic field lines in position. Let δW be the energy increment of the perturbed field $\underline{H}_0 + \delta \underline{H}$. Finally, introduce the

magnetostatic potential for \underline{H}_0 , writing $\underline{H}_0 = \text{grad } \phi$.

Now, on applying the necessary vector identity, an expression for δW is obtained, namely

$$8\pi \delta W = \int \delta \underline{H}^2 dV + 2 \int \text{div}(\phi \delta \underline{H}) dV$$

since $\text{div } \delta \underline{H} = 0$. In this equation the volume integrals are taken throughout the volume enclosed by the surface Σ . From Gauss's theorem the equation can be written

$$\delta W = \frac{1}{8\pi} \int \delta \underline{H}^2 dV + \frac{1}{4\pi} \int_{\Sigma} \phi \delta \underline{H} \cdot d\underline{S} \quad (2-14).$$

But since the flux on Σ is conserved the second term in equation (2-14) vanishes, and so $\delta W \geq 0$. Hence the potential field \underline{H}_0 is the field of minimum energy and, therefore, must be a configuration of stable equilibrium.

Since Dungey's analysis would seem to indicate that this field \underline{H}_0 is unstable at the neutral point, a dilemma is encountered, the resolution of which must be along the following lines.

Within the approximations of the method, namely assuming perfect conductivity and neglecting the gas pressure, Dungey's solution at the neutral point of the field is, in a sense, correct. These approximations break down at the neutral point, however, and the solution may, therefore, be physically unrealistic.

Under the approximations used, the only way in which one part of the fluid can influence another is by hydromagnetic effects, which will be propagated with the Alfvén velocity. This velocity of propagation goes to zero at the neutral point. As a consequence, the domain of dependence of any surface, however near to but not containing the neutral point, and on which the solution is known for a finite time, does not include the neutral point itself. The neutral point is, therefore, an isolated point, and the solution obtained there will not be relevant to the solution in the surrounding gas. On the other hand, when pressure and magnetic diffusion effects are included, the solution at the neutral point will indeed be influenced by the solution at neighbouring points. However, additional boundary conditions are then necessary to obtain this solution; and one cannot proceed by Dungey's very neat method. In short, Dungey's method relies on the fact that the neutral point is isolated, a fact that makes the solution obtained by this method inappropriate to the physical problem.

It must be concluded, therefore, that the neutral point is not unstable in any real sense. It is possible that a perturbation given to a potential field may initiate a discharge of the type envisaged by Dungey.

But the total energy dissipated in the discharge will be exactly equal to the perturbation energy and no more. The energy of the potential field itself is unassailable.

Dungey attempted to show that the inclusion of gas pressure would not inhibit the development of his discharge, arguing that the pressure gradient would reinforce the electromagnetic forces. In investigating this point, he examined a two-dimensional field configuration and proved that the condition of static equilibrium requires an infinite current density at an X-type neutral point.

This second conclusion of Dungey's work can be stated as follows. An isolated two dimensional magnetic field configuration containing an X-type neutral point cannot be in hydrostatic equilibrium. Dungey's proof of this theorem depends, however, on an assumption, albeit an explicit one, that the lines of force touch at the neutral point. The case where the lines of force cut at a finite angle is excluded by means of a qualitative argument. This argument is, however, misleading. In the present thesis, it is intended to demonstrate the existence of a two-dimensional isolated field which contains a neutral point and which is in equilibrium under hydrostatic pressure. In this context, by an isolated field is meant a magnetic

configuration whose outer boundary is a closed line of force. An isolated equilibrium field may be constructed as follows.

It is possible to specify a two-dimensional field that is independent of the z -coordinate, and whose lines of force are parallel to the x - y plane, by a vector potential $\underline{A} = (0, 0, A(x, y))$. An equilibrium field with two O-type neutral points and an X-type neutral point on a line of symmetry may be constructed as follows. Let the O-type neutral points be the points O_1 and O_2 at $x = \pm a$, $y = 0$, and take the X-type neutral point as the origin O . The type of field under discussion is illustrated in Figure (2-1).

The equation of hydrostatic equilibrium will simply be

$$\text{curl } \underline{H} \wedge \underline{H} = 4 \pi \text{ grad } \rho \quad (2-15).$$

Taking the curl of equation (2-15), and substituting the vector potential A for the magnetic field, yields the equation

$$\frac{\partial(\nabla^2 A, A)}{\partial(x, y)} = 0 \quad (2-16),$$

which indicates that the condition of equilibrium is that the current density $\nabla^2 A$ should be a function of A .

As a simple example, consider the solution

$$\nabla^2 A = -\lambda^2 A \quad (2-17).$$

By separation of the variables, the general solution of equation (2-17) can be expressed, in polar coordinates with origin 0, as

$$A = \sum_{n=0}^{\infty} A_{2n} J_{2n}(\lambda r) \cos 2n\theta \quad (2-18),$$

where J_{2n} denotes the Bessel function of the first kind of order $2n$. In equation (2-18) account has been taken of the fact that A is finite at the origin, and allowance has been made for the symmetry and single-value requirements of the type of field, illustrated in Fig (2-1).

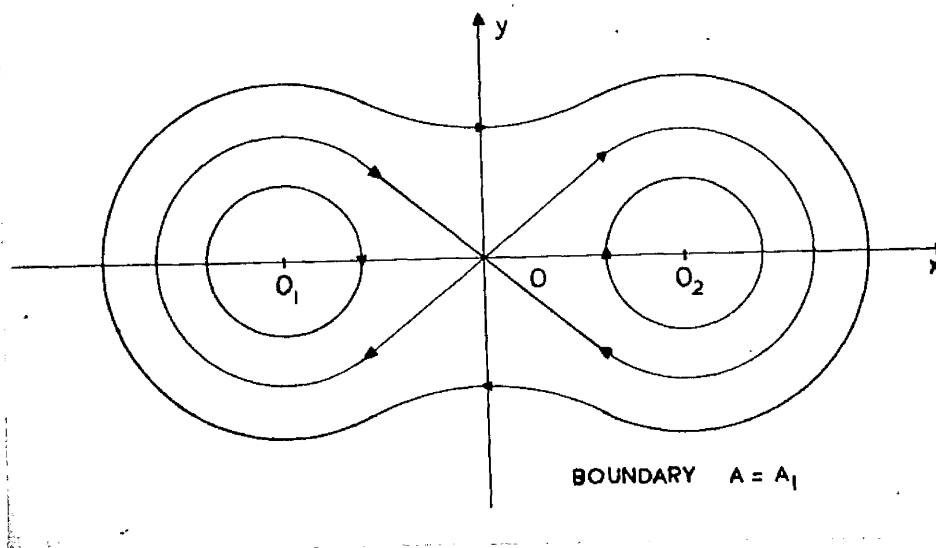


Fig (2-1) Equilibrium field with an X-type neutral point, bounded by the equipotential $A=A_1$.

It is more convenient, however, to work in bipolar coordinates, taking O_1, O_2 as the reference points of the coordinate system. If r_1, r_2 are the distances of a point from O_1, O_2 respectively, then a particular solution of equation (2-17) is

$$A = A_0 (J_0(\lambda r_1) + J_0(\lambda r_2)) \quad (2-19).$$

Here A_0 is a constant. In this solution the origin is automatically a neutral point. It will be an X-type neutral point, and O_1, O_2 will be O-type neutral points, if

$$\lambda = \frac{r_0}{2a} \quad (2-20),$$

where r_0 is the first positive zero of $J_1(r)$. The field given by equation (2-19) is then of the figure of eight form near the origin that is shown in Fig (2-1).

The complete field given by equation (2-19) has, of course, a much more complicated structure than that indicated in the diagram. It possesses other neutral points, in addition to the three O_1, O_2 , and O under discussion. It is possible, however, to construct a field of the simple type envisaged in the diagram, by the simple expedient of enclosing the field by a boundary that is a line of force, $A = A_1$, as shown in Fig (2-1). Numerical computations can readily verify the existence of such a line of force.

The example just considered, although rather artificial, does prove the existence of isolated two-dimensional fields which possess a neutral point and are in equilibrium under gas pressure. The existence of such equilibrium fields may be important in investigations of the development of certain types of instability in the field, on which some flare theories depend. There is, however, no reason why fields of the isolated type should specifically be considered in such problems. A field which has a flux distribution specified on its outer boundary seems more appropriate for the solar chromosphere. For the roots of such fields are expected to lie below the photosphere, in regions of high gas density, where the lines of force will be firmly held in position. The movements of the field lines at low levels, due to photospheric motions, then exert perturbations on the chromospheric field. Equilibrium configurations containing a neutral point, for fields of this type for which the magnetic flux is specified on the boundary, obviously exist. The potential configuration already considered on p. 73 is one very simple example.

(111) Subsequent Developments

Sweet⁽¹¹⁶⁾ has considered Dungey's type of discharge from a more satisfactory standpoint. He considered a two dimensional example in which the field lines were directed in the x-y plane and were independent of the z-coordinate. The field examined lay above a line in the x-y plane on which the magnetic flux was specified. The twin bipolar system considered is shown in Figure (2-2). A flux distribution has been specified on the line PQ, and it is assumed that the field above PQ is initially of potential form.

The two current systems A and B responsible for the magnetic field are now moved together. If infinite conductivity is assigned to the fluid, then the lines of force will move with the fluid during this displacement, and a new field configuration will be taken up. This new configuration will be referred to as the colliding field. In general, this field cannot be of potential form, and electric currents will be induced above PQ by the displacement.

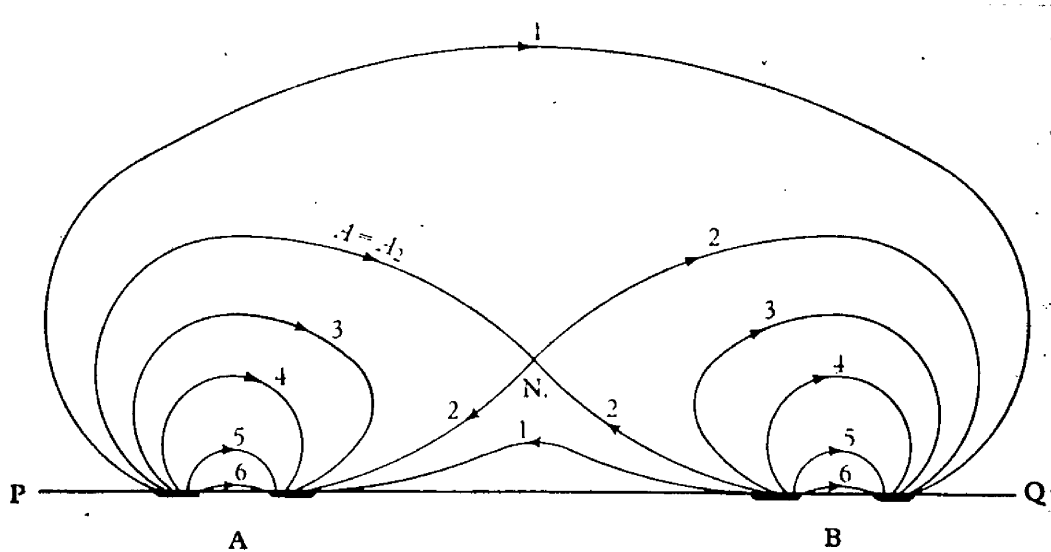


Fig. 1. Potential field of two bipolar systems.

Fig (2-2) The potential field of two bipolar systems. (116)

From an investigation of the field above PQ that is induced by a displacement of the current systems through a distance of the same order as their initial separation, Sweet derived the following important result. He showed by a detailed and rigorous argument that, if hydrostatic equilibrium is to be possible in the colliding field configuration, then there is a point M above PQ at which the gas pressure is at least of order $H_0^2/8\pi$, where H_0 is a typical value of the magnetic

intensity in the initial potential field.

This result was next applied to the solar atmosphere. Since the magnetic pressure above a spot group will greatly exceed the ambient gas pressure of the chromosphere or corona, Sweet argued that the large gas pressures required for equilibrium cannot be maintained by the chromospheric gas. He concluded, therefore, that in general a non-singular equilibrium configuration will not exist.

While this conclusion would seem a reasonable consequence of Sweet's result, it requires further justification. For, although the gas pressure in the initial potential field will be several orders of magnitude below the magnetic pressure, the displacement might conceivably induce a gas pressure sufficient to sustain equilibrium. Certainly a sufficiently high gas pressure, of order $H_0^2/8\pi$, may be produced by compression in the immediate neighbourhood of the neutral point. The condition of equilibrium in a two-dimensional field requires, however, that the pressure be constant along a line of force. The region of high gas pressure must, therefore, extend far from the neutral point, and, although the lines of force have their roots in the photosphere, it is difficult to see how the

necessary pressure configuration could exist at chromospheric levels.

A more rigorous treatment of this same question has been briefly reported by Sweet⁽¹⁰⁹⁾. His method may be outlined as follows.

A system is considered within a region D, bounded by a closed surface S, under the assumption that the electrical conductivity is infinite. Then the equation of hydrostatic equilibrium is simply equation (2-15). Now suppose that arbitrary small displacements \underline{q} are made to the fluid within D. Let the resulting perturbations on the pressure, density, and magnetic intensity be δp , $\delta \rho$, and $\delta \underline{H}$ respectively. Then it can be shown that these perturbations are related to the displacement vector \underline{q} by the following first order equations

$$\delta \rho = - \operatorname{div} \rho \underline{q} \quad (2-21),$$

$$\delta \underline{H} = \operatorname{curl} (\underline{q} \wedge \underline{H}) \quad (2-22),$$

$$\delta p = \bar{c}^2 \delta \rho \quad (2-23).$$

Here equations (2-21) and (2-22) are respectively the conditions of continuity and perfect electrical conductivity. Equation (2-23) depends on the assumption that the gas behaves isothermally; \bar{c} is the local velocity of sound.

Further, from equation (2-15), the equilibrium condition to first order can be written as

$$4\pi \text{grad } \delta p = \text{curl } \underline{H} \wedge \delta \underline{H} + \text{curl } \delta \underline{H} \wedge \underline{H} \quad (2-24).$$

Substitution may now be made for δp , $\delta \underline{H}$, and δp from equations (2-21) to (2-23); equation (2-24) will then yield a single partial differential equation for the displacement \underline{q} , namely

$$\begin{aligned} \text{curl } \underline{H} \wedge \text{curl } (\underline{q} \wedge \underline{H}) + \text{curl} [\text{curl} (\underline{q} \wedge \underline{H})] \wedge \underline{H} \\ + 4\pi \bar{c}^2 \text{grad } \text{div } p \underline{q} = 0 \end{aligned} \quad (2-25).$$

A solution for this second order equation is then sought within the region D. As a boundary condition the displacement vector \underline{q} is specified on the bounding surface S.

Sweet examined equation (2-25) for a cylindrical configuration, in which the field was independent of the z-coordinate. It was found that a non-singular solution of equation (2-25) under an arbitrary boundary displacement does not, in general, exist. Further, it was shown that a sufficient condition for this non-existence is that $(H_z^2 + 8\pi p)''$ should nowhere exceed a certain positive upper bound, which depends on the size of the region D under consideration. Here dashes have been used to denote differentiation with respect to a vector potential A of the form considered earlier in this

chapter. It should perhaps be stressed that the equation of hydrostatic equilibrium, (2-15), requires that both H_z and p be functions of A .

When a non-singular solution does not exist for g , a singularity of some form must be induced in the magnetic field as a result of the displacement. The form of this singularity must be a sheet current of finite length, since any other type of singularity, - such as a line current, for example, - would involve an infinite magnetic intensity, and thereby infinite magnetic energy.

Under the assumption of infinite conductivity, therefore, a general type of displacement of the lines of force on the boundary S will produce a sheet current within D . When, however, large but finite conductivity is allowed, such current sheets will be replaced by thin regions of large but finite current density. Within these regions magnetic diffusion will be important, and the approximation that the lines of force are frozen to the material breaks down. Reconnection of the lines of force will, therefore, take place allowing the field to move to configurations of lower energy that are ultimately non-singular.

The extreme thinness of the current region allows the magnetic diffusion to proceed at an enhanced rate.

Thus magnetic energy can be extracted from the system in a time-scale far shorter than the time of normal resistive diffusion. The main body of the present thesis is concerned with an investigation of the interpenetration and reconnection of the magnetic field lines in such regions of high current density. Separate investigations of this mechanism along similar lines have previously been made by Parker^(117,59), and these will be discussed in the course of the work.

CHAPTER 3

SINGULAR MAGNETOHYDROSTATIC CONFIGURATIONS

The general problem of the behaviour of a plasma under conditions of movement of flux systems cannot readily be studied in an exact manner. A two-dimensional system of a very simple nature will, therefore, be examined, since it lends itself to quantitative analysis. The magnetohydrostatics of the system is treated in detail in the present chapter, and this treatment will provide zero-order solutions that are required to solve the more general dynamical problem discussed in chapters 4 - 6.

(1) A Simple Two-Dimensional Model

Consider the field due to a system of two identical line currents, each of strength I_0 , acting along the positive directions of the lines $x = \pm a_0$, $y = 0$. Represent the magnetic field of this system by the vector $\underline{H} = (H_x, H_y, 0)$, and by the vector potential $\underline{A} = (0, 0, A)$. Then clearly H_x , H_y , and A are all functions of x and y only, and it is possible to represent the field by a complex potential $f(z)$, ($z = x + iy$), where

$$f(z) = - (2 I_0 / c) \log (z^2 - a_0^2) \quad (3-1).$$

Note that A is the real part of $f(z)$, and so

$$A = - (2 I_0 / c) \log |z^2 - a_0^2| \quad (3-2).$$

Then the magnetic intensity is given by

$$f'(z) = - H_y - i H_x \quad (3-3),$$

which yields the result that

$$i H_x + H_y = \frac{4 I_0}{c} \frac{z}{(z^2 - a_0^2)} \quad (3-4).$$

The field of this system is illustrated in Figure (3-1) in which the line currents are directed into the page, (i.e. $I_0 < 0$). The lines of force illustrated are the equipotentials $A = \text{constant}$, and form the well-known set of Cassinian ovals.

A finite boundary is now assigned to the system, and a finite thickness assigned to the wires, thus replacing the line currents by current cylinders of equal current strength. The exterior boundary is taken to be the equipotential (as calculated from equation (3-2)), going through the point $x = 0, y = R_0$. The boundaries of the wires will be taken, for convenience, to be the equipotentials through the points $x = \pm(a_0 - b_0), y = 0$; this step will involve no significant loss of generality. The system within these boundaries is, then, still represented by equations (3-1) to (3-4).

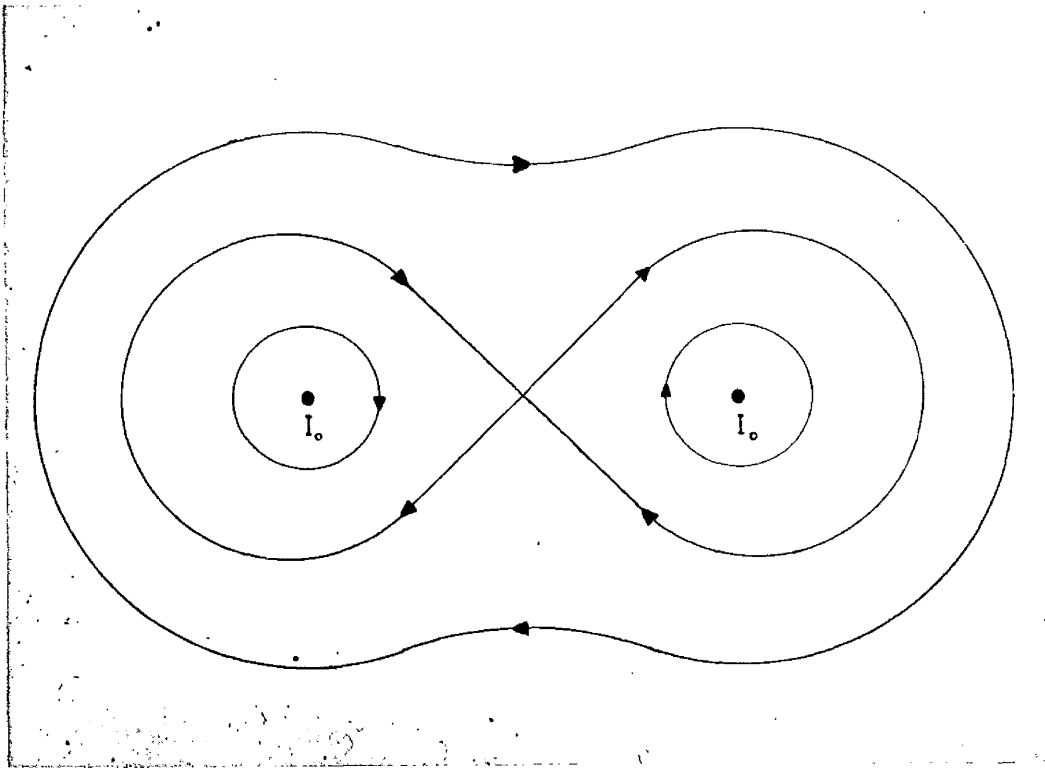


Fig. (3-1) The potential field of two line currents

Suppose now that F_0 is the magnetic flux (per unit z -length) crossing the x -axis between the neutral point and one of the current cylinders. Further, let F_0' be the value of the flux that crosses the y -axis between the neutral point and the outer boundary at the point $(0, R_0)$. Then from equation (3-2) two relations are obtained, namely

$$F_0 = \frac{2I_0}{c} \log \left[\frac{2b_0 a_0 - b_0^2}{a_0^2} \right] \quad (3-5),$$

$$F_0' = \frac{2I_0}{c} \log \left[\frac{R_0^2 + a_0^2}{a_0^2} \right] \quad (3-6).$$

In this system each wire is subjected by the magnetic field to an inward force. It is supposed, therefore, that initially the two wires are held apart by an external force. This latter force is then relaxed slightly, allowing the currents to move together at a rate sufficiently slow to enable the inertia of the system to be neglected. Let it be assumed, therefore, that at a subsequent time, the distance between the two currents has become $2a$, that their strengths have become I , and that the values of the two fluxes F_0 , F_0' , defined in the previous paragraph, have become F and F' respectively. In addition, it is assumed that the distance of the outer boundary is kept constant, and that the thickness of the current cylinders remains b_0 . As the displacement takes place the shapes of the boundaries are altered slightly so that they remain equipotentials. This is a convenient approximation to a system with rigid boundaries, and again will cause no essential loss of generality.

If the medium within these boundaries is non-conducting, the field readjusts itself during the displacement, retaining potential form. It follows that the magnetic field may be written as

$$i H_x + H_y = \frac{4I}{c} \frac{z}{z^2 - a^2} \quad (3-7).$$

From this equation the fluxes F and F' can be calculated. Then the condition of total flux conservation,

$$F + F' = F_0 + F_0' \quad (3-8),$$

will yield I as a function of a , for given values of a_0 , b_0 , and R_0 .

If, however, the medium is perfectly conducting the magnetic field moves with the material. Equation (3-8) is then supplemented by the additional flux condition,

$$F = F_0 \quad (3-9).$$

Now for a potential field, the ratio of F to F_0 is a prescribed function (following from equation (3-7)) of the displacement ($a_0 - a$). Thus the condition (3-9) indicates that the field resulting from a displacement of the kind described, in a perfectly conducting medium, can under no circumstances be potential, and electric currents will be induced by the displacement. The form of these currents, however, is not predetermined

by the separation a , but depends on the motion of the medium during the displacement.

(ii) Determination of the Sheet Current Induced by Displacements of a Perfectly Conducting Medium.

The work of Sweet⁽¹⁰⁹⁾, to which reference was made in the last chapter, shows that a general displacement of the system described in section (i) will involve the production of a sheet current. Here it is intended to consider only the special limiting case of zero gas pressure. Since it has already been shown that the displaced field cannot be potential, it is at once clear that, in this limit, a sheet current will be induced by any displacement of the two current cylinders.

For equilibrium it will be necessary that the Lorentz force have no component along the current sheet. This requirement will be satisfactorily met if the magnetic field is parallel to the sheet current; that is, no magnetic flux crosses the sheet. Now the conditions of symmetry require - in the limit of zero gas density - that the sheet current lie symmetrically along one of the coordinate axes. If it departed from these axes it would be subjected to an unbalanced magnetic force. In fact, for the displacement described

in section (i), a sheet current will be induced along the y -axis. Suppose that it is of length $2L$.

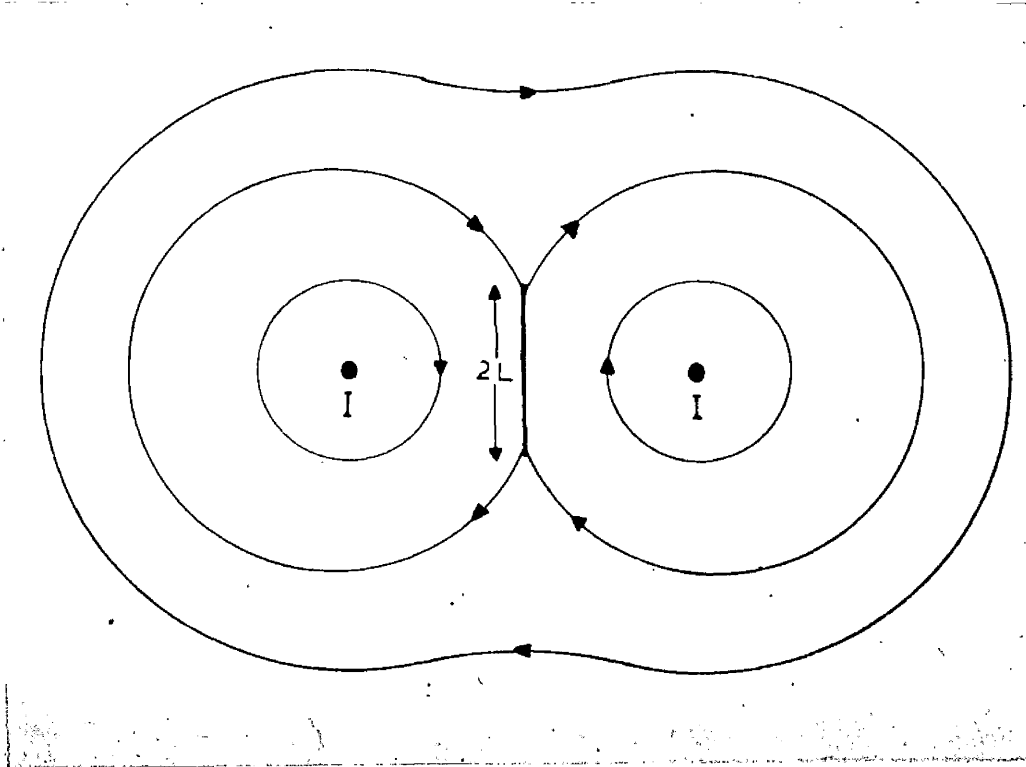


Fig (3-2). The field of two line currents and a sheet current of length $2L$

The problem is to find the magnetic field due to two line currents at the points $x = \pm a$, $y = 0$ and a sheet current of length $2L$, across which no flux passes. This magnetic configuration is illustrated in Figure (3-2). By working in elliptical coordinates, it is possible to show that the general solution for this problem can be written as

$$i H_x + H_y = \frac{I_1 (z^2 + L^2)^{1/2}}{z^2 - a^2} + \frac{I_2}{(z^2 + L^2)^{1/2}} \quad (3-10).$$

To remove the infinities in the magnetic intensity at the points $z = \pm iL$, it is necessary to take $I_2 = 0$. As the strength of the two current cylinders is known to be I , it is also possible to determine I_1 . The magnetic field resulting from the displacement is then found to be

$$i H_x + H_y = \frac{4Ia}{c(L^2 + a^2)^{1/2}} \frac{(z^2 + L^2)^{1/2}}{z^2 - a^2} \quad (3-11).$$

It is important to note that in both equation (3-10) and (3-11) $(z^2 + L^2)^{1/2}$ is to be interpreted as $z(1 + L^2/z^2)^{1/2}$, following the generally accepted conventions for the interpretation of non-integral powers in the theory of functions of the complex variable (118). This interpretation is necessary to ensure that the cut in the complex plane coincides with the sheet current.

Using equation (3-3), integration of equation (3-11) will yield the complex potential, viz

$$f(z) = -\frac{I}{c} \log \left[\frac{(L^2 + a^2)^{1/2} z - a(L^2 + z^2)^{1/2}}{(L^2 + a^2)^{1/2} z + a(L^2 + z^2)^{1/2}} \right] - \frac{4Ia}{c(L^2 + a^2)^{1/2}} \sinh^{-1} \frac{z}{L} \quad (3-12).$$

From equations (3-11) and (3-12) and two fluxes F and F' are obtained as follows:-

$$F = \frac{2I}{c} \left(\frac{a^2}{L^2 + a^2} \right)^{\frac{1}{2}} \left[2 \log \left(\frac{(a-b_0) + (L^2 + (a-b_0)^2)^{\frac{1}{2}}}{L} \right) + \left(\frac{L^2 + a^2}{a^2} \right)^{\frac{1}{2}} \log \left(\frac{a(L^2 + (a-b_0)^2)^{\frac{1}{2}} - (L^2 + a^2)^{\frac{1}{2}} (a-b_0)}{a(L^2 + (a-b_0)^2)^{\frac{1}{2}} + (L^2 + a^2)^{\frac{1}{2}} (a-b_0)} \right) \right] \quad (3-13),$$

$$F' = \frac{2I}{c} \left(\frac{a^2}{a^2 + L^2} \right)^{\frac{1}{2}} \left[2 \log \left(\frac{R_0 + (R_0^2 - L^2)^{\frac{1}{2}}}{L} \right) + \left(\frac{L^2 + a^2}{a^2} \right)^{\frac{1}{2}} \log \left(\frac{(L^2 + a^2)^{\frac{1}{2}} R_0 - a (R_0^2 - L^2)^{\frac{1}{2}}}{(L^2 + a^2)^{\frac{1}{2}} R_0 + a (R_0^2 - L^2)^{\frac{1}{2}}} \right) \right] \quad (3-14).$$

These results will now be applied to a system which has no outer boundary.

Let R_0 tend to infinity; for large R_0 , equations (3-6) and (3-14) respectively yield

$$F_0' \sim \frac{4I_0}{c} \log R_0 \quad (3-15),$$

$$\text{and } F' \sim \frac{4I}{c} \left(\frac{a^2}{L^2 + a^2} \right)^{\frac{1}{2}} \log R_0 \quad (3-16).$$

F and F_0' are, however, finite and independent of R_0 .

So, as $R_0 \rightarrow \infty$, equation (3-8), the condition of conservation of total flux, shows that

$$I = \left(\frac{a^2 + L^2}{a^2} \right)^{\frac{1}{2}} I_0 \quad (3-17).$$

It will be convenient to reduce a , b_0 , and L to dimensionless form; so put

$$X = \frac{a}{a_0}, \quad Y = \frac{L}{a_0}, \quad B = \frac{b_0}{a_0} \quad (3-18).$$

Then, with these substitutions, and using equations (3-5), (3-13), and (3-17), the second flux condition (3-9) can be written as

$$\log(2B - B^2) = 2 \log\left(\frac{(X-B) + (Y^2 + (X-B)^2)^{1/2}}{Y}\right) + \left(1 + \frac{Y^2}{X^2}\right)^{1/2} \log\left(\frac{X(Y^2 + (X-B)^2)^{1/2} - (X^2 + Y^2)^{1/2}(X-B)}{X(Y^2 + (X-B)^2)^{1/2} + (X^2 + Y^2)^{1/2}(X-B)}\right) \quad (3-19).$$

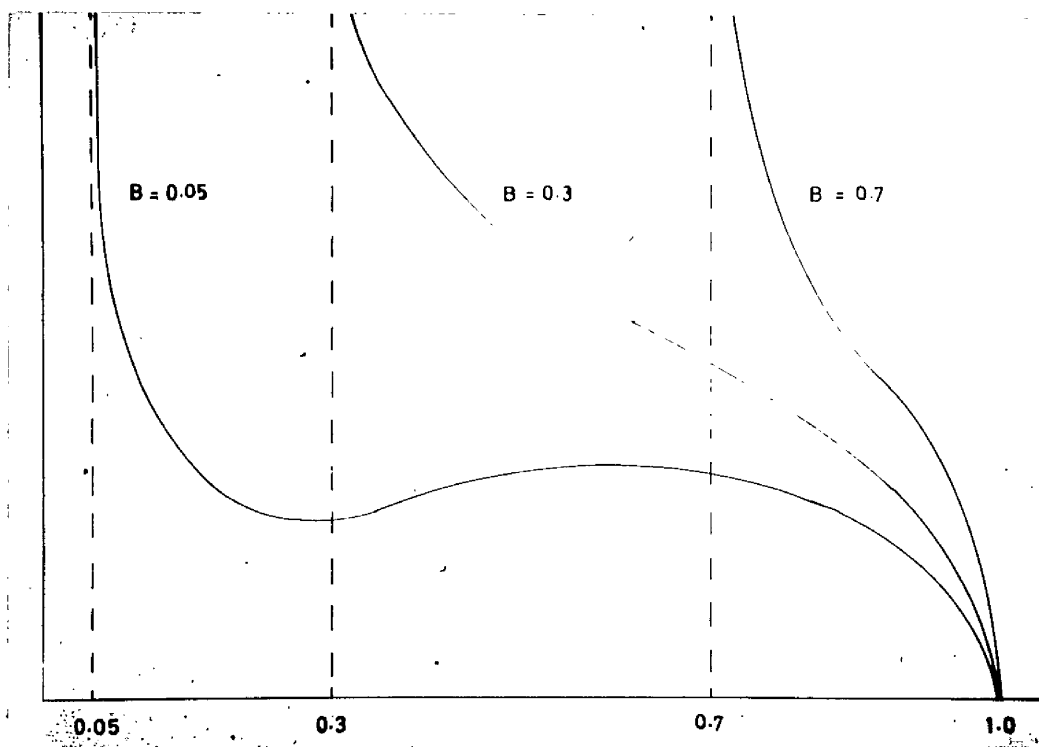


Fig (3-3). Length of the current sheet induced by the displacement of the current cylinders

Equation (3-19) gives a relationship between the dimensionless values of a , b_0 , and L . In particular, it enables the value of L to be determined for given values of a_0 , b_0 , and a , thus determining the length of the induced current sheet as a function of the displacement of the two current cylinders. Equation (3-19) may be solved numerically by a simple application of Newton's method of successive approximation. Three solutions are shown in Figure (3-3) as a graph of Y against X for three values of B , namely $B = 0.05$, 0.3 , and 0.7 .

As already mentioned, each current cylinder is in general subject to an inward magnetic force. The magnitude of this force, G say, can be evaluated by considering the magnetic stresses of one half plane upon the other. Since the integrated magnetic stress round the outer boundary goes to zero as this outer boundary goes to infinity - from (3-11), $H \sim 4Ia/c(a^2 + L^2)^{\frac{1}{2}}z$, for large z - , it is clear that the attractive force G is simply

$$G = \frac{1}{4\pi} \left(\int_L^\infty H_x^2 dy - \int_0^L H_y^2 dy \right) \quad (3-20).$$

Substitution for H from equation (3-11), and integration of (3-20) then yields

$$G = \frac{I^2 (a^2 - L^2)}{a c^2 (a^2 + L^2)} \quad (3-21).$$

It follows that equilibrium will be attained when the displacement has been allowed to proceed until $L = a$. The required externally applied forces on the current cylinders can then be entirely relaxed.

Suppose that equilibrium is attained when $a = a_1$. If the medium is taken as strictly perfectly conducting, the system will remain indefinitely in this equilibrium configuration with $L = a = a_1$. If, on the other hand, very large but finite conductivity is assigned to the medium, there must be a gradual leakage of flux through the sheet current due to magnetic diffusion. The flux F' will increase at the expense of the flux F between the current cylinders and the origin. The two current cylinders will continue to move together, and a and L will vary. The system will, however, retain its equilibrium configuration. The flux condition of equation (3-9) must, therefore, now be replaced by the condition of equilibrium, namely

$$L = a \quad (3-22).$$

The other flux condition, equation (3-8), however, holds as before, and, therefore, equation (3-17) which is based on this is still applicable. Due to (3-22), this equation can now be written in a simpler form, viz

$$I = \sqrt{2} I_0 \quad (2-23).$$

Making use of these two new conditions, the expression for the flux F can, from equation (3-13), be written in a new form,

$$F = \frac{2I_0}{c} \left[2 \log \left[1 - \frac{b_0}{a} + \left(1 + \left(1 - \frac{b_0}{a} \right)^2 \right)^{1/2} \right] + \sqrt{2} \log \left(\frac{\left(1 + \left(1 - b_0/a \right)^2 \right)^{1/2} - \sqrt{2} \left(1 - b_0/a \right)}{\left(1 + \left(1 - b_0/a \right)^2 \right)^{1/2} + \sqrt{2} \left(1 - b_0/a \right)} \right) \right] \quad (3-24).$$

Taken together equations (3-5) and (3-24) then yield

$$\frac{F}{F_0} = \left[2 \log \left(1 - \frac{b_0}{a} + \left(1 + \left(1 - \frac{b_0}{a} \right)^2 \right)^{1/2} \right) + \sqrt{2} \log \left(\frac{\left(1 + \left(1 - b_0/a \right)^2 \right)^{1/2} - \sqrt{2} \left(1 - b_0/a \right)}{\left(1 + \left(1 - b_0/a \right)^2 \right)^{1/2} + \sqrt{2} \left(1 - b_0/a \right)} \right) \right] \left[\log \frac{2b_0 a_0 - b_0^2}{a_0^2} \right]^{-1} \quad (3-25)$$

This last expression can be simplified in the case when the current cylinders are very thin, that is when $b_0/a \ll 1$. Then neglecting terms of order (b_0/a) , equation (3-25) can be reduced to give the separation of

the currents, a , as an explicit function of the fluxes and of the initial parameters of the system, a_0 and b_0 . This expression is found to be

$$\log \frac{4a}{b_0} = \frac{F}{\sqrt{2} F_0} \log \frac{a_0}{2b_0} + \sqrt{2} \log (1 + \sqrt{2}) \quad (3-26).$$

The above hydrostatic analysis will provide the zero-order solution of the dynamical system to be considered in the next chapter. When the effects of finite conductivity are allowed, the current sheet must be replaced by a thin finite region of high current density. The field outside this region is described to zero order by equation (3-11). Equation (3-26) is also of importance, in that it can be used to relate the rate of magnetic diffusion in the current sheet to the rate of displacement of the two current cylinders.

CHAPTER 4
 QUASI-STEADY MAGNETOHYDRODYNAMICS
 AT NEUTRAL LINES

(1) Order of Magnitude Considerations

As has already been stated, when the effects of large but finite conductivity are taken into account, the sheet current discussed in the last chapter is replaced by a thin region of high current density. The magnetic field within this region will have a neutral point and will be of the form shown in Figure (4-1).

As magnetic diffusion takes place, the fluid flows into this region and is squeezed out along the length of the region by the magnetic pressure on the sides. The direction of fluid motion has been indicated by the short arrows in Figure (4-1).

Let the length of the current region be $2L$ as before, and let its thickness be 2ℓ . Denote the velocity of inflow by v_0 , and the velocity of outflow by v_1 . Further, let H_0 and ρ_0 be typical values of the magnetic intensity and gas density respectively outside the current region. Finally let T be the temperature of the ambient gas, and denote the electrical conductivity by σ .

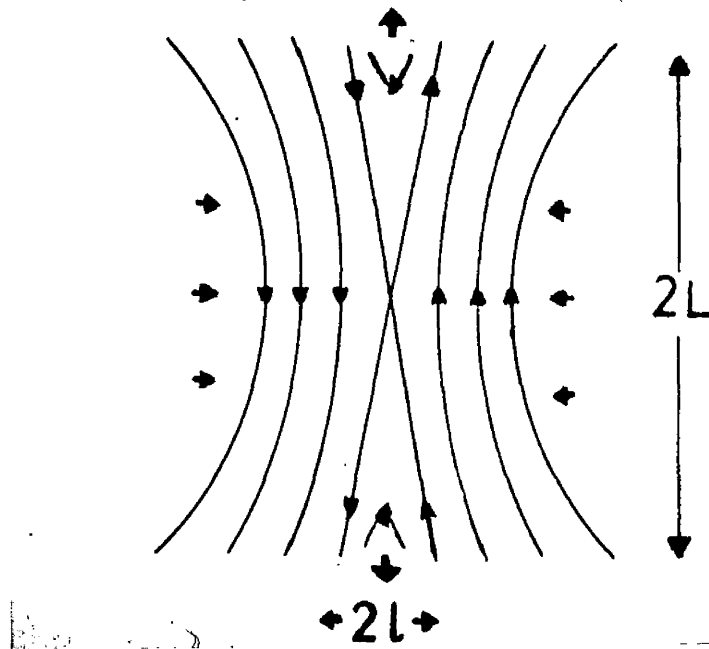


Fig (4-1) The field in the region of high current density

It will be convenient to work in terms of three characteristic velocities, defined as follows

$$v_A = \frac{H_0}{(4\pi\rho_0)^{1/2}} \quad (4-1),$$

$$v_S = \left(\frac{RT}{\mu}\right)^{1/2} \quad (4-2),$$

μ being the mean molecular weight of the gas in units of the mass of the hydrogen atom,

and
$$v_D = \frac{c^2}{4\pi\sigma L} \quad (4-3).$$

Then v_A is the Alfvén velocity, and v_S essentially the sound velocity, in the ambient gas. Further, v_D is the velocity of magnetic diffusion over a scale-length L . Two modes of interpenetration are distinguished, the compressible and the incompressible cases being treated separately.

The first of the order of magnitude solutions for quasi-stationary conditions that follow is essentially that originally given by Parker⁽¹¹⁷⁾. Parker has also developed a semi-quantitative treatment of this mode⁽⁵⁹⁾. In addition, he has included the effects of ambipolar diffusion, which will not be considered at this stage. Later it is intended to follow a slightly different line of argument, based on a more direct formulation of the differential equations. In this way it may be possible to examine the significance of an undetermined parameter (α) that appears in Parker's work.

Consider now the system illustrated in Figure (4-1). In the incompressible case, the density is ρ_0 throughout the current region, and the equation of continuity simply yields

$$v_1 \ell \sim v_0 L \quad (4-4).$$

The outflow velocity v_1 , or more correctly an upper limit for it, is obtained by equating the kinetic energy of the gas squeezed out along the layer with the magnetic energy convected into the layer. This gives

$$\frac{1}{2} \rho_0 v_1^3 \ell \sim \frac{H_0^2}{8\pi} v_0 L \quad (4-5).$$

From equations (4-4) and (4-5) it at once follows that $v_1 \sim v_A$, the Alfvén velocity.

Finally, since v_0 will simply be the velocity of magnetic diffusion across the current thickness ℓ , it follows that

$$v_0 \sim \frac{c^2}{4\pi\sigma\ell} \quad (4-6).$$

Equations (4-4) and (4-6) are now sufficient to determine a solution for v_0 and ℓ . In terms of the characteristic velocities this solution is

$$\ell \sim \left(\frac{v_0}{v_A} \right)^{1/2} L \quad (4-7),$$

$$v_0 \sim (v_A v_D)^{1/2} \quad (4-8).$$

Equations (4-7) and (4-8) form the basis of the order of magnitude solution for this incompressible mode. From these two equations it is a simple matter to

determine the magnitudes of the remaining physical variables. Since $v_A \gg v_D$ in most astrophysical problems, and particularly in the chromospheric conditions relevant to solar flares, it is clear from equation (4-8) that this mechanism, even in this slow mode, allows a much faster rate of magnetic field annihilation than is possible with normal magnetic diffusion. The rate is enhanced by a factor of order $(v_A/v_D)^{\frac{1}{2}}$.

The incompressible mode, just considered, would apply in the case where the gas pressure is greater than the magnetic pressure, or at least comparable with it. Such conditions certainly exist on the sun, - in or below the photosphere. Of more interest to the solar flare problem, however, are typical chromospheric or coronal conditions in which, at least above an active region, the magnetic pressure greatly exceeds the gas pressure. This implies that

$$\frac{H_0^2}{8\pi} \gg \rho_0 v_s^2 \quad (4-9),$$

and the incompressible analysis will no longer be a good physical approximation.

Consider again the configuration represented in Figure (4-1). The effects of compressibility will now be important. Only the simple case of isothermal

compression will be treated here. It may be imagined that radiative losses keep the gas at some constant value of the temperature, - a fair assumption in view of the extreme thinness of the current sheet that is derived. The high magnetic pressure on the sides of the current region compresses the gas in the interior to a very high density. The condition of pressure balance across the current region gives the result that

$$\rho_1 v_S^2 \sim H_0^2 / 8\pi, \text{ or equivalently}$$

$$\rho_1 \sim \frac{v_A^2}{v_S^2} \rho_0 \quad (4-10),$$

where ρ_1 is a typical value of the gas density inside the current region. A further relation is obtained from the equation of continuity, namely

$$\rho_1 l v_1 \sim \rho_0 L v_0 \quad (4-11).$$

If it is assumed that the field in the current region is of the form shown in Figure (4-1); to be more specific, if it is assumed that typically

$$H_x \sim \frac{l}{L} H_y \quad (4-12),$$

where l is the thickness of the current sheet, then the y-components of the gas pressure gradient and of the magnetic forces are of the same order, and work together in expelling the gas from the current region. On the

basis of this assumption it is readily seen that

$$v_1 \sim v_s \quad (4-13),$$

so that the ejection velocity is, from (4-10), essentially the Alfvén velocity in the compressed gas. Now equations (4-10), (4-11), and (4-13), together with equation (4-6), which still applies, are sufficient to derive the order of magnitude solution. This is found to be

$$l \sim \left(\frac{v_D v_s}{v_A^2} \right)^{1/2} L \quad (4-14),$$

$$v_0 \sim \left(\frac{v_D}{v_s} \right)^{1/2} v_A \quad (4-15).$$

The main effect of compression is to reduce the thickness of the current region by a factor $(v_s/v_A)^{1/2}$. The diffusion of the magnetic field then takes place across this reduced distance at a proportionately faster rate.

This order of magnitude solution, originally due to Sweet, was first given in a paper by Hoyle and Wickramasinghe⁽¹¹⁹⁾, who applied it to a coronal problem unconnected with solar flares. Later it was independently developed in a semi-quantitative manner by Parker⁽⁵⁹⁾ and applied to the flare problem. Parker's treatment, like his treatment of the incompressible mode, contains an

undetermined parameter. It is intended to show, however, that in this case of compressible flow, this parameter is indeterminate, and that this fact is indicative of the existence of a faster mode of interpenetration. The basis of Parker's mode is essentially the assumption contained in equation (4-12); this assumption requires justification by a consistency argument such as is attempted later in the present chapter. The assumption made in (4-12) about the size of H_x determines the order of magnitude of the magnetic force ejecting material from the current region. The fluid motion will, however, itself affect the magnetic field. It is not valid, therefore, to impose a boundary condition on H_x based on the analysis of chapter 3. To do so would incorporate the assumption of equation (4-12) and make the problem definitive. It is necessary, rather, to examine the correctness of such an assumption by means of a strictly quantitative investigation of the motion in the interior of the current region.

(ii) Hydromagnetic Equations

A quantitative treatment is now attempted of the two modes of interpenetration, discussed in order of magnitude in the last section. First of all the hydromagnetic equations are stated.

These comprise first the electromagnetic equations,
viz

$$\text{curl } \underline{H} = \frac{4\pi}{c} \underline{j} \quad (4-16),$$

$$\text{div } \underline{H} = 0 \quad (4-17),$$

$$\text{curl } \underline{E} = -\frac{1}{c} \frac{\partial \underline{H}}{\partial t} \quad (4-18),$$

$$\text{and } \frac{\underline{j}}{\sigma} = \underline{E} + \frac{1}{c} (\underline{v} \wedge \underline{H}) \quad (4-19).$$

In equation (4-16) normal practice has been followed in omitting the displacement current. In the conductivity equation (4-19) only ohmic effects have been included; the Hall current term has been neglected. Further, as already mentioned, the effects of ambipolar diffusion are not included in this treatment.

These electromagnetic equations will be supplemented by the hydrodynamic equations, namely

$$\text{div } \rho \underline{v} = -\frac{\partial \rho}{\partial t} \quad (4-20),$$

$$\rho \frac{\partial \underline{v}}{\partial t} + \rho (\underline{v} \cdot \text{grad}) \underline{v} = -\text{grad } \rho + \frac{\underline{j} \wedge \underline{H}}{c} \quad (4-21).$$

Notice that the effects of viscosity and gravity have both been omitted from the equation of motion, equation (4-21).

Owing to the two-dimensional form of the problem to be considered, it is possible to make a considerable simplification of these equations. So let us introduce a vector potential \underline{A} , where

$$\underline{A} = (0, 0, A(x, y)) \quad (4-22),$$

in the same way as in Chapter 2, section (ii). Then

$$\underline{H} = \left(\frac{\partial A}{\partial y}, -\frac{\partial A}{\partial x}, 0 \right) \quad (4-23).$$

Again, the two-dimensional form will allow one to write

$$\underline{j} = (0, 0, j_z) \quad (4-24),$$

$$\underline{E} = (0, 0, E_z)$$

Equation (4-16) can, therefore, be scalarized to give

$$j_z = - (c/4\pi) \nabla^2 A \quad (4-25).$$

Further, equation (4-17) can be integrated to yield

$$E_z = -\frac{1}{c} \frac{\partial A}{\partial t} + \text{grad } \psi \quad (4-26),$$

and the two-dimensional form requires that $\text{grad } \psi$ be a constant, independent of position. So put $\text{grad } \psi = E_0$;

then the value of E_0 will be determined by the choice of the zero for $\partial A / \partial t$. The logical step would be to take A constant on the boundaries of the flux systems, i.e. in the model of chapter 3, on the boundaries of the current cylinders. In this case, $E_0 = 0$. It is more convenient, however, to define A so that throughout the motion $A = 0$ at the neutral point. Then with this definition, $E_0 = E_z(0, 0)$.

Using equations (4-25) and (4-26), the four electro-magnetic equations can be reduced to the form:

$$\frac{\partial A}{\partial t} - \underline{v} \wedge \underline{H} - \frac{c^2}{4\pi\sigma} \nabla^2 A = c E_0 \quad (4-27).$$

The above equation (4-27), together with (4-20) and (4-21), are the equations that must be considered in the quantitative treatment of the interpenetration modes.

Before proceeding to the quantitative discussion, it might be profitable to pause a moment, in order to state the exact nature of the problem that is to be examined in the remainder of the chapter. The problem concerns the derivation of a solution, or at least the essential features of a solution, for the dynamics of the region of high current density that results from a breakdown of hydrostatic equilibrium due to the relative motions of two flux systems embedded in a gas

of high conductivity. For simplicity, the flux systems have been taken to be of the idealized two-dimensional form of two infinite parallel current cylinders.

Divide the domain of hydrodynamical flow into two regions as follows. Region I is defined as the region of high current density; the surrounding region of the gas is termed region II. As the conductivity tends to infinity, region I shrinks into a sheet current, and conditions in region II approach the magneto-hydrostatic conditions. The solutions derived in chapter 3 from purely hydrostatic considerations are then applicable in this region. In particular, in region II the zero-order magnetic field is given by equation (3-11). Dynamically the zero-order solution for region II is simply $\underline{v} = 0$. A zero-order solution does not exist in region I, since region I itself does not exist to zero-order.

A first order solution in region I is then sought, by attempting a solution of the dynamical equations in this region. The boundary conditions for these equations are provided by the zero-order solution in region II. It is here, then, that the analysis of chapter 3 is important. As with the earlier order of magnitude considerations, so in the quantitative discussions that follow, it will be necessary to treat separately the incompressible and the compressible cases.

(iii) Incompressible Mode.

Hydrostatic solutions were obtained in chapter 3 for the limiting case of zero gas pressure. In this case a single sheet current was obtained. The surrounding field was of potential form. Such analysis is directly applicable to the case where $v_A \gg v_S$, since the low gas pressure will be unable to sustain a non-force-free field. This corresponds to the compressible case to be considered in the next section. In the case under consideration in the present section, the gas pressure must be at least of the same order as the magnetic pressure, if not larger, and the magnetic field need no longer be of potential form. Electric currents may be induced provided only that the resulting magnetic forces are balanced by a gradient in the gas pressure.

When the gas pressure has been included, therefore, the condition of hydrostatic equilibrium is given by equation (2-15), or equivalently

$$\text{grad } p = \frac{\underline{j} \wedge \underline{H}}{c} \quad (4-28).$$

On introducing the vector potential A from (4-23) and (4-25), equation (4-28) can be written as

$$\text{grad } p = - \frac{\nabla^2 A}{4\pi} \text{grad } A \quad (4-29).$$

From (4-29) it is clear that the condition for magnetohydrostatic equilibrium is simply that the current density and the pressure be functions of A , and so are constant along a magnetic line of force. It follows from (4-29) that

$$\frac{dp}{dA} = - \frac{\nabla^2 A}{4\pi} \quad (4-30).$$

The presence of gas pressure allows the possibility of a different type of sheet current from that derived by ignoring pressure effects. In the earlier case a symmetrical displacement of the line currents produced a sheet current along a finite segment of one of the coordinate axes. No other type of sheet current was admissible. When the influence of gas pressure is taken into account, however, the possibility that the sheet current has the form shown in Figure (4-2) must be considered.

In this case the magnetic field changes non-symmetrically across the sheet, the resulting change in magnetic pressure being balanced by a change in the gas pressure. Such a current sheet clearly cannot exist in the absence of gas pressure, and was not considered in chapter 3. As the gas pressure tends to zero, the strength of the curved part of the current sheet in

Figure (4-2) must also tend to zero, while the strength of that part lying along the coordinate axis will remain finite. Thus in the case of very low gas pressure one is again led to the type of sheet current considered in chapter 3.

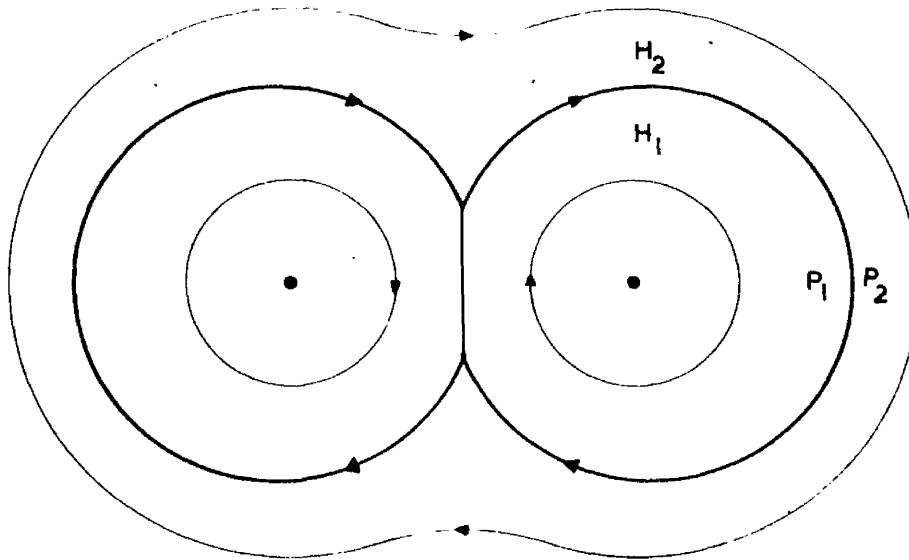


Fig (4-2) The field of two line currents and a sheet current following a closed line of force.

If H_1 and H_2 are the respective magnetic field strengths at a point on either side of this current sheet, then since it has already been seen that hydrostatic equilibrium requires that the gas pressure is constant on

a line of force, it is clear that

$$H_1^2 - H_2^2 = 8\pi (\rho_2 - \rho_1) = \text{constant} \quad (4-31),$$

where p_1 , p_2 are the values of the gas pressure on either side of the sheet.

When gas pressure is important, it is not clear which type of sheet current will be formed; it may well depend on the nature of the displacement of the flux systems. The rate of magnetic reconnection in the type of sheet current shown in Figure (4-2) will in general, be slower than the rate for the type illustrated in Figure (3-2), since the dynamical conditions that lead to enhanced interpenetration are not present in the curved part of the current sheet. The interpenetration across this part of the sheet reduces to virtually static diffusion. The thickness of this region adjusts itself so that the interpenetration through it keeps pace with that taking place in the straight part of the current sheet. Notice that the interpenetration in the straight part of the current sheet will be slowed down since the ejection of material will in part be opposed by the higher pressure p_2 (Figure (4-2)), which is always in excess of the pressure p_1 on the current region's sides. This may in part be compensated by the fact that the material, that would have been ejected from the current

sheet along the y -axis, can now flow out of the current sheet over an area distributed over the whole of the curved portion.

The existence of current sheets of this type has been examined by Sweet⁽¹⁰⁹⁾. His discussion concerned a compressible gas, though no assumption was made that the gas pressure was small. No treatment has yet been given for a strictly incompressible fluid. The present incompressible treatment is, however, only intended to represent the case where the magnetic pressure does not exceed the gas pressure by a large factor. Incompressibility is essentially only an approximation to be applied within region I; it is not to be regarded in any sense as a general feature of the fluid. With this proviso, then, with regard to the meaning of incompressibility, Sweet's work may be used, and the formation of a sheet current after sufficient distortion of the field may be assumed. Whether the induced sheet current will be of the 'straight' or of the 'curved' type, must, however, remain uncertain.

To determine the boundary conditions on region I, it will be assumed that a current sheet has been induced simply along the y -axis. Further, use is made of the field derived in chapter 3 for this sheet current

together with the two current cylinders. This is taken to represent the magnetic configuration in region II to zero-order, and can, near the y-axis, be written as

$$\begin{aligned} H_x &= 0 \\ H_y &= H_0 L \frac{(L^2 - y^2)^{1/2}}{L^2 + y^2} \end{aligned} \quad (4-32).$$

Here H_0 is the field on the positive x-axis just outside the current region. This, then, will be the boundary condition on region I.

It is important to remember that the field of equation (4-32) is the result of two assumptions made about the field in region II; - firstly that the induced current sheet is of the 'straight' type, and secondly that the field in region II is of potential form. Certainly such assumptions are consistent with the condition of hydrostatic equilibrium. Nonetheless the field in region II depends on the displacement of the field lines from the initial configuration, and the condition of equilibrium is simply that of pressure balance, given by (4-30). We are, however, entitled to adopt an initial configuration that will reduce to a potential configuration on arrival at the sheet current situation, just described. Equation (4-32) may then be taken for definiteness to provide boundary conditions on region I.

In the incompressible case the equation of continuity (4-20) reduces to

$$\operatorname{div} \underline{v} = 0 \quad (4-33),$$

when stationary conditions ($\partial/\partial t \equiv 0$) are assumed.

It is convenient, therefore, to introduce a stream function $\phi = (0, 0, \phi(x, y))$ so that

$$\underline{v} = \operatorname{curl} \phi = \left(\frac{\partial \phi}{\partial y}, -\frac{\partial \phi}{\partial x}, 0 \right) \quad (4-34).$$

If now substitution is made for \underline{v} and \underline{H} in terms of their respective potential functions, then, again under steady conditions, the hydromagnetic equation (4-27) can be rewritten as

$$\frac{\partial(A, \phi)}{\partial(x, y)} - \frac{c^2}{4\pi\sigma} \nabla^2 A = c E_0 \quad (4-35).$$

Further take the curl of the equation of motion, equation (4-21), to eliminate the pressure and the other gradient terms. Then this equation can, on introducing the two potential functions, be reduced to

$$\frac{\partial(\phi, \nabla^2 \phi)}{\partial(x, y)} = \frac{\rho}{4\pi} \frac{\partial(A, \nabla^2 A)}{\partial(x, y)} \quad (4-36).$$

The equations of the system are, therefore, reduced to the differential equations (4-35) and (4-36) in the two potential functions. In an appendix to his

recent paper, Parker⁽⁵⁹⁾ has suggested that solutions of the form

$$\begin{aligned}\nabla^2 \phi &= f(\phi) \\ \nabla^2 A &= h(A)\end{aligned}\tag{4-37},$$

might be possible, on the grounds that equation (4-36) would then be automatically satisfied. But it is easy to see that equations (4-37) impose on the solution conditions that are not met in the problem at hand. For the boundary of region I is defined by $A = 0$. The second of equations (4-37) requires this to be a line of force. Such a boundary is quite clearly not applicable to the type of current region under consideration, namely that corresponding to a straight current sheet, (Figure (3-2)). If the boundary were indeed a line of force, the current sheet would have to be of the curved type discussed earlier in this section, and shown in Figure (4-2). This type of current sheet would involve a rather different interpenetration mechanism to that envisaged by Parker and under discussion here.

It is clear, therefore, that a solution of the form of equation (4-37) that is relevant to the present problem cannot be found. Instead the equation of motion must be examined in more detail. In fact, the problem

is not readily treated in an exact manner. Nonetheless it is intended to state the relevant equations for the sake of completeness.

It will be more convenient to use the two components of the equation of motion directly, rather than to make further use of equation (4-36). Consider, then, the x-component of the equation of motion (4-21). Since the velocity of inflow is small, this equation reduces to a static equation of pressure balance, viz

$$\frac{1}{\rho} \frac{\partial p}{\partial x} + \frac{1}{4\pi\rho} \frac{\partial A}{\partial x} \nabla^2 A = 0 \quad (4-38).$$

Since the thickness of the current region is very small in comparison with its length, the following approximations are justified:

$$\begin{aligned} \nabla^2 A &= \frac{\partial^2 A}{\partial x^2} \\ \nabla^2 \phi &= \frac{\partial^2 \phi}{\partial x^2} \end{aligned} \quad (4-39).$$

On substituting for $\nabla^2 A$ from equation (4-39), equation (4-38) can be integrated to yield

$$p = F(y) - \frac{1}{8\pi} \left(\frac{\partial A}{\partial x} \right)^2 \quad (4-40),$$

where $F(y)$ is a function of y to be determined.

Now the boundary condition on the field in region I is, from equation (4-32),

$$\frac{\partial A}{\partial x} = - H_0 L \frac{(L^2 - y^2)^{1/2}}{L^2 + y^2} \quad (4-41).$$

$$\frac{\partial A}{\partial y} = \quad \bigcirc$$

Further, the gas pressure p must be constant on the boundary of the current region, since in region II the pressure will be constant along a line of force, due to the condition of hydrostatic equilibrium. Taken with the thinness of the current region the condition (4-41) shows that the boundary of region I is indeed a line of force to zero-order, - but not, of course, to higher orders. Moreover, since it has been assumed that the field in region II is of potential form, the pressure will be constant along the boundary a fortiori. Let p_0 , then, be the constant value of p on the boundary; using the condition (4-41), it is now possible to solve for $F(y)$ obtaining

$$F(y) = p_0 + \frac{H_0^2 L^2}{8\pi} \frac{L^2 - y^2}{(L^2 + y^2)^2} \quad (4-42).$$

The gas pressure is then known in terms of A from equation (4-40).

Next, again substituting the potential functions for the magnetic field and the fluid velocity, the y -component of the equation of motion (4-21) can be written as

$$J \left(\frac{\partial \phi}{\partial x}, \phi \right) = \frac{1}{\rho} \frac{\partial \rho}{\partial y} + \frac{\nabla^2 A}{4\pi\rho} \frac{\partial A}{\partial y} \quad (4-43),$$

where the symbol J denotes the Jacobian operator, i.e.

$$J(\phi_1, \phi_2) = \frac{\partial(\phi_1, \phi_2)}{\partial(x, y)}$$

Then, on using the approximations given in equation (4-39), and substituting for ρ from equations (4-40) and (4-42), this y -component can be rewritten as

$$J \left(\phi, \frac{\partial \phi}{\partial x} \right) = \frac{1}{4\pi\rho} J \left(A, \frac{\partial A}{\partial x} \right) + \frac{H_0^2 L^2 y}{4\pi\rho} \frac{(3L^2 - y^2)}{(L^2 + y^2)^3} \quad (4-44)$$

Further, by equation (4-39), the conductivity equation (4-35) can be slightly simplified to give

$$J(A, \phi) - \frac{c^2}{4\pi\sigma} \frac{\partial^2 A}{\partial x^2} = c E_0 \quad (4-45)$$

These last two equations, (4-44) and (4-45), must be solved for A and ϕ within region I. The boundary of this region must be determined from the solutions. It will be the curve on which $\partial^2 A / \partial x^2 = 0$. Denote this curve by C . Then it will be sufficient to solve for ϕ and A in the first quadrant; that is, within the region bounded by the positive x - and y -axes and by the curve C . The boundary conditions on ϕ and A within this region will be as follows :-

$$\text{On } x = 0, \quad \phi = 0$$

$$\text{On } y = 0, \quad \phi = 0$$

$$\text{On } C \quad \frac{\partial A}{\partial x} = - \frac{H_0 L (L^2 - y^2)^{1/2}}{L^2 + y^2} \quad (4-46).$$

$$\text{and} \quad \frac{\partial \phi}{\partial x} = 0$$

In equations (4-46), the first two conditions are conditions of symmetry, and the third is simply equation (4-41). The final condition is due to the fact that outside region I the fluid has not yet been accelerated and, therefore, $v_y = 0(v_x)$; inside region I, however, $v_y = 0(v_\Delta)$ and so $v_y \gg v_x$. Thus on the boundary, to a first approximation, $v_y = 0$.

The solution of equations (4-44) and (4-45) with these boundary conditions will, of course, depend on the value of the constant E_0 . Further, the shape of the boundary will also depend on the value of this parameter. If non-singular solutions with a closed boundary curve C exist only for a finite range of values of E_0 , then an upper limit for E_0 can clearly be obtained. The interpenetration of the system will speed up until the upper bound is attained, and then will remain steady at this maximum rate of interpenetration. If, on the other hand, such non-singular solutions exist for all

values of E_0 , this fact would be indicative of the existence of a faster mode of interpenetration.

As this is essentially a jury problem, it is not possible to derive, by any straightforward method, the main features of the solutions that would be necessary to determine whether the mode is definitive. Parker⁽⁵⁹⁾, in his semi-quantitative treatment of this mode, derived a solution along the x-axis. But this solution can shed no light at all on the question of the possible existence of an upper bound for E_0 . Parker's solution was not a solution of the two equations that are being considered here, the conductivity equation and the y-component of the equation of motion; - rather it was a solution of the conductivity equation and the equation of continuity, based on an empirical assumption. This assumption, which was justifiable only on an order of magnitude argument, was that on $y = 0$

$$\frac{\partial v_y}{\partial y} = \frac{\alpha^2}{L} \left[\frac{2(p-p_0)}{\rho} \right]^{1/2} \quad (4-47),$$

where α is a constant. In this way, Parker avoided solving the equation of motion, and determined his solution for v_x from only the conductivity equation. It was then possible to determine the value of E_0 in terms of α . This latter parameter, however, remains

undetermined and indeed quite arbitrary, as is the assumption (4-47) that introduced it. Moreover this assumption ignores the accelerating effect of the magnetic field. Clearly, then, Parker's solution can give no further insight into the question of the definitiveness of this incompressible mode.

Parker's derivation of a solution in the compressible case again follows the lines of argument described in the previous paragraph. In the next section it will be shown, however, that it is possible, at least in the compressible case, to obtain a solution along the x-axis without recourse to Parker's arbitrary assumption. Further, it will be possible to investigate the question of whether the mode is definitive, a vital question omitted from consideration in Parker's treatment.

(iv) Parker's Compressible Mode

The compressible case, which is more readily amenable to quantitative discussion, will now be examined. This analysis is more directly applicable to the case of solar flares. For under chromospheric or coronal conditions it is expected that the magnetic pressure will exceed the gas pressure by several orders of magnitude. At the outset, therefore, an assumption is

made to this effect, requiring that in the ambient gas

$$v_A \gg v_s \quad (4-48),$$

where the notation of section (1) of the present chapter has been used. This condition implies that the magnetic field in the ambient gas where hydrostatic conditions prevail is of a force-free form. In particular, if the field is of a two-dimensional type the field must also be potential.

Assuming, then, the simple two-dimensional model of two infinite current cylinders, the comments of the previous paragraph show that, in the ambient gas, the magnetic field will to a first approximation be of the form derived in chapter 3, and will be given by equation (3-11). Thus, on the boundary curve C of region I, one is entirely justified in applying the boundary condition that is given by equation (4-32), namely

$$\begin{aligned} H_x &= 0 \\ H_y &= \frac{H_0 L (L^2 - y^2)^{1/2}}{L^2 + y^2} \end{aligned} \quad (4-32),$$

where H_0 is again the y -component of the field at the point where the boundary cuts the x -axis. It is important to note that equation (3-11) can only be used

to zero-order, and no knowledge of the variation of H_x along the boundary can be obtained. With this boundary condition a solution is now sought in region I..

In section (ii) of the present chapter the equations of the system were reduced to the equations of continuity and motion, equations (4-20) and (4-21), together with the hydromagnetic equation (4-27).

Writing

$$\frac{D}{Dt} = \frac{\partial}{\partial t} + \underline{v} \cdot \text{grad} \quad (4-49),$$

these equations can be expressed in scalar form as

$$\frac{DA}{Dt} = c E_0 + \frac{c^2}{4\pi\sigma} \nabla^2 A \quad (4-50),$$

$$\frac{Dv_x}{Dt} = - \left(v_s^2 \frac{\partial}{\partial x} (\log \rho) + \frac{\nabla^2 A}{4\pi\rho} \frac{\partial A}{\partial x} \right) \quad (4-51),$$

$$\frac{Dv_y}{Dt} = - \left(v_s^2 \frac{\partial}{\partial y} (\log \rho) + \frac{\nabla^2 A}{4\pi\rho} \frac{\partial A}{\partial y} \right) \quad (4-52),$$

$$\frac{D\rho}{Dt} = - \rho \text{div } \underline{v} \quad (4-53).$$

In equations (4-51) and (4-52) it has been assumed that the gas behaves isothermally under compression.

It is intended to transform the four physical equations (4-50) - (4-53) to dimensionless form. This transformation is made in terms of five physical

constants H_0 , ρ_0 , L , σ and v_S , which have essentially the same meanings as in section (i) of this chapter. The precise definition of these constants is made as follows:-

Choose an arbitrary epoch, at which it is intended to examine the solution of the system, as the time origin $t = 0$. Let P_0 be the point at which the boundary curve of region I cuts the positive x-axis. Then the physical parameters H_0 , ρ_0 , σ , and v_S are respectively defined as the y-component of the magnetic intensity, the gas density, the electrical conductivity, and the local velocity of sound, all taken at the point P_0 and at the time $t = 0$. Further, $2L$ is defined as the greatest length (in the y-direction) of the current region, again taken at this same epoch. The solution is then sought that corresponds to the epoch $t = 0$.

The parameters σ , v_S , and ρ_0 can be assumed to be independent of the particular epoch chosen in the above definition. L and H_0 , on the other hand, will be dependent on the separation of the two current cylinders, which will vary with the epoch chosen as the time origin.

In terms of these redefined physical parameters, the two typical velocities, v_A and v_D , are defined in the same way as in section (i), viz

$$v_A = \frac{H_0}{(4 \pi \rho)^{1/2}} \quad (4-1),$$

$$v_D = \frac{c^2}{4 \pi \sigma L} \quad (4-3).$$

The transformation to dimensionless form will be based on Parker's order of magnitude solution, equations (4-14) - (4-15). For convenience, therefore, define ℓ and v_0 in terms of the newly defined physical parameters in exactly the same way as in section (i), writing

$$\ell = \left(\frac{v_D v_S}{v_A^2} \right)^{1/2} L$$

$$v_D = \left(\frac{v_D}{v_S} \right)^{1/2} v_A \quad (4-54).$$

Then, ℓ and v_0 , now respectively a precisely defined length and velocity, are of the same order of magnitude as the thickness of the current sheet and the velocity of interpenetration.

Now transform to dimensionless variables as follows, putting

$$\begin{aligned}
 x &= \frac{l}{\Gamma_0} \xi & y &= L \eta \\
 t &= \frac{L}{\Gamma_0 v_0} \tau & E_0 &= \frac{v_0 H_0}{c} \Gamma_0 \\
 A &= \frac{H_0 l}{\Gamma_0} \alpha & \rho &= \frac{v_A^2}{v_s^2} \rho_0 \tilde{\omega} \\
 v_x &= \frac{\Gamma_0 l}{L} v_s \frac{u_x}{\tilde{\omega}} & v_y &= \Gamma_0^2 v_s \frac{u_y}{\tilde{\omega}}
 \end{aligned} \tag{4-55}$$

In these equations, Γ_0 is a dimensionless numerical parameter of order unity, assumed a priori to be independent of the physical parameters of the system. Essentially Γ_0 is the dimensionless electric intensity. It is, however, convenient to include Γ_0 in many of the transformation equations, since this will normalise the resulting differential equations and tend to algebraic simplification. The fact that Γ_0 is of order unity must be verified by a consistency argument. This is attempted below, and indeed this verification and the determination of Γ_0 are the main objects of the subsequent analysis.

Finally it is convenient to introduce two further dimensionless parameters, ϵ_1 and ϵ_2 , defined by

$$\begin{aligned} \epsilon_1 &= \left(\frac{v_s}{v_A} \right)^2 \\ \epsilon_2 &= \left(\frac{v_A^2 v_D}{v_s^3} \right)^{1/2} \end{aligned} \quad (4-56).$$

On applying the transformations (4-55), and on using the simplification afforded by equations (4-56), the physical equations of the system, (4-50) - (4-53), can be written in dimensionless form as follows :

$$\begin{aligned} 1 + \frac{\partial^2 \alpha}{\partial \xi^2} &= \frac{\epsilon_1}{\bar{\omega}} \left(u_\xi \frac{\partial \alpha}{\partial \xi} + u_\eta \frac{\partial \alpha}{\partial \eta} \right) \\ &\quad \frac{\epsilon_1 \epsilon_2}{\Gamma_0^2} \left(\Gamma_0 \frac{\partial \alpha}{\partial \tau} - \epsilon_1 \epsilon_2 \frac{\partial^2 \alpha}{\partial \eta^2} \right) \end{aligned} \quad (4-57),$$

$$\begin{aligned} \frac{\partial \bar{\omega}}{\partial \xi} + \frac{\partial \alpha}{\partial \xi} \frac{\partial^2 \alpha}{\partial \xi^2} + \epsilon_1^2 \epsilon_2^2 \left[\frac{1}{\Gamma_0^2} \frac{\partial \alpha}{\partial \xi} \frac{\partial^2 \alpha}{\partial \eta^2} + \epsilon_2 \Gamma_0 \bar{\omega} \frac{\partial}{\partial \tau} \left(\frac{u_\xi}{\bar{\omega}} \right) \right. \\ \left. + \Gamma_0^2 \left(u_\xi \frac{\partial}{\partial \xi} \left(\frac{u_\xi}{\bar{\omega}} \right) + u_\eta \frac{\partial}{\partial \eta} \left(\frac{u_\eta}{\bar{\omega}} \right) \right) \right] = 0 \end{aligned} \quad (4-58),$$

$$\begin{aligned} u_\xi \frac{\partial}{\partial \xi} \left(\frac{u_\eta}{\bar{\omega}} \right) + u_\eta \frac{\partial}{\partial \eta} \left(\frac{u_\eta}{\bar{\omega}} \right) + \frac{1}{\Gamma_0^4} \left(\frac{\partial \bar{\omega}}{\partial \eta} + \frac{\partial \alpha}{\partial \eta} \frac{\partial^2 \alpha}{\partial \xi^2} \right) \\ + \frac{\epsilon_2}{\Gamma_0} \bar{\omega} \frac{\partial}{\partial \tau} \left(\frac{u_\eta}{\bar{\omega}} \right) + \frac{\epsilon_1^2 \epsilon_2^2}{\Gamma_0^6} \frac{\partial \alpha}{\partial \eta} \frac{\partial^2 \alpha}{\partial \eta^2} = 0 \end{aligned} \quad (4-59),$$

$$\frac{\partial u_\xi}{\partial \xi} + \frac{\partial u_\eta}{\partial \eta} = - \frac{\epsilon_2}{\Gamma_0} \frac{\partial \bar{\omega}}{\partial \tau} \quad (4-60).$$

The assumption has already been made that

$v_A \gg v_S$. From equation (4-56) this implies that $\epsilon_1 \ll 1$.

It is less easy to see the order of magnitude of ϵ_2 .

However, one may examine the order of ϵ_2 for values of the physical parameters that are expected to occur in a

solar flare. Assuming chromospheric conditions, take

$T \sim 10^4$ °K, $\sigma \sim 2 \cdot 10^{13}$ e.s.u. Observations of

solar flares suggest that $L \sim 10^4$ km and that

$\rho_0 \sim 2 \cdot 10^{-13}$ gm/cm³. Finally, energy considerations

require that $H_0 \sim 500$ gauss.

With these values the three typical velocities involved in the definitions of ϵ_1 and ϵ_2 are approximately given by

$$\begin{aligned} v_A &\sim 3 \cdot 10^8 \text{ cm/sec} \\ v_S &\sim 1.6 \cdot 10^6 \text{ cm/sec} \\ v_D &\sim 4 \cdot 10^{-3} \text{ cm/sec} \end{aligned} \quad (4-61).$$

From these values it is readily calculated that

$\epsilon_1 \sim 3 \cdot 10^{-5}$, and $\epsilon_2 \sim 9 \cdot 10^{-3}$. Thus it is seen that, at least under solar flare conditions, $\epsilon_1 \ll 1$, $\epsilon_2 \ll 1$.

Now the dimensionless functions α , ω , u_ξ , and u_η that are the solutions of equations (4-57) - (4-60) will be functions of six variables, - the three dedimensionalized space and time coordinates ξ , η , and τ , and the three dimensionless parameters Γ_0 , ϵ_1 , and

ϵ_2 . Write, therefore,

$$\begin{aligned}
 \alpha &= \alpha(\xi, \eta, \tau, \Gamma_0, \epsilon_1, \epsilon_2) \\
 \omega &= \omega(\xi, \eta, \tau, \Gamma_0, \epsilon_1, \epsilon_2) \\
 u_\xi &= u_\xi(\xi, \eta, \tau, \Gamma_0, \epsilon_1, \epsilon_2) \\
 u_\eta &= u_\eta(\xi, \eta, \tau, \Gamma_0, \epsilon_1, \epsilon_2)
 \end{aligned}
 \tag{4-62}.$$

Now both ϵ_1 and ϵ_2 are small quantities. The order of magnitude solutions, therefore, suggest that the dimensionless variables in (4-62) are expansible as shown below

$$\begin{aligned}
 \alpha &= \alpha_0(\xi, \eta, \tau, \Gamma_0) + \sum_{\substack{i=0 \\ ij \neq 0}}^{\infty} \sum_{j=0}^{\infty} \epsilon_1^i \epsilon_2^j \alpha_{ij}(\xi, \eta, \tau, \Gamma_0) \\
 \omega &= \omega_0(\xi, \eta, \tau, \Gamma_0) + \sum_{\substack{i=0 \\ ij \neq 0}}^{\infty} \sum_{j=0}^{\infty} \epsilon_1^i \epsilon_2^j \omega_{ij}(\xi, \eta, \tau, \Gamma_0) \\
 u_\xi &= u_{\xi 0}(\xi, \eta, \tau, \Gamma_0) + \sum_{\substack{i=0 \\ ij \neq 0}}^{\infty} \sum_{j=0}^{\infty} \epsilon_1^i \epsilon_2^j u_{\xi ij}(\xi, \eta, \tau, \Gamma_0) \\
 u_\eta &= u_{\eta 0}(\xi, \eta, \tau, \Gamma_0) + \sum_{\substack{i=0 \\ ij \neq 0}}^{\infty} \sum_{j=0}^{\infty} \epsilon_1^i \epsilon_2^j u_{\eta ij}(\xi, \eta, \tau, \Gamma_0)
 \end{aligned}
 \tag{4-63}.$$

In equations (4-63) the functions α_0 and α_{ij} etc. are simply the appropriate coefficients of powers of ϵ_1 and ϵ_2 in the Taylor expansions about the point $\epsilon_1 = 0, \epsilon_2 = 0$.

Substitution of these expansions into the dimensionless equations (4-57) - (4-60) will yield the following results, on equating the terms independent of ϵ_1 and ϵ_2 ,

$$\bar{\omega}_0 \left(1 + \frac{\partial^2 \alpha_0}{\partial \xi^2} \right) = 0 \quad (4-64),$$

$$\frac{\partial \bar{\omega}_0}{\partial \xi} + \frac{\partial \alpha_0}{\partial \xi} \frac{\partial^2 \alpha_0}{\partial \xi^2} = 0 \quad (4-65),$$

$$u_{\xi 0} \frac{\partial}{\partial \xi} \left(\frac{u_{\eta 0}}{\bar{\omega}_0} \right) + u_{\eta 0} \frac{\partial}{\partial \eta} \left(\frac{u_{\eta 0}}{\bar{\omega}_0} \right) + \frac{1}{r_0^4} \left(\frac{\partial \bar{\omega}_0}{\partial \eta} + \frac{\partial \alpha_0}{\partial \eta} \frac{\partial^2 \alpha_0}{\partial \xi^2} \right) = 0 \quad (4-66),$$

$$\frac{\partial u_{\xi 0}}{\partial \xi} + \frac{\partial u_{\eta 0}}{\partial \eta} = 0 \quad (4-67).$$

It is intended to derive the essential features of the solution of these last four equations within region I. From symmetry considerations it will be sufficient to solve them in a single quadrant, that is in a domain, D say, bounded by the positive x- and y-axes and the boundary curve C of the region of high current density.

The following boundary conditions are available for the dimensionless vector potential α . By the symmetry of the magnetic configuration, it is necessary that

$$\text{On } \xi = 0, \quad \frac{\partial \alpha_0}{\partial \xi} = 0 \quad (4-68).$$

$$\text{On } \eta = 0, \quad \frac{\partial \alpha_0}{\partial \eta} = 0$$

Further, in region II the magnetic field is given by (4-32). The continuity of \underline{H} across the boundary of the current region yields the condition that

$$\text{On } C \quad \frac{\partial \alpha_0}{\partial \xi} = - \frac{(1-\eta^2)^{1/2}}{1+\eta^2} \quad (4-69),$$

when equation (4-32) is reduced to dimensionless form. The condition on H_x in equation (4-32) is automatically satisfied by the form of the dimensionless transformations (4-55).

Now, in region I, $\alpha_0 \neq 0$. Within this region, therefore, equation (4-64) reduces to

$$\frac{\partial^2 \alpha_0}{\partial \xi^2} = -1 \quad (4-70).$$

This indicates that to zero order the current density is constant throughout the region. Integration of equation (4-70) and application of the boundary conditions (4-68) yields α_0 within region I :

$$\begin{aligned} \alpha_0 &= F_0(\eta) - \xi^2/2 \\ F_0'(0) &= 0 \end{aligned} \quad (4-71).$$

Here $F_0(\eta)$ is a function of η still to be determined. Further, the application of the external boundary condition (4-69) will yield an equation for the boundary curve C. This is found to be the oval, given by

$$\xi^2(1+\eta^2)^2 + \eta^2 = 1 \quad (4-72).$$

Attention is next turned to the dimensionless gas density $\bar{\omega}$. In region II the gas density $\rho = O(\rho_0)$. It follows, then, from the form of the dimensionless transformations that

$$\text{On } C \quad \bar{\omega}_0 = 0 \quad (4-73).$$

On substitution for α_0 from (4-71), equation (4-65) can be integrated directly to give

$$\bar{\omega}_0 + \xi^2/2 = F_1(\eta)$$

where $F_1(\eta)$ is a function of η only. $F_1(\eta)$ can be determined by the external boundary condition (4-73), since the equation for C is now known. Solving for $F_1(\eta)$ then yields

$$\bar{\omega}_0 = \frac{1}{2} \left[\frac{1-\eta^2}{(1+\eta^2)^2} - \xi^2 \right] \quad (4-74)$$

In region II the gas has not yet been accelerated and, therefore, $v_y = O(v_0) \ll v_S$. Hence the continuity of v_y across the boundary requires that, in region I,

$$\frac{u_{\eta_0}}{\bar{\omega}_0} \rightarrow 0 \quad \text{on } C.$$

Now, since $\bar{\omega}_0$ itself tends to zero on C , this last equation will give the boundary conditions that

$$\text{On } C \quad u_{\eta_0} = 0 \quad (4-75),$$

$$\text{and} \quad \frac{\partial u_{\eta_0}}{\partial \xi} = 0 \quad (4-76)$$

A further boundary condition can be obtained from the continuity of mass flow across C . In region II hydrostatic conditions prevail; as shown in the last section, therefore, the gas density will be constant along a line of force. To a first approximation the boundary curve of region I is such a line of force, and, therefore, the gas density is, to this order, constant along it. In dimensionless form this requires that in region II the leading non-zero term in the expansion (4-63) of the dimensionless density $\tilde{\omega}$ be constant along the curve C . It is readily seen that this term is $\tilde{\omega}_{10}$. Further, from the definition of β_0 and the transformation equations (4-55), it follows that

$$\text{on } C \quad \tilde{\omega}_{10} = 0 \quad (4-77).$$

The above argument is hardly rigorous. It can be made so, however, by a straightforward but tedious examination of higher order terms of the dimensionless expansions (4-63).

Now, in region II, the gas and current densities are zero, to zero order, that is

$$\omega_0 = \frac{\partial^2 \alpha_0}{\partial \xi^2} = 0$$

Taking equation (4-57) to order ϵ_1 , the following result, applicable to region II, is obtained

$$\omega_{10} = u_{\xi_0} \frac{\partial \alpha_0}{\partial \xi} + u_{\eta_0} \frac{\partial \alpha_0}{\partial \eta} \quad (4-78).$$

Substitution can now be made for $\partial \alpha_0 / \partial \xi$ from (4-69). Then, on using the results of equations (4-75) and (4-77), (4-78) will reduce to

$$u_{\xi_0} = - \frac{1 + \eta^2}{(1 - \eta^2)^{1/2}} \quad (4-79).$$

This last result has been derived for region II. The continuity of mass flow across the boundary of the current region requires that it should also hold in region I in the limit on C.

Putting $\underline{u} = (u_{\xi_0}, u_{\eta_0}, 0)$, equation (4-67) can be written as

$$\text{div } \underline{u} = 0$$

It is possible, therefore, to replace the two components of \underline{u} by a stream function, writing

$$u_{\xi_0} = \frac{\partial Q}{\partial \eta} \quad (4-80).$$

$$u_{\eta_0} = -\frac{\partial Q}{\partial \xi}$$

This will allow considerable simplification of the remaining differential equation (4-66). Upon substitution for ω_0 from equation (4-74), and for α_0 from equation (4-71), this last equation reduces to the form :

$$J \left(Q, \frac{2(1+\eta^2)^2}{1-\eta^2-\xi^2(1+\eta^2)^2} \frac{\partial Q}{\partial \xi} \right) = F_2(\eta) \quad (4-81).$$

The symbol J is now used to denote the two-dimensional Jacobian operator in the (ξ, η) plane, so that

$$J(\phi_1, \phi_2) = \frac{\partial(\phi_1, \phi_2)}{\partial(\xi, \eta)}$$

The function $F_2(\eta)$ that appears in (4-81) is a function of η only, which is to be determined by the solution of this differential equation. The unknown functions $F_2(\eta)$ and $F_0(\eta)$ are related by the equation

$$F_2(\eta) = \frac{1}{\Gamma_0^4} \left(\frac{\eta(3-\eta^2)}{(1+\eta^2)^3} + F_0'(\eta) \right) \quad (4-82).$$

Clearly, the equation (4-81) can be written as a partial differential equation in Q only, namely

$$\frac{\partial}{\partial \xi} \left[J \left(Q, \frac{2(1+\eta^2)^2}{1-\eta^2-\xi^2(1+\eta^2)^2} \frac{\partial Q}{\partial \xi} \right) \right] = 0 \quad (4-83).$$

As boundary conditions on this final differential equation, there are firstly the conditions of symmetry, that

$$\begin{aligned} \text{on } \xi = 0, & \quad Q = 0 \\ \text{on } \eta = 0, & \quad Q = 0 \end{aligned} \quad (4-84),$$

on choosing a suitable origin for Q . Further, there are in addition the two conditions to be applied on the boundary curve C . These are given by equations (4-76) and (4-79). Upon transformation into expressions in terms of Q , these two equations will provide the boundary conditions that

$$\text{on } C \quad \frac{\partial^2 Q}{\partial \xi^2} = 0 \quad (4-85)$$

$$\text{on } C \quad \frac{\partial Q}{\partial \eta} = - \frac{1+\eta^2}{(1-\eta^2)^{1/2}} \quad (4-86)$$

The four conditions contained in equations (4-84) - (4-86) may be expected, in general, to be sufficient to determine a unique solution for the third order partial differential equation (4-83). This is illustrated by the following argument. Consider the partial differential equation in its second order form, - that

is equation (4-81). It is then a quasi-linear hyperbolic equation of the second order. It is readily seen that on the ξ -axis the equation can be reduced to a second order non-linear ordinary differential equation in $\partial Q / \partial \eta$, for which the boundary conditions, when applied on $\eta = 0$, are sufficient. In point of fact, the solution on $\eta = 0$ will be derived in the next chapter. Thus the boundary conditions are sufficient to extend the solution to a neighbourhood of $\eta = 0$. Special conditions apply on $\eta = 0$, since the differential equation (4-81) is parabolic on that line. The more general problem of extending the solution at a point away from the ξ -axis must next be considered.

Suppose, therefore, that the solution has been successfully derived from the ξ -axis up to the line $\eta = \eta_0$. Further, suppose Q_0 is the value of Q at the point A_0 at which the line $\eta = \eta_0$ cuts the boundary curve. Now, suppose that it is intended to extend the solution up to $\eta = \eta_1$ ($\eta_1 > \eta_0$). For convenience, call the point $(0, \eta_1)$ B_0 . The characteristics of the differential equation (4-81) are the curves

$$\begin{aligned} \eta &= \text{constant} \\ Q &= \text{constant} \end{aligned} \quad (4-87).$$

So from the first of conditions (4-84) it is seen that Q is now known on two intersecting characteristics $Q_0(\xi, \eta)$ $\eta = \eta_0$ and $Q = 0$ ($\eta_0 \leq \eta \leq \eta_1$). It follows, therefore, from the theory of partial differential equations ~~It follows,~~ that a unique solution can be obtained for Q within the shaded area in Figure (4-3); that is, within the area bounded by the two characteristics just mentioned, and the two characteristics of the opposite systems through the end points, A_0 and B_0 .

Clearly then to extend the solution to the region $\eta \leq \eta_1$, $Q < Q_0$ (Q is negative), a further boundary condition on C will be required. This is provided by equation (4-85). Finally, the last boundary condition on C , equation (4-86), will be necessary to eliminate the unknown function $F_2(\eta)$ that occurs in equation (4-81).

From the above argument, it is reasonable, therefore, to conclude that the conditions (4-84) - (4-86) will be sufficient (and necessary) to determine a unique solution of the differential equation (4-83). Let us postulate, therefore, the existence of such a solution, denoting it by $Q_0(\xi, \eta)$. Since the differential equation (4-83) and the boundary conditions (4-84) - (4-86) are all independent of Γ_0 , this solution must also be independent of the value of Γ_0 . The solution $Q_0(\xi, \eta)$ will determine $F_2(\eta)$ from equation

(4-81), and the function $F_2(\eta)$ will also be independent of Γ_0 . The only effect of Γ_0 will be on the determination of α_0 , the dimensionless vector potential. From equations (4-82) and (4-71) one may readily obtain an expression for α_0 in terms of $F_2(\eta)$, namely:

$$\alpha_0 = \Gamma_0^4 \int_0^{\eta} F_2(\eta') d\eta' + \frac{1}{2} \left[\frac{1-\eta^2}{(1+\eta^2)^2} - \xi^2 \right] \quad (4-88).$$

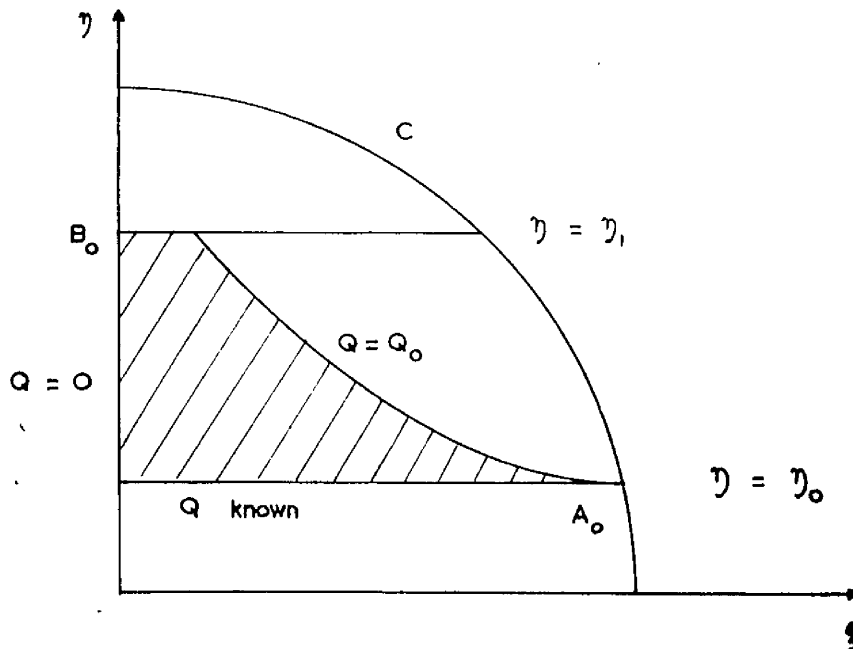


Fig (4-3). Domain of dependence for equation (4-81).

From the above considerations it is clear that non-singular solutions exist for the hydromagnetic equations for all values of the parameter Γ_0 , provided only that a non-singular solution $Q_0(\xi, \eta)$ exists for the differential equation (4-83) subject to its boundary conditions. Further, if a non-singular solution exists for one value of Γ_0 , this solution will define $Q_0(\xi, \eta)$ and hence determine solutions for every other value of Γ_0 .

It is seen, therefore, that this mode, as proposed by Parker is indeterminate. The reason for this indeterminacy is that the behaviour, to a first approximation, of all the physical variables with the exception of H_x , is homogeneous in Γ_0 . The x-component of the magnetic field increases monotonically with Γ_0 , thus providing an increasing accelerating force that is responsible for the enhanced interpenetration. It may be expected, therefore, that the magnetic field will distort itself into configurations allowing faster and faster interpenetration, until the parameter Γ_0 is no longer of order unity, and terms neglected in this treatment become important. A possible faster mode taking these features into account will be considered in chapter 6.

CHAPTER 5
DISCUSSION OF THE SOLUTION FOR
THE COMPRESSIBLE MODE

The argument just considered shows conclusively that within the approximations of this mode, Γ_0 possesses no upper bound. On the other hand, it will be possible to show that Γ_0 is bounded below; the purpose of the present chapter is to determine this lower bound, and thus set a lower limit to the rate of interpenetration of the colliding magnetic fields. To investigate the significant aspects of the solutions for different values of Γ_0 , it will be necessary only to determine the solution for $\partial Q / \partial \eta$ on the ξ -axis. The section which follows will be concerned entirely with the derivation of this solution.

(i) Solution for Q on the ξ -Axis.

It will be convenient to consider the partial differential equation for Q derived in the last chapter in its second order form, equation (4-81), which is restated here for reference purposes as equation (5-1), viz

$$\mathcal{J} \left(Q, \frac{2(1+\eta^2)^2}{1-\eta^2-\xi^2(1+\eta^2)^2} \frac{\partial Q}{\partial \xi} \right) = F_2(\eta) \quad (5-1).$$

The second condition of equation (4-8⁴), namely the symmetry condition that the ξ -axis is a stream-line, requires that

$$\text{on } \eta = 0 \quad Q = 0 \quad (5-2).$$

Substitution of this result into the differential equation (5-1) will, however, only yield

$$F_2(0) = 0 \quad (5-3).$$

It is clear, then, that the partial differential equation, as it stands, gives no information about the behaviour of $\partial Q / \partial \eta$ on the ξ -axis. Therefore, differentiate equation (5-1) partially with respect to η . On putting $\eta = 0$ and applying equation (5-2), an ordinary differential equation for $\partial Q / \partial \eta$ on the ξ -axis is obtained with ξ as the independent variable. It is convenient to write

$$g(\xi) = - \left(\frac{2}{F_2'(0)} \right)^{\frac{1}{2}} \left(\frac{\partial Q}{\partial \eta} \right)_{\eta=0} \quad (5-4).$$

Then this ordinary differential equation will become

$$(1 - \xi^2) (g'^2 - g g'') - 2\xi g g' = (1 - \xi^2)^2 \quad (5-5).$$

In this last equation dashes are used to denote differentiation with respect to ξ .

Equation (5-5), a second order ordinary differential equation, requires two boundary conditions to determine its solution. One of these is provided by equation (4-85). By equation (5-2), equation (4-85), as it stands, is satisfied automatically on $\eta = 0$.

However, if the equation for the curve C is written as

$\xi = \xi_0(\eta)$, then

$$\frac{d}{d\eta} \left[\left(\frac{\partial^2 Q}{\partial \xi^2} \right)_c \right] = \left(\frac{\partial^3 Q}{\partial \xi^3} \right)_c \frac{d\xi_0}{d\eta} + \left(\frac{\partial^3 Q}{\partial \xi^2 \partial \eta} \right)_c \quad (5-6).$$

The left hand side of equation (5-6) is zero by the boundary condition (4-85), and, on using equation (5-2), equation (5-6) will reduce to the condition that

$$\text{on } \eta = 0 \quad \left(\frac{\partial^3 Q}{\partial \xi^2 \partial \eta} \right)_c = 0 \quad (5-7).$$

Finally, by the definition of $g(\xi)$, this last condition (5-7) becomes

$$g''(1) = 0 \quad (5-8),$$

since the boundary cuts the ξ -axis at the point (1, 0).

The second boundary condition follows at once from the first condition of equation (4-84), namely the symmetry condition that the η -axis is a streamline.

This condition is

$$g(0) = 0 \quad (5-9).$$

The immediate problem involves the solution of the non-linear differential equation (5-5), with the two point boundary conditions, given in equations (5-8) and (5-9). This problem is considered in detail in Appendix (5-1), where the complete solution of equation (5-5) has been obtained. Of particular interest is the value of $g(\xi)$ on the boundary curve C. For convenience, therefore, denote $g(1)$ by the symbol Λ_0 . Then, from the solutions that have been derived in Appendix (5-1), one obtains the important numerical result that

$$\Lambda_0 = 0.5578 \quad (5-10).$$

(ii) Determination of the Minimum Value of Γ_0 .

It is now possible to apply the results of the solution of equation (5-5) to the differential equation (5-1). From the definition of $g(\xi)$, given in equation (5-4), it follows that

$$\Lambda_0 = - \left(\frac{2}{F_2'(0)} \right)^{\frac{1}{2}} \left[\left(\frac{\partial Q}{\partial \eta} \right)_{\eta=0} \right]_{\xi=1} \quad (5-11).$$

At the end of chapter 4, four boundary conditions were obtained for Q ; they are given in equations (4-84) to (4-86). Three of these conditions have already been applied in determining $g(\xi)$; the fourth condition, equation (4-86), is still free, however. Applying this condition on the ξ -axis readily yields the result that

$$\left(\frac{\partial Q}{\partial \eta} \right)_{\substack{\xi=1 \\ \eta=0}} = -1 \quad (5-12).$$

Substitution of this result into equation (5-11) will now allow a solution to be obtained for $F_2'(0)$, viz

$$F_2'(0) = \frac{2}{\Lambda_0^2} \quad (5-13).$$

From equation (5-10), this can be written in numerical form as

$$F_2'(0) = 6.429 \quad (5-14).$$

The next step involves an examination of the behaviour of the magnetic field. It is convenient, therefore, to restate the equation for the dimensionless vector potential α_0 , that is equation (4-88), as follows

$$\alpha_0 = \Gamma_0^4 \int_0^{\eta} F_2(\eta') d\eta' + \frac{1}{2} \left[\frac{1-\eta^2}{(1+\eta^2)^2} - \xi^2 \right] \quad (5-15).$$

Now by symmetry the origin must be a neutral point of the magnetic field. This requires that both $\partial\alpha_0/\partial\xi$ and $\partial\alpha_0/\partial\eta$ are zero at the origin. It can be seen from equation (5-15) that this condition is automatically satisfied, since it has been shown that $F_2(0) = 0$. There is, however, a further condition to be fulfilled; for not only must the origin be a neutral point, it must in addition be an X-type, not an O-type, neutral point. This is seen from the general topological form of the magnetic field, as introduced in chapter 3. There is, therefore, the additional requirement that the lines of force through the origin be real.

Expand α_0 in a Taylor series about the origin. Then, in the neighbourhood of that point, the lines of force can, to first order, be written as

$$\left(\frac{\partial^2\alpha_0}{\partial\xi^2}\right)_0 \xi^2 + 2\left(\frac{\partial^2\alpha_0}{\partial\xi\partial\eta}\right)_0 \xi\eta + \left(\frac{\partial^2\alpha_0}{\partial\eta^2}\right)_0 \eta^2 = \text{constant} \quad (5-16).$$

In equation (5-16) the suffix zero is used outside the brackets to indicate that the derivative in question is evaluated at the origin. The algebraic expressions for these derivatives can readily be obtained from equation (5-15). The equation for the lines of force through the neutral point can then be written as

$$\xi^2 + (3 - \Gamma_0^4 F_2'(0)) \eta^2 = 0 \quad (5-17).$$

Now these lines of force can only be real if the coefficients of ξ^2 and η^2 have opposite signs. It is, therefore, required that

$$\Gamma_0^4 F_2'(0) \geq 3 \quad (5-18).$$

Now substitute for $F_2'(0)$ from equation (5-13); then the condition (5-18) will become

$$\Gamma_0 \geq \Gamma_{\min} \quad (5-19),$$

where Γ_{\min} is given by

$$\Gamma_{\min} = \left(\frac{3 \Lambda_0^2}{2} \right)^{1/4} \quad (5-20).$$

On substitution of the result of equation (5-10), the last result can be written in numerical form as

$$\Gamma_{\min} = 0.8265 \quad (5-21).$$

(iii) Application to the Idealised model.

It is now intended to apply the results of the last two sections to the idealized model developed in chapter 3. From the minimum value of Γ_0 that has just been determined it will be possible to obtain a

maximum time of interpenetration for the colliding magnetic fields of the model.

Before making any detailed application of the numerical results to the model, it will be advisable, for the sake of clarity, to expand the definitions of some of the quantities originally introduced in chapter 3. Basically the model has the two-dimensional form of two infinite parallel current cylinders of radius b_0 . The initial field was assumed to be potential with a current separation of $2a_0$. The two current cylinders were then allowed to approach each other under the influence of their mutual attraction. It was assumed that the two current cylinders approached each other sufficiently slowly to enable the inertia of the system to be neglected. It was further assumed that during this approach phase no interpenetration takes place. This is effectively an assumption about the value of the electrical conductivity. The consistency of these two assumptions requires justification, which can be provided by the determination of the actual rate of interpenetration that is considered in the subsequent quasi-steady phase of interpenetration. Consistency can be achieved, provided that the velocity of interpenetration eventually derived is significantly less than the Alfvén velocity.

As the two current cylinders are allowed to approach each other, under the assumption of infinite conductivity, a sheet current of length $2L$ will be formed. The formula relating L to the current separation, $2a$, is given in equations (3-18) and (3-19). The magnetic field of the induced current sheet produces forces which oppose the approach of the two current cylinders. An equilibrium configuration is reached when $L = a$.

The second phase mentioned earlier is concerned with the interpenetration of the field through a series of quasi-equilibrium configurations. It is to this phase that the analysis of chapter 4 applies. It is assumed that equilibrium is first attained when $a = L = a_1$. The value of a_1 , in terms of a_0 and b_0 , can be obtained from the solutions of equations (3-18) and (3-19). Once this equilibrium configuration has been attained the system is left to itself (the applied external forces required for the approaching phase are now zero), and interpenetration will take place. The system then remains in an equilibrium configuration with $L = a$, and the separation (2a) of the current cylinders decreases as interpenetration takes place.

From equations (3-11) and (3-23) the field of this equilibrium configuration is

$$i H_x + H_y = \frac{4I_0}{c} \frac{(z^2 + a^2)^{\frac{1}{2}}}{z^2 - a^2} \quad (5-22)$$

where I_0 is the initial strength of each current cylinder. Now the parameter H_0 , which will have the meaning assigned to it in chapter 4, (page 130) will be a function of a . From equation (5-22) one can write

$$H_0(a) = - \frac{4 I_0}{c a} \quad (5-23).$$

In chapter 3, an expression was derived for the magnetic flux F during this second interpenetration phase; - here F is the flux crossing the x -axis between the neutral point and each of the current cylinders. This expression, which is given in equation (3-25), determines F as a function of a , a_0 , and b_0 . Considerable simplification was possible in the case where $b_0 \ll a$, and attention will be confined to this particular case. With this assumption, equation (3-25) was reduced to equation (3-26), which, for convenience, is restated here, namely

$$\log \frac{4a}{b_0} = \frac{F}{\sqrt{2} F_0} \log \frac{a_0}{2b_0} + \sqrt{2} \log(1 + \sqrt{2}) \quad (5-24).$$

Now, differentiating equation (5-24) with respect to t , it is possible to obtain a relation between the rate of interpenetration, which is simply dF/dt , and the

rate at which the two current cylinders are moving together. In fact, this relation is

$$\frac{l}{a} \frac{da}{dt} = \frac{l}{\sqrt{2} F_0} \log\left(\frac{a_0}{2b_0}\right) \frac{dF}{dt} \quad (5-25).$$

As a first step in the interpretation of (5-25), express F as the integral

$$F = \int_0^{a-b_0} H_y(x, 0) dx \quad (5-26).$$

Then differentiate equation (5-26) totally with respect to t to obtain, since a is a function of t ,

$$\frac{dF}{dt} = \int_0^{a-b_0} \left(\frac{\partial H_y}{\partial t} \right)_{y=0} dx + \frac{da}{dt} H_y(a-b_0, 0) \quad (5-27).$$

Next one can apply Faraday's law to the integrand occurring in equation (5-27) and integrate to obtain the form

$$\frac{dF}{dt} = c \left[E_z(a-b_0, 0) - E_0 \right] + \frac{da}{dt} H_y(a-b_0, 0) \quad (5-28),$$

on using the definition of E_0 from chapter 4, viz

$$E_0 = E_z(0, 0) \quad (5-29).$$

Finally, substitute for $E_z(a-b_0, 0)$ from the conductivity equation, remembering that to a first approximation at this point $j = 0$, and that $v_x(a-b_0, 0) = da/dt$. Equation (5-28) will then

reduce to

$$\frac{dF}{dt} = -c E_0 \quad (5-30).$$

The electric field E_0 is related to the dimensionless parameter Γ_0 by the transformation equations (4-55). These give

$$E_0 = \frac{v_0 H_0}{c} \Gamma_0 \quad (5-31),$$

where v_0 is defined as

$$v_0 = \left(\frac{v_0}{v_s} \right)^{1/2} v_A \quad (5-32).$$

Now the velocities that appear on the right hand side of equation (5-32) depend upon the values of H_0 , L and f_0 , all of which will be functions of a . Let us, therefore, put $v_0 = v_0(a)$.

Now it is intended to evaluate a time-scale τ_0 for the interpenetration. So define this time-scale by the equation

$$\tau_0 = -a_1 / \left(\frac{da}{dt} \right)_{a=a_1} \quad (5-33).$$

Then from equations (5-25), (5-30), and (5-31), τ_0 is given by

$$\tau_0 = \frac{\sqrt{2} F_0}{\Gamma_0 v_0(a_1) H_0(a_1)} \left[\log \left(\frac{a_0}{2b_0} \right) \right]^{-1} \quad (5-34)$$

Finally, one may substitute for τ_0 from equation (3-5). Since it has been assumed that $b_0 \ll a_1$, it follows a fortiori that $b_0 \ll a_0$. So neglecting terms of order (b_0/a_0) in equation (3-5), this equation will yield

$$\tau_0 = \frac{2\tau_0}{c} \log \frac{2b_0}{a_0} \quad (5-35).$$

Then, using the results of (5-23) and (5-35), equation (5-34) will reduce to the simpler form

$$\tau_0 = \frac{a_1}{\sqrt{2} \Gamma_0 \sigma_0(a_1)} \quad (5-36).$$

From the work of the previous section, this last result can clearly be written in the alternative form, that

$$\tau_0 \leq \tau_{max} \quad (5-37),$$

where τ_{max} is the maximum time-scale of interpenetration. This is defined by

$$\tau_{max} = \frac{a_1}{\sqrt{2} \Gamma_{min} \sigma_0(a_1)} \quad (5-38).$$

which by equation (5-21) can be written in numerical form as

$$\tau_{max} = 0.8555 \frac{a_1}{\sigma_0(a_1)} \quad (5-39).$$

A maximum time-scale of interpenetration is, therefore, unambiguously defined in terms of a_1 and v_0 , that is in terms of the physical parameters of the system.

The application of this result to chromospheric conditions will be made in chapter 7.

CHAPTER 6.

POSSIBLE ENHANCEMENT OF PARKER'S COMPRESSIBLE MODE.

(i) General Description of a Possible Faster Mode.

It has been shown in chapter 4 (page 146) that a maximum, in contrast to a minimum, rate of interpenetration cannot be determined for Parker's mode; in other words this mode is not definitive. Since the existence of a lower bound for Γ_0 has been established, this fact is indicative of the existence of a faster mode of interpenetration.

The key to a possible faster mode is provided by the solution for the dimensionless vector potential α in the slow mode. From equation (4-88), this solution is

$$\alpha_0 = \Gamma_0^4 \int_0^\eta F_2(\eta') d\eta' + \frac{1}{2} \left[\frac{1-\eta^2}{(1+\eta^2)^2} - \xi^2 \right] \quad (6-1)$$

The form of this solution suggests that one should make the substitution

$$\alpha = \alpha^*(\xi, \eta, \tau) + \Gamma_0^4 F(\eta, \tau) \quad (6-2)$$

Substituting this into equations (4-57) to (4-59), the dimensionless equations of the system can be written in the form

$$\begin{aligned} 1 + \frac{\partial^2 \alpha^*}{\partial \xi^2} &= \frac{\epsilon_1}{\omega} \left(u_\xi \frac{\partial \alpha^*}{\partial \xi} + u_\eta \frac{\partial \alpha^*}{\partial \eta} \right) + \frac{\epsilon_1 \Gamma_0^4}{\omega} u_\eta \frac{\partial F}{\partial \eta} \\ + \frac{\epsilon_1 \epsilon_2}{\Gamma_0^2} \left(\Gamma_0 \frac{\partial \alpha^*}{\partial \tau} + \Gamma_0^5 \frac{\partial F}{\partial \tau} - \epsilon_1 \epsilon_2 \frac{\partial^2 \alpha^*}{\partial \eta^2} - \epsilon_1 \epsilon_2 \Gamma_0^4 \frac{\partial^2 F}{\partial \eta^2} \right) \end{aligned} \quad (6-3)$$

$$\frac{\partial \bar{\omega}}{\partial \xi} + \frac{\partial \alpha^*}{\partial \xi} \frac{\partial^2 \alpha^*}{\partial \xi^2} + \epsilon_1^2 \epsilon_2^2 \left[\frac{1}{\Gamma_0^2} \frac{\partial \alpha^*}{\partial \xi} \frac{\partial^2 \alpha^*}{\partial \eta^2} + \Gamma_0^2 \frac{\partial \alpha^*}{\partial \xi} \frac{\partial^2 F}{\partial \eta^2} \right. \\ \left. + \Gamma_0^2 \left(u_\xi \frac{\partial}{\partial \xi} \left(\frac{u_\xi}{\bar{\omega}} \right) + u_\eta \frac{\partial}{\partial \eta} \left(\frac{u_\xi}{\bar{\omega}} \right) \right) + \epsilon_2 \Gamma_0 \bar{\omega} \frac{\partial}{\partial \tau} \left(\frac{u_\xi}{\bar{\omega}} \right) \right] = 0 \quad (6-4)$$

$$u_\xi \frac{\partial}{\partial \xi} \left(\frac{u_\eta}{\bar{\omega}} \right) + u_\eta \frac{\partial}{\partial \eta} \left(\frac{u_\eta}{\bar{\omega}} \right) + \frac{1}{\Gamma_0^4} \left(\frac{\partial \bar{\omega}}{\partial \eta} + \frac{\partial \alpha^*}{\partial \eta} \frac{\partial^2 \alpha^*}{\partial \xi^2} \right) + \frac{\partial F}{\partial \eta} \frac{\partial^2 \alpha^*}{\partial \xi^2} \\ + \frac{\epsilon_2}{\Gamma_0} \bar{\omega} \frac{\partial}{\partial \tau} \left(\frac{u_\eta}{\bar{\omega}} \right) + \frac{\epsilon_1^2 \epsilon_2^2}{\Gamma_0^6} \left(\frac{\partial \alpha^*}{\partial \eta} \frac{\partial^2 \alpha^*}{\partial \eta^2} + \Gamma_0^4 \frac{\partial \alpha^*}{\partial \eta} \frac{\partial^2 F}{\partial \eta^2} \right. \\ \left. + \Gamma_0^4 \frac{\partial F}{\partial \eta} \frac{\partial^2 \alpha^*}{\partial \eta^2} + \Gamma_0^8 \frac{\partial F}{\partial \eta} \frac{\partial^2 F}{\partial \eta^2} \right) = 0 \quad (6-5)$$

The final equation, the dimensionless equation of continuity (4-60) remains unchanged by the substitution and is

$$\frac{\partial u_\xi}{\partial \xi} + \frac{\partial u_\eta}{\partial \eta} = - \frac{\epsilon_2}{\Gamma_0} \frac{\partial \bar{\omega}}{\partial \tau} \quad (6-6)$$

An examination of these equations indicates that, as Γ_0 increases, the first term in the ϵ 's previously neglected to become of order unity will be the term $(\epsilon_1 \Gamma_0^4 / \bar{\omega}) u_\eta \partial F / \partial \eta$ in equation (6-3). Therefore, put

$$\Gamma_0 = G_0 / \epsilon_1^{1/4} \quad (6-7)$$

where G_0 is a constant.

A mode of interpenetration will now be sought in which G_0 is independent of ϵ_1 and ϵ_2 , and in which the dimensionless variables that have been introduced are of order unity within region I. As a further

simplification, introduce the dimensionless quantities

κ_1, κ_2 , defined by

$$\begin{aligned}\kappa_1 &= \epsilon_1 \\ \kappa_2 &= \epsilon_1^{1/4} \epsilon_2\end{aligned}\quad (6-8)$$

Since it has been shown in chapter 4 that $\epsilon_1 \ll 1, \epsilon_2 \ll 1$, it follows a fortiori from the definition (6-8) that

$$\kappa_1 \ll 1, \kappa_2 \ll 1.$$

Now, substituting from equations (6-7) and (6-8), the equations (6-3) - (6-6) can be tidied up to give the dimensionless equations of the system in a form appropriate to further investigation of the faster mode.

These equations become

$$\begin{aligned}1 + \frac{\partial^2 \alpha^*}{\partial \xi^2} - G_0^4 \frac{u_\eta}{\bar{\omega}} \frac{\partial F}{\partial \eta} &= \frac{\kappa_1}{\bar{\omega}} \left(u_\xi \frac{\partial \alpha^*}{\partial \xi} + u_\eta \frac{\partial \alpha^*}{\partial \eta} \right) + \frac{\kappa_1 \kappa_2}{G_0} \frac{\partial \alpha^*}{\partial \tau} \\ + \kappa_2 G_0^3 \frac{\partial F}{\partial \tau} - \frac{\kappa_1^2 \kappa_2^2}{G_0^2} \frac{\partial^2 \alpha^*}{\partial \eta^2} - \kappa_1 \kappa_2^2 G_0^2 \frac{\partial^2 F}{\partial \eta^2}\end{aligned}\quad (6-9)$$

$$\frac{\partial \bar{\omega}}{\partial \xi} + \frac{\partial \alpha^*}{\partial \xi} \frac{\partial^2 \alpha^*}{\partial \xi^2} + \frac{\kappa_1^2 \kappa_2^2}{G_0^2} \frac{\partial \alpha^*}{\partial \xi} \frac{\partial^2 \alpha^*}{\partial \eta^2} + \kappa_1 \kappa_2^2 G_0^2 \frac{\partial \alpha^*}{\partial \xi} \frac{\partial^2 F}{\partial \eta^2} +$$

$$\kappa_1 \kappa_2^3 G_0 \bar{\omega} \frac{\partial}{\partial \tau} \left(\frac{u_\xi}{\bar{\omega}} \right) + \kappa_1 \kappa_2^2 G_0^2 \left(u_\xi \frac{\partial}{\partial \xi} \left(\frac{u_\xi}{\bar{\omega}} \right) + u_\eta \frac{\partial}{\partial \eta} \left(\frac{u_\xi}{\bar{\omega}} \right) \right) = 0 \quad (6-10)$$

$$u_\xi \frac{\partial}{\partial \xi} \left(\frac{u_\eta}{\bar{\omega}} \right) + u_\eta \frac{\partial}{\partial \eta} \left(\frac{u_\eta}{\bar{\omega}} \right) + \frac{\partial F}{\partial \eta} \frac{\partial^2 \alpha^*}{\partial \xi^2} + \frac{\kappa_1}{G_0^4} \left(\frac{\partial \bar{\omega}}{\partial \eta} + \frac{\partial \alpha^*}{\partial \eta} \frac{\partial^2 \alpha^*}{\partial \xi^2} \right) + \frac{\kappa_2}{G_0} \bar{\omega} \frac{\partial}{\partial \tau} \left(\frac{u_\eta}{\bar{\omega}} \right) +$$

$$\frac{\kappa_1 \kappa_2^2}{G_0^6} \left[\kappa_1^2 \frac{\partial \alpha^*}{\partial \eta} \frac{\partial^2 \alpha^*}{\partial \eta^2} + \kappa_1 G_0^4 \left(\frac{\partial \alpha^*}{\partial \eta} \frac{\partial^2 F}{\partial \eta^2} + \frac{\partial F}{\partial \eta} \frac{\partial^2 \alpha^*}{\partial \eta^2} \right) + G_0^3 \frac{\partial F}{\partial \eta} \frac{\partial^2 F}{\partial \eta^2} \right] = 0 \quad (6-11)$$

$$\frac{\partial u_{\xi}}{\partial \xi} + \frac{\partial u_{\eta}}{\partial \eta} + \frac{\kappa_2}{G_0} \frac{\partial \omega}{\partial \tau} = 0 \quad (6-12)$$

Equations (6-9) to (6-12) are the complete equations of the system in dimensionless form. It is intended to treat them in a manner very similar to the treatment of the equivalent equations, (4-57) - (4-60), in the slow mode. The limiting solution is sought as κ_1 and κ_2 tend to zero. As before, the subscript zero is used to denote the values of the dimensionless functions at a point on the G_0 -axis, this time in the $\kappa_1 = \kappa_2 = G_0$ space. On this axis the dimensionless equations reduce to

$$1 + \frac{\partial^2 \alpha_0^*}{\partial \xi^2} = G_0^4 \frac{u_{\eta_0}}{\omega_0} \frac{\partial F_0}{\partial \eta} \quad (6-13)$$

$$\frac{\partial \omega_0}{\partial \xi} + \frac{\partial \alpha_0^*}{\partial \xi} \frac{\partial^2 \alpha_0^*}{\partial \xi^2} = 0 \quad (6-14)$$

$$u_{\xi_0} \frac{\partial}{\partial \xi} \left(\frac{u_{\eta_0}}{\omega_0} \right) + u_{\eta_0} \frac{\partial}{\partial \eta} \left(\frac{u_{\eta_0}}{\omega_0} \right) + \frac{\partial F_0}{\partial \eta} \frac{\partial^2 \alpha_0^*}{\partial \xi^2} = 0 \quad (6-15)$$

$$\frac{\partial u_{\xi_0}}{\partial \xi} + \frac{\partial u_{\eta_0}}{\partial \eta} = 0 \quad (6-16)$$

As equations (6-13) - (6-16), and the boundary conditions to be derived later, do not contain τ explicitly, we may take all the dimensionless variables independent of τ .

From equation (6-16) it is possible to introduce the stream function Q , defined by

$$\begin{aligned}
 u_{\xi_0} &= \frac{\partial Q}{\partial \eta} \\
 u_{\eta_0} &= - \frac{\partial Q}{\partial \xi}
 \end{aligned}
 \tag{6-17}$$

Further, since α_0^* and F_0 appear in the equations (6-13) to (6-16) only in derivative form, it will be convenient to write

$$\begin{aligned}
 \frac{\partial \alpha_0^*}{\partial \xi} &= -k(\xi, \eta) \\
 \frac{dF_0}{d\eta} &= f(\eta)
 \end{aligned}
 \tag{6-18}$$

Both k and f are then effectively dimensionless components of the magnetic field. From now on, one may work in terms of these components rather than in terms of the associated potential functions.

As in the slow mode, there is a boundary condition on the magnetic field provided by the analysis of chapter 3. This condition is given by equation (4-32), which in the new dimensionless form reduces to

$$k = \frac{(1-\eta^2)^{1/2}}{1+\eta^2}
 \tag{6-19}$$

at the boundary of the current region. If this boundary curve is again denoted by C , then equation (6-19) will define C .

Now equation (6-14) can be integrated directly to give

$$\omega_0 = F_1(\eta) - k^2/2$$

The function $F_1(\eta)$ can be determined directly from equation (6-19), by noting that on C $\omega_0 = 0$. Hence the result follows that

$$\omega_0 = \frac{1}{2} \left[\frac{1-\eta^2}{(1+\eta^2)^2} - k^2 \right] \quad (6-20)$$

The remaining two equations, (6-13) and (6-15), can, on applying the relations given in (6-17) and (6-18), be written as differential equations in Q and k . They are

$$\frac{\partial k}{\partial \xi} = 1 + \frac{G_0^4}{\omega_0} f(\eta) \frac{\partial Q}{\partial \xi} \quad (6-21)$$

$$\text{and } J\left(Q, \frac{1}{\omega_0} \frac{\partial Q}{\partial \xi}\right) = f(\eta) \left(1 + \frac{G_0^4}{\omega_0} f(\eta) \frac{\partial Q}{\partial \xi} \right) \quad (6-22)$$

In equation (6-22), J denotes the Jacobian operator with ξ and η as the independent variables.

The problem has, therefore, been reduced to two simultaneous partial differential equations with Q and k as the dependent variables; for ω_0 can readily be eliminated by using equation (6-20). For the present, it is convenient to retain ω_0 in equation (6-22), since substitution for it will merely complicate the algebra unnecessarily. For the same reason, there is no point in 'simplifying' the problem further by the elimination of one of the dependent variables from equations (6-21) and (6-22), thus reducing the problem to a single partial differential equation. The function $f(\eta)$ that appears in these equations is a function of η only that must be

determined by the solution of the two differential equations.

The solutions for Q and k must be obtained within a quadrant bounded by the positive ξ - and η -axes and by the boundary curve C , given by equation (6-19). In this mode, unlike the slow mode considered in chapter 4, the boundary curve is not known and must be determined step by step from the solution for k and equation (6-19).

The boundary conditions on Q can be obtained by an argument almost completely identical with that used to determine the boundary conditions in the slow mode.

The resulting boundary conditions are, in fact, identical, and are, therefore, exactly those given in equations (4-84) to (4-86), namely

$$\begin{aligned}
 \text{on } \xi &= 0, & Q &= 0 \\
 \text{on } \eta &= 0, & Q &= 0 \\
 \text{on } C & & \frac{\partial^2 Q}{\partial \xi^2} &= 0 & (6-23) \\
 \text{on } C, & & \frac{\partial Q}{\partial \eta} &= -\frac{1 + \eta^2}{(1 - \eta^2)^{1/2}}
 \end{aligned}$$

These conditions must be supplemented by a single boundary condition for k as demanded by equation (6-21). This is simply the condition of symmetry that

$$\text{on } \xi = 0, \quad k = 0 \quad (6-24)$$

Equation (6-22) is of the same order as the equivalent differential equation for Q , namely (4-81), in the slow mode; moreover, they are very similar in form. Each is a quasi-linear hyperbolic equation of the second order involving a function of η that requires determination stage by stage as the solution is developed. The main differences between the two equations are, firstly, that in equation (6-22) Q is coupled with the function k , to which it is also related by the first order differential equation (6-21) - this evidently requires the single boundary condition supplied by equation (6-24) - and, secondly, that the boundary conditions for Q are specified, in equations (6-23), on a curve C that is still to be determined. This second point does not, however, affect the boundary condition requirements in any way, since examination of the characteristics on this curve shows that they are of the same form as those considered earlier; that is, the characteristics of equation (6-22), considered as a second order partial differential equation in Q , touch on the curve C . The arguments, therefore, that were used in chapter 4 to justify the number and form of the boundary conditions on Q can be carried over to the present problem with only minimal

modifications. . . It is expected, therefore, that the problem as stated in equations (6-21) to (6-24) will be definitive for a given value of G_0 .

The most important difference between the two modes, however, is not a question of the application of the boundary conditions, but rather the fact that, in this fast mode, the parameter G_0 appears explicitly in the differential equations. . . In general, therefore, the solution for Q will depend on G_0 . . . In the slow mode, on the other hand, Q was independent of this parameter.

It should be noticed from equation (6-21) that, for $G_0 = 0$, equation (6-20) reduces to the form

$$\omega_0 = \frac{1}{2} \left(\frac{1 - \eta^2}{(1 + \eta^2)^2} - \xi^2 \right) \quad (6-25)$$

In this case, then, the boundary curve C is identical with that obtained in the slow mode. . . For this curve is simply given by $\omega_0 = 0$. . . Further, with $G_0 = 0$, the differential equation for Q will reduce to

$$\mathcal{J} \left(Q, \frac{2(1 + \eta^2)^2}{1 - \eta^2 - \xi^2(1 + \eta^2)^2} \frac{\partial Q}{\partial \xi} \right) = f(\eta) \quad (6-26)$$

which is identical in form with the equivalent equation, (4-81), in the slow mode. . . Since the boundary conditions on Q are in any event identical in the two modes, it is clear that in this special case the solution for Q is the same as the equivalent function in the slow mode. . . This, indeed, would be expected.

For a general value of G_0 , however, the curve C will, as already mentioned, depend on the solutions for Q and k , and must be determined from these solutions. So the shape of the boundary will itself depend on the value of G_0 . Indeed, unlike the slow mode, in which the shape of the boundary is always given by the same closed curve, namely the oval

$$1 - \eta^2 - \xi^2(1 + \eta^2)^2 = 0 \quad (6-27)$$

it is now possible that, for certain values of G_0 , the boundary derived from the solutions may be an open curve. Before discussing further the shape of the boundary, it should be stressed that, should the boundary curve C splay out and become parallel to the ξ -axis at any point, a singularity will be encountered at that point, and it will be impossible to proceed with the solution above that level. Such a point will, therefore, be referred to as the end-point of the boundary curve C .

There are five possibilities for the siting of such an end-point. They are as follows:-

- (i) The end-point is the point $(0, 1)$, as in the slow mode.
- (ii) The end-point is a finite point on the line $\eta = 1$.
- (iii) The end-point is a point at infinity on the line $\eta = 1$.

(iv) The end-point is a finite point for which $\eta < 1$.

(v) The end-point is a point at infinity for which the limiting value of η as $\xi \rightarrow \infty$ is less than 1.

Of these five possibilities for the site of the end-point only the first two will provide acceptable solutions.

It is possible that these considerations may provide a criterion to determine an upper bound for G_0 which would make this fast mode definitive. For the mode will indeed be definitive if the conditions (i) and (ii), cited above, break down for sufficiently large G_0 . Such a possibility is entirely absent in the slow mode. A complete discussion of this point must, however, await the complete evaluation of the solutions of Q and k , and their determination of the shape of the boundary curve. Such complete solutions are not attempted in the present thesis.

(ii) Solutions on the ξ -Axis.

Although no attempt is made to determine complete solutions of equations (6-21) - (6-24), the remainder of this chapter will examine some solutions of these equations on the ξ -axis, in the hope that some insight may be given regarding the definitiveness of the solution. In particular, the curvature of the boundary will be investigated at the point where it crosses the ξ -axis.

From the second condition in equation (6-23), it follows that $\partial Q/\partial \xi$ (and its ξ -derivatives) are zero on the line $\eta = 0$. Equation (6-21), therefore, integrates to give, on using (6-24),

$$K(\xi, 0) = \xi \quad (6-28)$$

Equation (6-20) can now be written as

$$\omega_0(\xi, 0) = \frac{1}{2} (1 - \xi^2) \quad (6-29)$$

To obtain any significant information from the remaining equation (6-22) one must first differentiate it partially with respect to η . The results of equations (6-28) and (6-29) can then be substituted into the differentiated form of this equation. In addition, make a substitution analogous to that made in chapter 5, putting

$$g(\xi) = - \left(\frac{2}{f'(0)} \right)^{1/2} \left(\frac{\partial Q}{\partial \eta} \right)_{\eta=0} \quad (6-30)$$

An ordinary differential equation is then obtained for $g(\xi)$, viz.

$$(1 - \xi^2)(g'^2 - g g'') - 2\xi g g' = (1 - \xi^2)^2 \quad (6-31)$$

It will be immediately noticed that this equation is identical with the equivalent equation, (5-5), developed in chapter 5. And since, as already observed, the boundary conditions on Q are identical in the two modes, the same must be true for the solutions of the

functions $g(\xi)$. The whole of the numerical analysis of chapter 5 may, therefore, be carried over into the new mode, and the solutions for $g(\xi)$ and $h(\xi)$ are as tabulated in Appendix (5-2). The function $h(\xi)$ is defined in the same manner as in Appendix (5-1), namely

$$h(\xi) = g(\xi) g'(\xi) \quad (6-32)$$

In particular, the following result is obtained from the application of the analysis of chapter 5,

$$f'(0) = \frac{2}{\Lambda_0^2} = 6.429 \quad (6-33)$$

on using the result given by equation (5-14).

The solutions for k and $\partial Q/\partial \eta$, therefore, are known on $\eta = 0$, and these may be used to examine the curvature of the boundary at the point where it cuts the ξ -axis. It will again be convenient to represent the boundary curve C by the equation

$$\xi = \xi_0(\eta) \quad (6-34)$$

Moreover, on the ξ -axis, one may state at once that

$$\begin{aligned} \xi_0(0) &= 1 \\ \xi_0'(0) &= 0 \end{aligned} \quad (6-35)$$

the latter condition must follow from symmetry. The curvature of the boundary is determined by the second derivative of $\xi_0(\eta)$. This curvature will clearly be outwards or inwards (i.e. away from or towards the

η -axis), according as $\xi_0''(0)$ is greater or less than zero.

Let us write the boundary condition on the magnetic field, equation (6-19), in the form

$$k(\xi_0, \eta) = \frac{(1-\eta^2)^{1/2}}{1+\eta^2} \quad (6-36)$$

Now differentiate this equation twice totally with respect to η to obtain, on $\eta = 0$.

$$\frac{d^2}{d\eta^2} \left[\frac{(1-\eta^2)^{1/2}}{1+\eta^2} \right] = \frac{\partial^2 k}{\partial \eta^2} + \frac{\partial k}{\partial \xi} \frac{d^2 \xi_0}{d\eta^2} \quad (6-37)$$

The other differentiated terms that have been omitted from the right hand side of equation (6-37) vanish due to the second condition of equation (6-35).

Substitution can now be made for $\partial k / \partial \xi$ from equation (6-28), and if the necessary differentiation is carried out to evaluate the left hand side for $\eta = 0$, equation (6-37) will take the form

$$\left[\frac{d^2 \xi_0}{d\eta^2} \right]_0 = -3 - \left(\frac{\partial^2 k}{\partial \eta^2} \right)_0 \quad (6-38)$$

Here the subscript zero has been used outside the brackets to indicate that the function in question is evaluated at the point $\xi = 1, \eta = 0$.

The final term on the right hand side of equation (6-38) must now be evaluated. Differentiate equation (6-21) twice partially with respect to η . On throwing

away the terms that vanish on the ξ -axis for reasons of symmetry, one is left with the following equation on that line

$$\frac{\partial^3 k}{\partial \xi \partial \eta^2} = \frac{1}{\omega_0} \frac{\partial^2 \omega_0}{\partial \eta^2} \left(1 - \frac{\partial k}{\partial \xi} \right) + 2 G_0^4 \frac{f'(0)}{\omega_0} \frac{\partial^2 Q}{\partial \xi \partial \eta} \quad (6-39)$$

Next substitute for k on the ξ -axis from equation (6-28).

Then the first term on the right hand side vanishes.

Further, since by equation (6-24), $\partial^2 k / \partial \eta^2 = 0$ at the origin, equation (6-39) can be written in integral form

as

$$\left(\frac{\partial^2 k}{\partial \eta^2} \right)_0 = 2 G_0^4 f'(0) \int_0^1 \left(\frac{1}{\omega_0} \frac{\partial^2 Q}{\partial \xi \partial \eta} \right)_{\eta=0} d\xi \quad (6-40)$$

Finally, substitute for $f'(0)$, $\omega_0(\xi, 0)$, and $Q(\xi, 0)$ from equations (6-33), (6-29) and (6-30) respectively, to obtain

$$\left(\frac{\partial^2 k}{\partial \eta^2} \right)_0 = - \frac{8 G_0^4}{\Lambda_0^3} J \quad (6-41)$$

Here J is the definite integral given by the equation

$$J = \int_0^1 \frac{h(\xi) d\xi}{(1-\xi^2) g(\xi)} \quad (6-42)$$

Then from equation (6-38) it follows that

$$\left(\frac{d^2 \xi_0}{d\eta^2} \right)_0 = \frac{8 G_0^4}{\Lambda_0^3} J - 3 \quad (6-43)$$

Let G_M be the value of G_0 that makes the right hand side of equation (6-43) zero; that is define G_M as

$$G_M = \left(\frac{3 \Lambda_0^3}{8 J} \right)^{1/4} \quad (6-44)$$

Then G_M is the value of the parameter G_0 which divides those solutions whose boundaries curve outwards from the ξ -axis ($G_0 > G_M$) from those whose boundaries curve in ($G_0 < G_M$). It is thus seen that for large G_0 the boundaries will have radically different shapes from those obtained for small values of G_0 , which in the limit approach the same closed oval as found in the slow mode. An argument can be advanced to suggest that, if this fast mode is definitive, and if, therefore, G_0 is restricted to a finite range of values, then the maximum value of G_0 will be less than G_M . This argument, however, is not complete and must remain speculative until the entire solutions of the problem are obtained. Nonetheless, it is possible that G_M may give an order of magnitude estimate of the maximum value of G_0 , should this maximum exist.

Finally, for completeness, the value of G_M is derived. The functions $g(\xi)$ and $h(\xi)$ are tabulated with considerable accuracy in Appendix (5-2). These values can readily be used in a numerical integration of equation (6-42) to determine J . Owing to the fact that in Appendix (5-2) both $g(\xi)$ and $h(\xi)$ are tabulated at a fairly close interval - in fact, an interval of 0.01 - Simpson's rule provides a simple and entirely

adequate method of integration. Integrating, then, by this method it is found that $J = 0.6951$. Using this value and that obtained for Δ_0 from equation (5-10), the result

$$G_M = 0.4651 \quad (6-45)$$

is readily obtained from equation (6-44). Lacking the final solutions one may tentatively regard this value as an order of magnitude estimate for G_0 appropriate to the new mode.

CHAPTER 7.

THE PARKER MODES UNDER SOLAR CONDITIONS

(1) Time-Scales

In previous chapters three distinct modes of interpenetration have been considered. These were Parker's incompressible mode and the two compressible modes that were studied in detail in chapters 4 - 6. In testing the application of the mechanism to solar flares, it will be convenient to compare the rates of these three different modes of field annihilation. For this purpose, Parker's incompressible mode, and the slow and the fast compressible modes will be referred to as the first, second and third modes respectively, and designated by the subscripts 1, 2, 3.

The velocity of interpenetration has already been estimated to order of magnitude for the first two modes. The formulae are given in equations (4-8) and (4-15). If it is assumed that the dimensionless parameter G_0 , used in the analysis of the fast mode, is of order unity, then the velocity of interpenetration for this mode can readily be evaluated from equations (6-7) and (4-56). For convenience, let us restate the formulae for the velocity of interpenetration; they are

$$\begin{aligned}
 v_1 &\sim (v_D v_A)^{\frac{1}{2}} && \text{(incompressible)} \\
 v_2 &\sim \left(\frac{v_D}{v_S}\right)^{\frac{1}{2}} v_A && \text{(Parker compressible)} \\
 v_3 &\sim \frac{(v_D v_A^3)^{\frac{1}{2}}}{v_S} && \text{(fast compressible)}
 \end{aligned}
 \tag{7-1}$$

It will be noted that the three velocities of interpenetration are in geometrical progression, the common ratio being the fourth root of the compression factor $(v_A/v_S)^2$. This central compression, which is the same in each of the compressible modes, is simply the compression required to provide a gas pressure along the neutral line sufficient to balance the external magnetic pressure. Its effect, in each compressible mode, is to decrease the thickness of the current sheet, thereby reducing the distance across which resistive diffusion must act. The essential difference between the two compressible modes lies in the velocity of ejection along the current sheet. In the slow compressible mode this is the sound velocity, i.e. the Alfvén velocity for the compressed gas. In the fast mode, however, the ejection velocity is the Alfvén velocity calculated for the ambient gas. In the latter case more lines of force from the external field cross the current sheet. The rate of ejection is then not

determined by the high density of the small amount of material in the current region, but rather by conditions exterior to the pinch.

The total energy dissipated in the simple model that has been discussed above will be of order $(H_0^2 / 8\pi) L^2 L_z$, where L_z is the extension of the assumed two-dimensional system in z-direction. From the discussion of chapter I, it follows that, to account for a large flare event, this energy must be of order 10^{32} ergs. This could be achieved with the following values

$$\begin{aligned} H_0 &= 500 \text{ gauss} \\ L &= 10^9 \text{ cm} \\ L_z &= 10^{10} \text{ cm} \end{aligned} \tag{7-2}$$

which are not inconsistent with the expected chromospheric conditions. The magnetic intensity given is perhaps a slightly large, but not unreasonable, value for the field in the chromosphere above an active region. The choice of the relative sizes of L and L_z is somewhat arbitrary. This particular choice is suggested by the observed filamentary structure in the early stages of the development of some flares. It may be significant that the values of L and L_z that have been chosen correspond quite well with the half-widths and lengths that are

typical of large flare filaments. Hence equations (7-2) provide reasonable values for the parameters H_0 , L and L_z that will supply sufficient energy for a large flare.

In equations (4-1) to (4-3) the characteristic velocities v_A , v_S and v_D were expressed in terms of five physical parameters, namely H_0 , L , σ , T , and ρ_0 . Of these parameters, σ will be a function of temperature. In a highly ionized gas one may write with sufficient accuracy

$$\sigma \sim 1.3 \cdot 10^7 T^{3/2} \quad (7-3)$$

Further, it will be convenient to work in terms of a particle density rather than the gas density ρ_0 .

Let N_0 denote the ambient particle density. Then, on using the values given in equations (7-2) and (7-3), the definitions of the characteristic velocities yield the following results:

$$\begin{aligned} v_A &\sim 1.1 \cdot 10^{14} N_0^{-1/2} \\ v_S &\sim 1.3 \cdot 10^4 T^{1/2} \\ v_D &\sim 6 \cdot 10^3 T^{-3/2} \end{aligned} \quad (7-4)$$

Now let τ_i denote the time-scale of interpenetration of the i -th mode, based on the values given in equation (7-2). Then one can write with sufficient accuracy

$$\tau_i = \frac{10^9}{v_i} \quad i = 1, 2, 3 \quad (7-5)$$

Justification of this is provided by the analysis of chapter 5 section (iii). From equations (7-1), (7-4) and (7-5) it follows that

$$\begin{aligned}
 \tau_1 &= 1.2 T^{3/4} N_0^{1/4} \\
 \tau_2 &= 1.3 \cdot 10^{-5} T N_0^{1/2} \\
 \tau_3 &= 1.5 \cdot 10^{-10} T^{5/4} N_0^{3/4}
 \end{aligned} \tag{7-6}$$

From equations (7-6) it should be noted that the rate of interpenetration of any of the modes will decrease with increasing temperature or particle density.

It is of interest to examine the variations of the time-scales with height in the chromosphere and low corona. A similar investigation has been made by Hoyle and Wickramasinghe⁽¹¹⁹⁾ of the variation in the high corona of the rate of interpenetration in the second of the modes under discussion here. In the solar atmosphere the temperature and particle density gradients are in opposite directions, and whereas the decrease in density with height tends to allow faster rates of interpenetration, the increasing temperature tends to counteract any such increase. The time-scales for the three modes have been plotted in Figure (7-1), using equations (7-6). The distribution of T and N_0 with height is taken from the composite model given by Allen⁽¹²⁰⁾. The full details of this distribution

and the resulting values of the τ_i 's are given in Appendix (7-1).

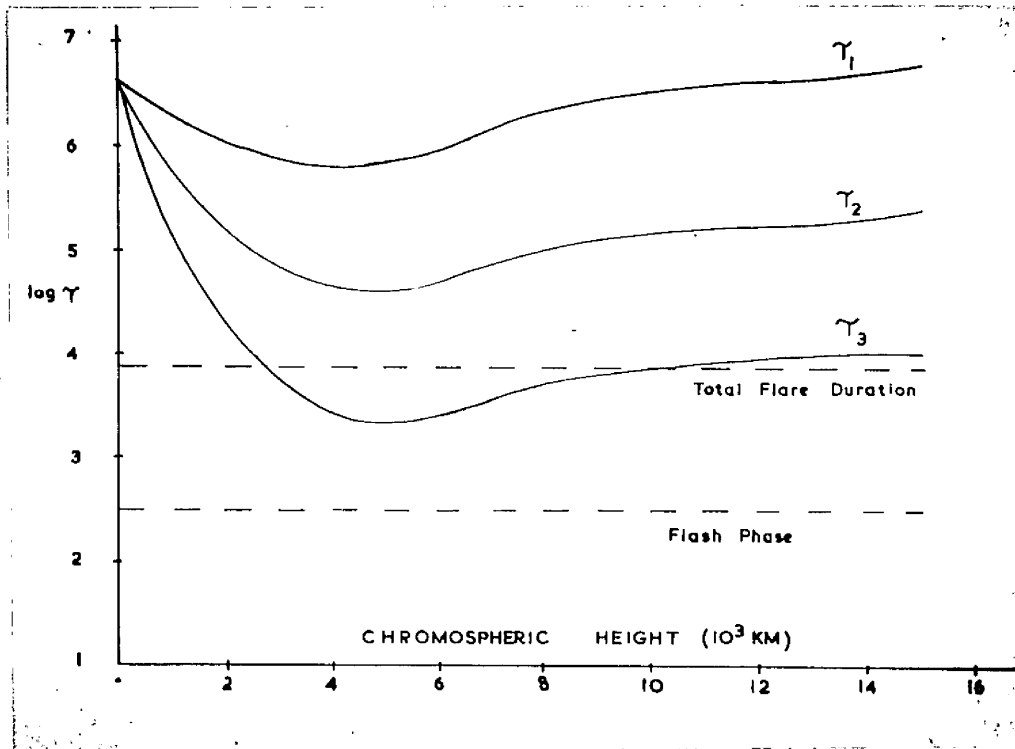


Fig (7-1). Plot of the time-scales of the three modes of field annihilation against chromospheric height. ($H_0 = 500$ gauss, $L = 10^4$ km).

From the graphs of Figure (7-1), it is seen at once that all three modes of interpenetration have maximum annihilation rates in the middle chromosphere. The effect of the decrease of magnetic field strength with height, neglected in Figure (7-1), is to increase the interpenetration time with increasing height, but

this will not destroy the feature of the maximum interpenetration rate shown in the diagram.

The time-scales of the three modes must be compared with the equivalent time-scales of solar flares. It has for many years been normal practice to attempt to identify the annihilation time with the duration of the flash phase. Certainly the flash phase is a predominant feature of the flare event, and the subsequent decay could be a relaxation process. Wentzel⁽¹²¹⁾ has criticized this interpretation on the grounds that this point of view requires that all the magnetic energy be dissipated into heat during the flash phase, and that all subsequent radiation is at the expense of this thermal energy store. He argues that if this were the case, the flare should be very hot at the time of maximum intensity which would be followed by a gradual decrease in temperature. Electron temperatures determined throughout the flare are, however, comparatively constant. Wentzel maintained, therefore, that the identification of the annihilation time with the flash phase was inconsistent with observation. It must be remembered, however, that such electron temperatures are extremely uncertain. Nevertheless, there is certainly a case for arguing that the relevant time-scale of the flare to be

compared with the rate of dissipation of magnetic energy is not the flash phase but the total duration of the flare.

For a 3+ flare, the mean total duration⁽¹²⁾ is more than two hours. The flash phase, on the other hand, lasts about five minutes. In Figure (7-1) these time-scales have been indicated, and it is at once seen that only the fastest mode can give interpenetration times shorter than either of these two time-scales.

As pointed out in chapter 1, flare observations indicate ambient particle densities in the flare region of order 10^{11} particles per cm^3 , and temperatures of the order of 10^4 °K. It should perhaps be noticed that a particle density of 10^{11} particles per cubic cm corresponds closely with the height at which the interpenetration rate is a maximum. In fact, substitution of the values just given into equations (7-6) yields

$$\begin{aligned} \tau_1 &\sim 6.8 \cdot 10^5 \text{ sec} \\ \tau_2 &\sim 4.1 \cdot 10^4 \text{ sec} \\ \tau_3 &\sim 2.7 \cdot 10^3 \text{ sec} \end{aligned} \quad (7-7)$$

From these values, it is again clear that only the fast mode can give a time of interpenetration appropriate to the solar flare problem. The shortest time-scale derived in equations (7-7), of about $\frac{3}{4}$ hour, is sufficiently rapid to account for the decay phase of a

solar flare. An interpenetration time of the order of the flare rise-time cannot be achieved by the present theory.

The results, therefore, are not wholly satisfactory. The best that can be said is that the fast mode can account for the decay times of large flares over a wide range of heights in the chromosphere and low corona. As it is intended to show, however, this fast mode requires rather special circumstances that will not, in general, be met in actual magnetic configurations. Although the rates of interpenetration do seem too slow to account satisfactorily for solar flares, it should be pointed out that it has not been proved that the fast mode is definitive; and the development of the form of the current sheet, as the parameter G_0 is increased, is unknown. The fast mode should, therefore, be regarded as a lower limit to the interpenetration rate, for the case where compressibility is important.

(ii) Effects of Ambipolar Diffusion

Gold and Hoyle⁽⁴⁰⁾ have suggested that an enhanced dissipation of magnetic energy can be provided in the solar flare problem by the effects of ambipolar diffusion. Parker⁽⁵⁹⁾ has criticized this suggestion, however, pointing out that the compression of the gas will reduce

such effects. This objection is most easily demonstrated in the following way.

Let n be the ion density, and f the fraction of neutral atoms that are present in the gas, which, it is supposed, is composed entirely of hydrogen. Let N be the total density of ion and neutral particles. Next let V_i, V be the collision frequencies for the ions with neutral particles and electrons respectively; and let ω, ω_i be the angular gyro-frequencies of electrons and ions respectively, so that

$$\omega = \frac{eH}{mc}, \quad \omega_i = \frac{eH}{m_i c} \quad (7-8)$$

where m, m_i are the electron and ion masses. Finally introduce the dimensionless parameters

$$\kappa = \frac{V}{\omega}, \quad \kappa_i = \frac{V_i}{\omega_i} \quad (7-9)$$

Now following Cowling's treatment⁽¹²²⁾, one may include the effects of ambipolar diffusion in the conductivity equation, writing it, with sufficient accuracy for conditions in the solar atmosphere, as

$$\underline{E} + \frac{\underline{v} \wedge \underline{H}}{c} = \frac{\underline{j}}{\sigma} - \frac{2f^2}{\kappa_i nec H} (\underline{j} \wedge \underline{H}) \wedge \underline{H} \quad (7-10)$$

However, it should be noted that the conductivity σ can be written as

$$\sigma = \frac{ne^2}{m \kappa \omega} = \frac{nec}{\kappa H} \quad (7-11)$$

Now in the two-dimensional model $\underline{j} \cdot \underline{H} = 0$. So it is clear that the conductivity equation (7-10) can be written as

$$\underline{E} + \frac{\underline{v} \wedge \underline{H}}{c} = \frac{\underline{j}}{\sigma'} \quad (7-12)$$

where σ' is a modified conductivity. On using equations (7-10) to (7-12), this modified conductivity will be given by

$$\frac{1}{\sigma'} = \frac{1}{\sigma} \left(1 + \frac{2f^2}{\kappa \kappa_i} \right) \quad (7-13)$$

In this problem, then ambipolar diffusion is equivalent to a reduction in the effective conductivity. Parker⁽⁵⁹⁾ has made clear the physical effects of ambipolar diffusion in the type of current region under discussion. The ambipolar diffusion cannot itself produce the actual reconnection of the lines of force; the flux linkages can only be altered as a result of Joule dissipation. However, ambipolar diffusion allows the ionized component to drift through the neutral gas, and allows the magnetic field which is frozen to this ionized component to proceed to configurations of lower energy. Near the neutral line the lines of force pile up to produce a very steep field gradient. Thus a thin region of increased Joule dissipation is formed which produces the necessary reconnection of the magnetic field lines. The presence of ambipolar diffusion, therefore,

enhances the rate of interpenetration by allowing the region of current density to constrict itself, so reducing the distance over which resistive diffusion must operate. The total Joule dissipation, though confined to a narrower region, is increased, but the main dissipation process of magnetic energy is obtained from collisions of the ionized component with neutral particles occurring over a much wider area.

The reduction in the conductivity will be important if

$$\frac{2f^2}{\kappa \kappa_i} \gg 1 \quad (7-14)$$

It will be convenient to denote the left hand side of this inequality by R . Now from equations (7-1), it is seen that in all three modes the rate of interpenetration is directly proportional to $v_D^{\frac{1}{2}}$. The time-scales, then, are directly proportional to $\sigma^{\frac{1}{2}}$. If ambipolar diffusion is important, and, therefore, $R \gg 1$, then as a rough approximation, one may replace σ in the formulae for the time-scales of field annihilation by the modified form of the conductivity given in equation (7-13). Thus ambipolar diffusion has the effect of reducing the time-scale by a factor of order $R^{\frac{1}{2}}$.

To estimate the significance of ambipolar diffusion, R must be computed. From equations (7-8), (7-9) and

(7-11) the result is obtained that

$$R = \frac{2 f^2 \sigma H^2}{c^2 n m_i v_i} \quad (7-15)$$

Write

$$f = \frac{n_a}{N} \quad (7-16)$$

$$v_i = n_a A_i w_i$$

Here n_a is the density of neutral atoms, A_i is the collisional cross-section for collisions between the ions and the neutral particles, and w_i is the ion thermal velocity. Then from equations (7-15) and (7-16), it follows that

$$R = \frac{\sigma H^2 n_a}{c^2 m_i A_i w_i n N^2} \quad (7-17)$$

For the present purpose, only a rough order of magnitude value of R is required. So let us take the following values of the physical parameters, which will be reasonably appropriate to the flare problem

$$\begin{aligned} H &\sim 500 && \text{gauss} \\ \sigma &\sim 10^{13} && \text{e.s.u.} \\ w_i &\sim 10^6 && \text{cm sec}^{-1} \\ N &\sim 10^{11} && \text{cm}^{-3} \end{aligned} \quad (7-18)$$

Finally take $A_i \sim 10^{-16} \text{ cm}^2$ in what follows. With these values equation (7-17) gives

$$R \sim 1.7 \cdot 10^9 \frac{n_a}{n} \quad (7-19)$$

From this equation it must be concluded that, for values of the parameters given by equation (7-18), only a very small percentage of neutral atoms is required to make the effects of ambipolar diffusion rather important.

From equation (7-19) one would expect a very significant enhancement of the annihilation rate under flare conditions. As Parker has pointed out, however, the result is illusory. Under steady conditions, the appropriate value of the total particle density N in equation (7-17) is not that of the ambient gas, but rather that of the compressed gas in the current region. For pressure balance it is necessary that

$$N \sim \left(v_A / v_s \right)^2 N_0 \quad (7-20)$$

where N_0 is specifically the ambient particle density - as in the last section. Denote the value of R resulting from this substitution by R_1 . Now, substituting for N and H in terms of the characteristic velocities, and further putting $w_1 = v_s$, it is found that equation (7-17) will be replaced by

$$R_1 = \frac{4 \pi \sigma v_s^3 n_a}{c^2 A_i N_0 v_A^2 n} \quad (7-21)$$

It is this equation, not (7-17), which must be used to determine the value of R , on which any increase in the reconnection rate depends.

The effects of ambipolar diffusion on either of the two compressible modes considered in earlier chapters can now be computed. Substitute into (7-21) the values of σ , v_A , and v_S from equations (7-3) and (7-4), which are based on a 500 gauss magnetic field. Equation (7-21) can then be written in numerical form as

$$R_1 = 3.3 \cdot 10^{-13} T^3 \frac{n_a}{h} \quad (7-22)$$

In Figure (7-2) $\log_{10} R_1$ has been plotted as a function of height in the solar atmosphere. As before, Allen's data has been used to give the temperature variation and the total particle density in the chromosphere and low corona. In the upper half, allowance has been made for the fact that at higher levels ionization is caused primarily by electron collisions and recombinations are radiative. A formula for the degree of ionization given by Allen⁽¹²³⁾ was used.

While the values of R_1 shown in Figure (7-2) must be rather uncertain, they are sufficient to show that no large increase can be achieved in the interpenetration rate due to the effects of ambipolar diffusion. The high gas density in the pinch, necessary to balance the external magnetic pressure, chokes any relative motion between the ionized and neutral components of the gas.

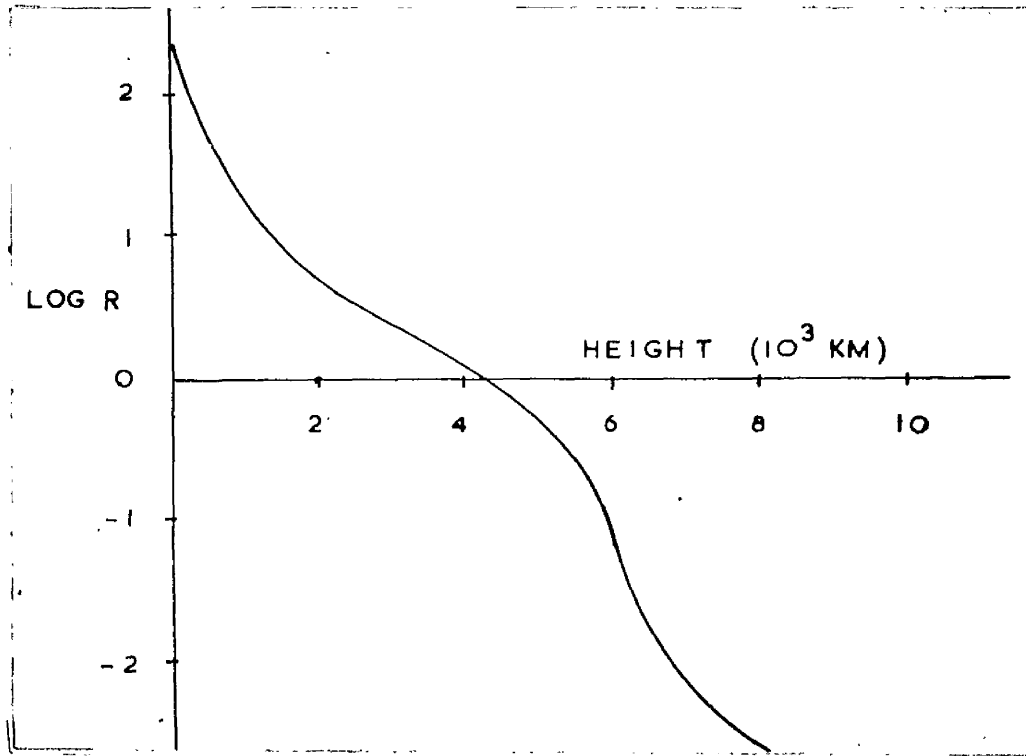


Fig (7-2). Variation of the parameter R_1 with chromospheric height.

(iii) The Effects of a z-Field.

The models considered up to this stage have been two-dimensional; the magnetic field was independent of the z-coordinate and had no component in the z-direction. These assumptions are, of course, quite artificial, and one cannot expect them to be satisfied, in general, in the solar atmosphere. What is more important is the fact that the second assumption affects significantly the rate of interpenetration derived.

To examine this point, suppose that in addition to the components of the field that lie in the $x - y$ plane, there is a component in the z -direction. The two colliding fields are then not exactly antiparallel. The neutral line in the two-dimensional field is now a line of force. Whereas the y -component of the field changes sign across the sheet current, the z -component does not. Now, in the two-dimensional case, to achieve pressure balance in the x -direction, a high gas pressure was required along the centre of the current sheet. In every mode this condition of pressure balance was expressed by the x -component of the equation of motion. When a z -field is present, however, this z -component is not zero along the centre of the sheet current, and the compression of the gas need only be sufficient to compress this component so that $H_z^2/8\pi$ can balance the total external magnetic pressure. The x -component of the equation of motion, when $v_S^2 \ll v_A^2$, can be written to a first approximation as

$$(\text{curl } \underline{H} \wedge \underline{H})_x = 0 \quad (7-23)$$

On neglecting the x -component of the magnetic field, this equation integrates to give

$$\frac{H_y^2 + H_z^2}{8\pi} = F(y) \quad (7-24)$$

If the z-component of the field is of the same order in the ambient gas as the component lying in the x - y plane, then only a moderate compression of the gas will be required to provide the increase in the H_z -field necessary to satisfy equation (7-24).

In the general case, therefore, where the field has a significant z-component, high compression is prevented by the presence of this component, and the rate of interpenetration is correspondingly reduced. The system behaves, therefore, as in the incompressible mode, and, as Figure (7-1) indicates, throughout the solar atmosphere this mode is quite inadequate to account for the features of solar flares.

A complete treatment of the case where a z-field is present would be extremely involved. For all the difficulties encountered in the two-dimensional incompressible mode in chapter 4 are present, and, in addition, the situation is complicated by gas motions induced in the z-direction which cannot be ignored. In deriving the order of magnitude solution, however, it is noted that the same equations are valid as for the incompressible case, namely (4-4), (4-5) and (4-6). Consequently the order of magnitude solution is identical with that of the incompressible mode and is, therefore given by

$$\begin{aligned} v_0 &\sim (\nu_D \nu_A)^{1/2} \\ l &\sim \left(\frac{\nu_D}{\nu_A}\right)^{1/2} L \end{aligned} \quad (7-25)$$

It might at first appear that the z-field's inhibition of the compression of the gas might allow ambipolar diffusion effects to be significant. As equation (7-23) shows, however, the field must be force-free in the x-direction, and, therefore, the ambipolar diffusion term in equation (7-10), which would otherwise be dominant, is zero to first order. But the field need not be completely force-free, and so ambipolar diffusion might still be important. In the equation of motion the magnetic force term must be as large as the pressure gradient, and this could still be sufficient to make the ambipolar diffusion term significant in the conductivity equation. Further and more detailed investigations of the effects of ambipolar diffusion in this connection are required before any definite conclusions can be reached. It is quite certain, however, that the ambipolar diffusion term does not have the dominance that would be suggested by equations (7-17) and (7-19).

CHAPTER 8

THE SEVERNY-WENTZEL MECHANISM

The complexity of the problem has prevented anything other than a steady two-dimensional analysis of the process of the dissipation of magnetic energy. In the work of Parker, in the present analysis, and in the work of Petschek to be discussed later, time-independent configurations have been examined in two dimensions. Dungey⁽¹²⁴⁾ and Severny⁽³¹⁾, on the other hand, have argued that the collapse resulting from an instability in the magnetic configuration near a neutral point does not lead to the setting up of a steady state. Severny has, therefore, considered a time-dependent system. The model adopted was one-dimensional. The argument in a crude form, is that as the collapse proceeds the magnetic field and the gas density are built up at the same rate. However, the magnetic pressure which is responsible for the compression increases as the square of the field, while the gas pressure is proportional to ρ^γ , and in all cases $\gamma < 2$. Hence the magnetic forces causing the collapse are built up more rapidly than the pressure forces reacting against it. As Syrovatskii⁽¹²⁵⁾ has pointed out in a criticism of Severny's work, however, considerable care is required

in applying this kind of argument. In the discussion of Severny's mechanism (31,34,126) that follows, it is intended to point out the restrictive conditions under which Severny's analysis may be applied.

Let us consider the magnetic field configuration which is represented by

$$\begin{aligned} \underline{H} &= (0, H(x, t), 0) \\ H(0, t) &= 0 \end{aligned} \quad (8-1)$$

So the field is directed everywhere in the y-direction and depends only on the x-coordinate. Moreover, the plane $x = 0$ is a neutral plane. For simplicity, symmetry is assumed about this plane; then the discussion may be confined to the field on one side of it.

It will be convenient to use the Lagrangian form of the fluid equations, so put

$$x = x(X, t) \quad (8-2)$$

where x is the coordinate of a fluid particle whose coordinate was initially X . Hence

$$x(X, 0) = X \quad (8-3)$$

Finally, suppose that, at time $t = 0$, the field, the density, and the pressure distributions are respectively given by

$$\begin{aligned} H &= H_0(X) \\ \rho &= \rho_0(X) \\ P &= P_0(X) \end{aligned} \quad (8-4)$$

In this simple one-dimensional case, the equation of motion in Lagrangian form can be written as

$$\int \frac{\partial^2 x}{\partial t^2} = - \frac{\partial}{\partial x} \left(\frac{H^2}{8\pi} + P \right) \quad (8-5)$$

The equation for the conservation of mass becomes

$$\int dx = \int_0 dX \quad (8-6)$$

Substituting from this equation into (8-5) will yield a simpler form of the equation of motion, viz.

$$\int_0 \frac{\partial^2 x}{\partial t^2} = - \frac{\partial}{\partial X} \left(\frac{H^2}{8\pi} + P \right) \quad (8-7)$$

Next perfect conductivity is assumed; the condition for the resulting conservation of magnetic flux can be written as

$$H dx = H_0 dX \quad (8-8)$$

Finally if radiative and other energy losses are neglected, there is the adiabatic equation, viz.

$$P = P_0 \left(\frac{\rho}{\rho_0} \right)^\gamma \quad (8-9)$$

From equations (8-8), (8-9) and (8-6), the variables H and P may be eliminated from the equation of motion, replacing them with the initial distributions, H_0 and P_0 . Equation (8-7) then becomes

$$\int_0 \frac{\partial^2 x}{\partial t^2} = - \frac{\partial}{\partial X} \left[\frac{H_0^2}{8\pi} \left(\frac{\partial x}{\partial X} \right)^{-2} + P_0 \left(\frac{\partial x}{\partial X} \right)^{-\gamma} \right] \quad (8-10)$$

Up to this point, with the physical assumptions made, the treatment has been exact. Equation (8-10) is, therefore, the complete differential equation of the system.

It should be noted - in passing - that it is a non-linear partial differential equation of the second order, and, therefore, of a rather complicated nature. Its solution for x , when the initial distributions ρ , H_0 , and P_0 are specified, requires a single external boundary condition. The initial boundary condition on x is given by equation (8-3).

To simplify the problem, Severny^(31,34) considered the case of homologous or what he termed 'automodal' compression. He assumed that the form of the material distribution was independent of time, and that, therefore, the solution of equation (8-10) had the simple separable form

$$\begin{aligned} x &= a(t) X \\ a(0) &= 1 \end{aligned} \quad (8-11)$$

With this substitution a very considerable simplification of the equation of motion is possible. Equation (8-10) reduces to the form

$$\rho X \frac{d^2 a}{dt^2} = - \frac{d}{dX} \left[\frac{H_0^2}{8\pi} \frac{1}{a^2} + \frac{P_0}{a\gamma} \right] \quad (8-12)$$

Suppose now that the system was initially in equilibrium, then one can write

$$H_0^2/8\pi + P_0 = P_n \quad (8-13)$$

where P_n is a constant - in fact, the initial value of the gas pressure on the neutral plane.

Now let X_0 be the initial half-width of the transition region of the magnetic field. Substitute for H_0 in equation (8-12) using the equilibrium condition (8-13), and integrate the resulting equation with respect to X , from $X = 0$ to $X = X_0$. The following equation is then obtained

$$\frac{d^2 a}{dt^2} = Q \left(\frac{1}{a^\gamma} - \frac{1}{a^2} \right) \quad (8-14)$$

where Q is given by

$$Q = \left[P_0 - P(X_0) \right] / \int_0^{X_0} \rho X dX \quad (8-15)$$

Equation (8-14) is essentially the equation studied and solved by Severny. Since $\gamma < 2$ - and of necessity $Q > 0$ - it is clear from this equation that a compression once started will proceed at an ever increasing rate. From this, Severny deduced that the equilibrium configuration of a magnetic field with a neutral plane is unstable. He concluded further that a compression, once it has begun, will proceed to an indefinite extent, since equation (8-14) indicates that there can be no equilibrium configuration other than $a = 1$, and this, it is claimed, is unstable.

Severny argued, therefore, that the compression proceeds until shocks are developed, which eventually stop the compression, and lead to an impulsive heating of the gas. The collapse towards the neutral surface was identified with the flash phase of the flare.

It proceeds at approximately the Alfvén velocity, which scale short enough to account for the flare's sudden even for a small field (~ 50 gauss) will provide a time-scale short enough to account for the flare's sudden rise to maximum. This 'instability' of the field, then, and the consequent collapse are the basis of Severny's theory of flares and of the theory of the acceleration of charged particles that he developed with Shabanskii (102,127).

Several criticisms can be made of the theory. For the present, attention will be concentrated on the restrictions that are imposed by Severny's approximation of automodal compression. Even if the assumption of equation (8-11) is made, it should be remembered that the equation of motion must still be examined in the form of equation (8-12), and not simply in its integrated form (8-14). Substituting the equilibrium condition, equation (8-13), it is possible to write (8-12) in the form

$$\left(\frac{1}{a\gamma} - \frac{1}{a^2} \right)^{-1} \frac{d^2 a}{dt^2} = - \frac{1}{\rho_0 X} \frac{d\rho_0}{dX} \quad (8-16)$$

Now by the definition of equation (8-11), the left hand side of this equation is a function of t only, the right hand side a function only of X . It follows that, in addition to equation (8-14), it is also required that

$$\frac{d\rho_0}{dX} + Q \rho_0 X = 0 \quad (8-17)$$

Thus for Severny's automodal compression to operate, the initial distributions P_0 and β_0 must satisfy the differential equation (8-17). A special class of equilibrium configuration is, therefore, required for Severny's analysis to be legitimate. Further, the condition (8-17), though necessary, is not sufficient for the compression to be of the uniform type specified by equation (8-11). The solution of the general form of the differential equation of the system, namely equation (8-10), requires two boundary conditions for a unique solution. Firstly there is the initial condition which is simply $x = X$, or in Severny's case $a(0) = 1$, and secondly there is the external boundary condition which, it may be supposed, is applied on the plane $X = X_0$. Such a condition will be of the form

$$x(X_0, t) = f(t) \quad (8-18)$$

For the compression to be of the automodal form considered by Severny, $f(t)$ must clearly, for self-consistency, be of the form

$$f(t) = X_0 a(t) \quad (8-19)$$

where $a(t)$ is the solution of the differential equation (8-14).

Equation (8-19) is the boundary condition that corresponds, not to the free collapse of the field, but

rather to a forced compression. From equations (8-6) and (8-11), it is seen that the pressure that must be applied on the external boundary, $X = X_0$, in order to sustain the automodal compression, is given by

$$P = P(X_0) \left(\frac{1}{a(t)} \right)^{\gamma} \quad (8-20)$$

From this equation it is clear that the automodal compression will only proceed to an indefinite extent if the externally applied pressure is increased without limit.

The principal criticism, then, of Severny's work is similar to that made of Dungey's discharge theory⁽¹¹⁵⁾ in chapter 2 (page 76). If a perturbation is made on the type of one-dimensional magnetic field with a neutral plane under consideration here, then the energy available to distort the magnetic configuration is precisely the perturbation energy and no more. The illusion of a free collapse of the field is created by forcing the boundary conditions, and the existence of an instability, in any real sense, has not been demonstrated.

To summarize, by his assumption of a uniform compression of the type given in equation (8-11), Severny claimed to give an example of a collapse of the magnetic field towards a neutral plane that would result in shock phenomena and a consequent severe heating of

the flare region. On the basis of this example, he drew rather general conclusions about the stability of such magnetic configurations. As the present analysis has shown, however, only a special class of initial equilibrium configurations can lead to such automodal compression under any external boundary conditions. Again, granted that such an initial configuration is attainable in practice, internal consistency requires that the external boundary condition be of the form of equation (8-20). The physical interpretation of such a boundary condition must be that the compression is of a special and forced type, and that the initial equilibrium configuration was such as to allow the compression to remain uniform. These considerations greatly reduce the generality of Severny's analysis, and any conclusion about the stability of the field resulting from it must be disregarded.

A theory similar to that of Severny has been developed very recently by Wentzel⁽¹²⁸⁾. Again a uni-dimensional time-dependent system was considered. In addition to the field components as represented by equation (8-1), however, Wentzel included a component in the z-direction that was initially uniform. The direction of the magnetic vector, therefore, instead of reversing across the transition region, is turned through

an angle of $\pi - 2\theta$ where $0 < \theta < \pi/2$, the size of θ depending on the relative strengths of the y- and z-components. The neutral plane is then replaced by a plane of minimum resultant field strength and, therefore, of minimum magnetic pressure.

Wentzel considered the collapse of the magnetic field towards this surface. In treating the dynamics, only the magnetic forces were considered; the effects of gas pressure were neglected. This is no doubt a reasonable approximation, since at the chromospheric levels at which flares occur, it is expected that the magnetic forces will be dominant. Thus the forces that react against the collapse and ultimately halt it are the magnetic forces built up by the compression of the constant z-field. Wentzel carried out an extensive numerical analysis of this type of collapse and of the resulting shock formation. A number of initial magnetic configurations were examined, and the effects of varying the angle of inclination θ were also computed. The situations initially assumed, however, did not correspond to equilibrium configurations. Such a theory, therefore, merely describes the behaviour of a system after an instability has fully developed, and thus has no bearing on the circumstances giving rise to the flare.

Probably Wentzel's work is quantitatively the most detailed that has been attempted in connection with solar flares. Reference has already been made to his contention⁽¹²⁴⁾ that the flash phase corresponds to the time of onset of the first visible effects of an initial instability, and that the proper time-scale for identification with the rate of magnetic energy dissipation is the total duration of the flare. On this point of view, the actual rate of optical emission in the flare will correspond to the rate of magnetic energy dissipation.

Wentzel proposed that the collapse towards the surface of minimum field strength leads to an onset of turbulence, if the velocity of collapse exceeds a certain arbitrary fraction of the local Alfvén velocity. He supposed that this turbulence persists throughout the flare, and that the emission of the optical flare is due to Joule dissipation of magnetic energy in the turbulent field of flow. He pointed to observations by Suemoto and Hiei⁽³²⁾ of the premaxima spectra of two small flares. These authors found that the electron densities derived from a Stark interpretation could only be reconciled with the electron densities derived from the line intensities if the total emission depth was as small as

10 km. Wentzel suggested, therefore, that the Joule dissipation is confined to the boundary layers of the turbulent eddies. The thickness of these layers is determined by the skin-depth through which the field can diffuse while the eddies are in contact. From order of magnitude calculations Wentzel concluded that his interpretation of the optical flare as Joule dissipation in a turbulent region was in accord with these observations. It must be remembered, however, that a thickness of 10 km is also consistent with the release of the whole of the magnetic energy in the flash phase by the current sheet mechanism.

Although there is some observational justification, therefore, for this important aspect of Wentzel's theory, it is felt that the identification of the magnetic dissipation time-scale with the total flare duration is somewhat arbitrary. Further, despite the detailed nature of his analysis of the collapse, Wentzel could only justify the onset of turbulence by a qualitative argument. The required turbulence is no more than hypothetical. Finally, as mentioned previously, the initial configurations that are studied in the numerical analysis are non-equilibrium configurations.

Consequently both the nature and the existence of the field instability are in this theory, unlike that of Severny, completely ignored.

CHAPTER 9

PETSCHER'S MECHANISM

The slowness of the interpenetration rate in the Parker current sheet mechanism prompted further attempts to show how this mechanism might be speeded up. It was suggested by Jaggi⁽¹²⁹⁾ that the type of resistive instability examined by Furth, Killeen and Rosenbluth⁽¹³⁰⁾ might develop in a current sheet of the kind that has been under discussion. This development would lead to a shortening of the scale length L and a corresponding enhancement of the interpenetration rate. The work of Furth, Killeen and Rosenbluth, however, is not of direct application to the solar flare problem, and Jaggi's analysis fails to give a clear estimate of what the revised interpenetration rate ought to be. A more satisfactory approach has been developed by Petschek⁽¹³¹⁾, who examined the effects of wave propagation on the interpenetration rate. Owing to the existence of a small component of the magnetic field perpendicular to the sheet current, it is possible that at a certain distance from the neutral point the velocity of propagation of Alfvén waves across the sheet may exceed the diffusion velocity. Wave propagation will then predominate over the diffusion mechanism, and the current sheet can bifurcate, leading to

a significant shortening of its effective length. An enhanced rate of interpenetration can thus be obtained. The discussion of flare mechanisms will be concluded with a fairly detailed account of Petschek's work. The account mainly concerns his adaptation of Parker's incompressible mode.

Petschek considered a two-dimensional system involving the collision of two regions of constant but oppositely directed magnetic field. If these magnetic fields are $\underline{H} = (0, \pm H_0, 0)$, one may assume a field of flow given by $\underline{v} = (\bar{v}_0, 0, 0)$ to apply outside the transition region of high current density. Here v_0 will be a constant. The assumed field of flow will be consistent with the condition required for a steady state, namely $\text{curl } \underline{E} = 0$. These two fields are taken as the zero order fields, and perturbations will be caused on them by the presence of an interpenetration region of finite dimensions. Petschek showed that in addition to the type of current sheet that has already been considered, which lies wholly along the y-axis, another rather different type is possible, at least over part of the range of y. This arrangement consists of two separate sheet currents each inclined at a small angle $\pm\beta$ to the y-axis. Between the two sheets the

field is zero in the y-direction, that is the field is effectively perpendicular to the sheets. This type of field is shown in Figure (9-1).

It will be convenient to refer to the region between the two sheet currents as region A, and to the exterior region as region B. The regions have been appropriately labelled in Figure (9-1). Petschek derived a very neat solution for this configuration, which is self-consistent for small β , and which in each region is independent of x and y. The magnetic field of this solution is illustrated in Figure (9-1); the details of the solution are given in Table (9-1). In this table the signs of the various terms are those appropriate to the first quadrant. Further, from the Rankine-Hugoniot conditions at the shock faces together with the equation of continuity in region A, it can be shown that the angle of inclination β of the current sheets to the y-axis is independent of y and is given by

$$\beta = \sin^{-1} \left(\frac{v_0}{v_A} \right) \quad (9-1)$$

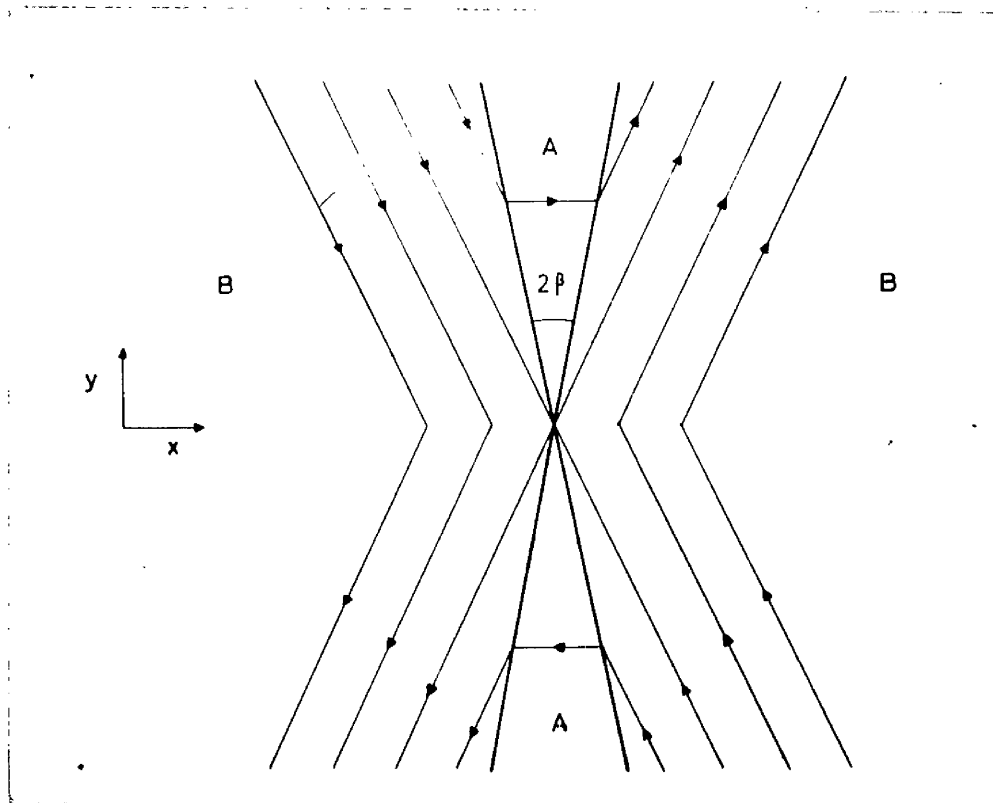


Fig (9-1). Field due to two sheet currents each making an angle β with the y-axis.

| <u>Physical Variable</u> | <u>Region A</u> | <u>Region B</u> |
|--------------------------|----------------------|------------------|
| Gas density | ρ_0 | ρ_0 |
| Fluid velocity (x-comp.) | 0 | $-v_0$ |
| Fluid velocity (y-comp.) | v_A | 0 |
| Magnetic field (x-comp.) | $v_0 H_0 / v_A$ | $2v_0 H_0 / v_A$ |
| Magnetic field (y-comp.) | 0 | H_0 |
| Gas pressure | $P_0 + H_0^2 / 8\pi$ | P_0 |

Table (9-1). Petschek's solution for regions A and B, for a small inclination β . (i.e. $v_0 \ll v_A$).

The magnetic configuration illustrated in Figure (9-1) is not physically realistic as it stands. It involves a sheet current along the x-axis, along which there would be an undesired component of the Lorentz force. This sheet current arises because the region of wave propagation has been assumed to extend right to the origin. At an X-type neutral point, however, the transverse field must go smoothly to zero. In a neighbourhood of the neutral point, then, the two sheet currents must coalesce to form a single sheet current of finite length. In this region interpenetration is due to resistive diffusion, while at a greater distance up the y-axis the transverse field builds up and wave propagation becomes the dominant mechanism. At such distances the field will indeed be of the form shown in Figure (9-1), while near the origin the field corresponds to that of a single diffusion region with an X-type neutral point, similar to that illustrated in Figure (4-1). The complete magnetic configuration is illustrated in Figure (9-2).

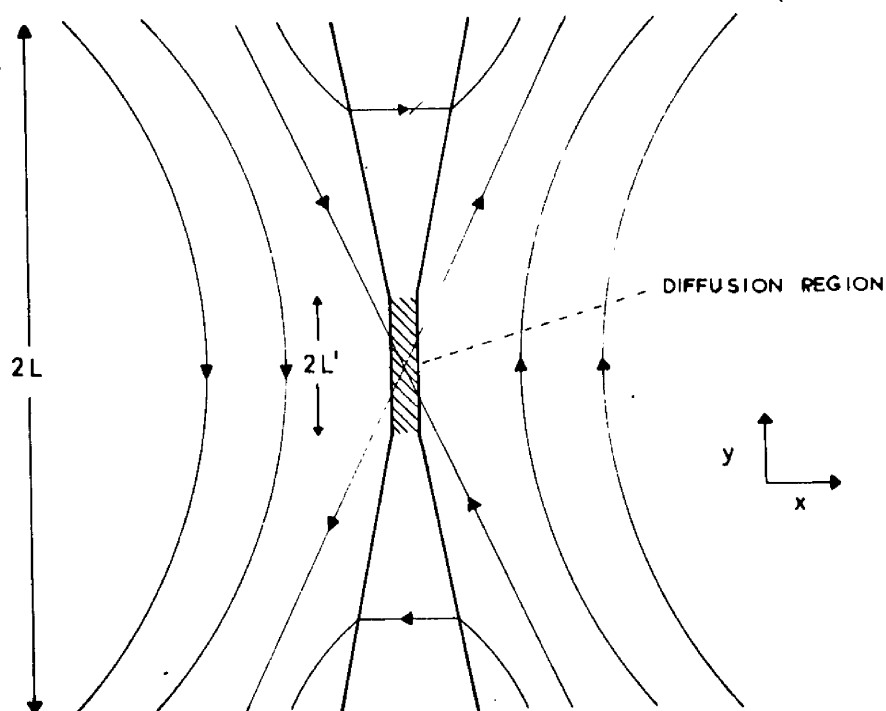


Fig (9-2). Complete magnetic configuration for the interpenetration region.

The solution in table (9-1) can be satisfied by any value of the interpenetration velocity v_0 . This value depends essentially on the nature of the complete system, including the central diffusion sheet. To obtain this complete solution, one must fit the solution given in Table (9-1) to a region of normal resistive diffusion of length L' say. From the analysis of the incompressible mode, considered earlier, it follows that

$$v_0 \sim (v_D' v_A)^{\frac{1}{2}} \quad (9-2)$$

Here v_0 is the common interpenetration velocity of the diffusion and of the wave dominated region. In equation (9-2) v_D' is the diffusion velocity across a distance L' , viz.

$$v_D' = \frac{c^2}{4\pi\sigma L'} \quad (9-3)$$

If, as before, the diffusion velocity across the total scale-length L is denoted by v_D , then from equations (9-2) and (9-3)

$$v_0 \sim (v_D v_A)^{1/2} \left(\frac{L}{L'}\right)^{1/2} \quad (9-4)$$

Equation (9-4) indicates that as v_0 is increased the length of the diffusion region is shortened in order to accommodate this increased rate of interpenetration.

The next point considered by Petschek was the determination of a minimum value for L' , and hence a maximum interpenetration rate. Now in the external field of flow it is possible to write the fluid velocity and the magnetic field as

$$\begin{aligned} \underline{v} &= v_0 (\underline{i} + \underline{u}) \\ \underline{H} &= H_0 (\underline{j} + \underline{h}) \end{aligned} \quad (9-5)$$

In equations (9-5) \underline{i} and \underline{j} are respectively unit vectors in the x- and y-directions. The vectors \underline{u} and \underline{h} represent the perturbations on the fluid velocity and the magnetic field due to the presence of a finite interpenetration region. As $v_0/v_A \rightarrow 0$, the moduli of

the vectors \underline{u} and \underline{h} will also tend to zero. Petschek used the condition that $|\underline{h}|$ be of order unity as a criterion to determine the maximum interpenetration rate, v_{\max} .

Petschek assumed that the perturbation field \underline{h} was of potential form in the external region. Though this assumption is certainly arbitrary, he showed that with it internal consistency could be maintained. Now the thickness of the whole of region A is small compared with the extent of the external field of flow; so, in discussing the exterior region, one may to a first approximation regard the analysis of region A as providing boundary conditions on the y-axis. The solution in Table (9-1) then provides the normal component of \underline{h} on this line; this component is given by

$$\begin{aligned} L' \leq y < L & \quad h_x = \frac{2v_0}{v_A} \\ -L' \gg y > L & \quad h_x = -\frac{2v_0}{v_A} \\ |y| < L' & \quad h_x = \frac{2v_0}{v_A} \frac{y}{L'} \end{aligned} \quad (9-6)$$

The last condition in (9-6) has been taken simply as an approximation for h_x over the boundary of the diffusion region. The precise value taken over this region is probably not important.

From equations (9-6) and the assumption of a potential field, \underline{h} is determined uniquely in the external region. Petschek found that the modulus of \underline{h} had its greatest value at the point where the x-axis meets the boundary of the interpenetration region. At this point

$$|h| = \frac{2}{\pi} \frac{v_0}{v_A} \log\left(\frac{L}{L'}\right) \quad (9-7)$$

Taking $|\underline{h}| = O(1)$ at this point, and using equations (9-4) and (9-7), v_{\max} may be determined as follows:

$$v_{\max} \sim v_A \left(\log \frac{v_A}{v_D} \right)^{-1} \quad (9-8)$$

Petschek extended his analysis to the compressible case. The effects of compressibility do not significantly alter the form of the magnetic field or the general configuration of the field of fluid motion. Further, the interpenetration rate is unchanged to order of magnitude. It is important to note that a significant difference between the Petschek and Parker compressible modes, which both correspond to the situation where $H_0^2/8\pi \gg P_0$, is that in Petschek's analysis there is no great compression in region A. The effects of compression, however, will probably still be important in the diffusion region of length L' .

While considerable refinement is still required in the analysis, in particular, in the relationship and fit

between the regions of wave propagation and diffusion, Petschek's work does bear out the conclusion that the Parker modes are not definitive, although it must be realized that there is still no clear proof of definitiveness even in this mode. A considerable enhancement of the interpenetration rate is, however, clearly possible. Further, no artificial assumption about the exact alignment of the colliding magnetic fields is required, since the result of equation (9-8) is largely independent of compressibility. Moreover, the result is almost independent of the conductivity which appears only logarithmically, and so the result cannot be affected significantly by any heating of the gas.

One final point should perhaps be made. The scale length L used in the analysis of both Parker and Petschek is arbitrary. The importance of the work in chapter 3 of the present treatment is that it relates this parameter to the displacement of flux systems in a perfectly conducting medium.

In conclusion, the mechanism will be applied to the flare problem in the same manner as the other modes. Assuming, therefore, a 500 gauss magnetic field and a scale-length of 10^9 cm, the values given in equation

(7-4) may be used for v_A and v_D . The minimum time-scale for interpenetration is then given numerically by

$$\tau_{\min} \sim 2.1 \cdot 10^{-5} K N^{1/2} \quad (9-9)$$

where $K = 10.3 + (3/2) \log T - (1/2) \log N$ (9-10)

The values of the minimum time-scale derived from the application of these two equations have been plotted in Figure (9-3). Allen's values⁽¹²⁰⁾ have again been used for the chromospheric temperature and density distributions. The full details of the numerical values on which Figure (9-3) is based are tabulated in Appendix (9-1). The time-scales appropriate to the total flare duration (~ 2 hours) and the flash phase (~ 5 minutes) have both been marked in Figure (9-3). Since the time-scale of interpenetration depends mainly on the gas density and is virtually independent of temperature, there is a steady decrease in its minimum value with increasing chromospheric height. From Figure (9-3) it is at once clear that Petschek's mode can account for the rapidity of the rise to flare maximum for any chromospheric height above about 2000 km. In fact, the interpenetration time is of the same order as the flash phase duration, or even shorter, for particle densities less than $4 \cdot 10^{12}$ particles per cm^3 .

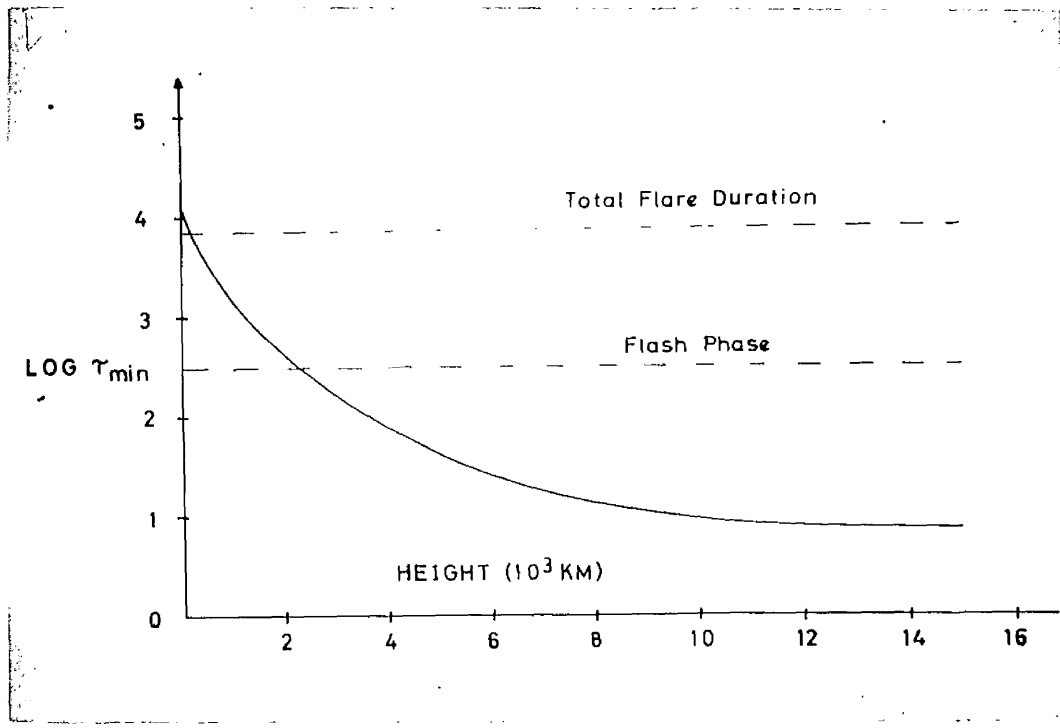


Fig (9-3). Minimum time-scale of interpenetration in Petschek's mode against chromospheric height.

CHAPTER 10.

GENERAL REQUIREMENTS OF A FLARE THEORY

The essential requirements of a complete theory of solar flares may be summarized under the following four main headings:-

- (1) Energy Storage Mechanism.
- (2) Breakdown Mechanism.
- (3) Singular Magnetic Configurations.
- (4) Dissipation Mechanism.

The energy storage mechanism must be capable of storing up to $2 \cdot 10^{32}$ ergs at chromospheric or coronal heights in the solar atmosphere. This energy must be stored in force-free perturbations of the potential field of the associated active region. The energy of the potential field itself is not available to supply the flare.

A breakdown mechanism must be provided to account for the explosive onset of the flare. Two types of instability have been considered in this connection, namely a dynamical instability, and what we shall term a macroscopic resistive instability.

In the limit of infinite conductivity the magnetic field must be capable of giving rise to singular

configurations. The need for such configurations is obvious in the current sheet mechanisms of Parker and Petschek, but singular configurations are also required in the alternative theories of Severny and Wentzel.

The essential differences between the two alternative types of theory that have been discussed lie in their respective accounts of dissipation mechanism. Here the main problem has been to find means by which the magnetic energy can be converted into heat sufficiently rapidly to account for the flare. There is not, however, complete agreement as to whether the dissipation time should be identified with the flash phase or with the total flare duration.

In the course of the present chapter, it is intended to discuss the extent to which specific theories that have been put forward successfully meet the above four requirements.

(1) Introduction

Some of the requirements of a flare theory have been described by Gold and Hoyle⁽⁴⁰⁾ as follows:

- "(a) magnetic field configurations must be found which are usually stable and which can store energy with a density a hundred times greater than in any other form;
- (b) a rather rare situation must occasionally arise

that leads to an instability in the magnetic field configuration, and to the dissipation of this energy as heat and mass motion." Up to this point the present discussion has been largely confined to mechanisms concerned in the actual dissipation process. To place such mechanisms in a context relevant to the flare problem, it is necessary to supply both a storage and a triggering mechanism. The first of these requirements will receive a full discussion in the second and third sections of this chapter; in the present section it is intended to say a brief word of introduction about possible triggering mechanisms.

Gold and Hoyle have pointed out that the instability responsible for setting off the flare need not require an external triggering mechanism. A breakdown might occur in the process of energy storage, and a dynamical instability might develop, when the stored energy exceeded a certain critical value. The authors, however, could find no firm justification for this conclusion, and, therefore, proposed that the triggering mechanism was in fact external and not directly connected with the storage process. Nevertheless the idea of a dynamical instability is certainly very attractive, and could provide a satisfactory initiatory device for the

dissipative mechanisms that have been considered in earlier chapters.

Certainly to initiate the collapse described in the theories of Severny and Wentzel, a dynamical instability is required. A complete theory would involve an investigation into the possibilities of such an instability and its development from stable equilibrium configurations. A dynamical instability is undoubtedly the most plausible suggestion to account for the sudden onset of a flare; further, it would be equally applicable to the initiation of the steady conditions of current-sheet mechanisms. No significant work has been done, however, on the question of the existence or development of a dynamical instability in connection with solar flares. While other possibilities do exist that can lead to the steady conditions of the current-sheet mechanism, it would seem that the type of collapse envisaged by Severny and Wentzel can only be started by a dynamical instability.

Even if a dynamical instability were to occur in the chromospheric magnetic field, this would be followed by a flare only if the field collapsed to a singular current-sheet configuration. These configurations are an essential feature of all four dissipation mechanisms

that have been discussed (Parker, Severny, Wentzel and Petschek). Magnetic fields must be found, therefore, which, in the limit of infinite conductivity, are capable under displacement of giving rise to singular configurations. It is in attempting to meet this requirement that investigations of magnetic fields with neutral points have been important.

(ii) The Role of Neutral Points and the Acceleration of Charged Particles.

Sweet⁽¹³²⁾ has examined the topology of an idealised sunspot field at chromospheric levels. His discussion is based on the assumption that sunspots arise when flux tubes that would normally lie at a lower level protrude through the photosphere and emerge into chromospheric regions. The field examined was that of a complex spot group, consisting of two simpler bipolar groups. The boundary of the field may be mapped on to a plane Σ , which is referred to as the photosphere. The field of interest then lies above Σ , and the magnetic flux crosses Σ in four regions A, B, C, D, as shown in Figure (10-1).

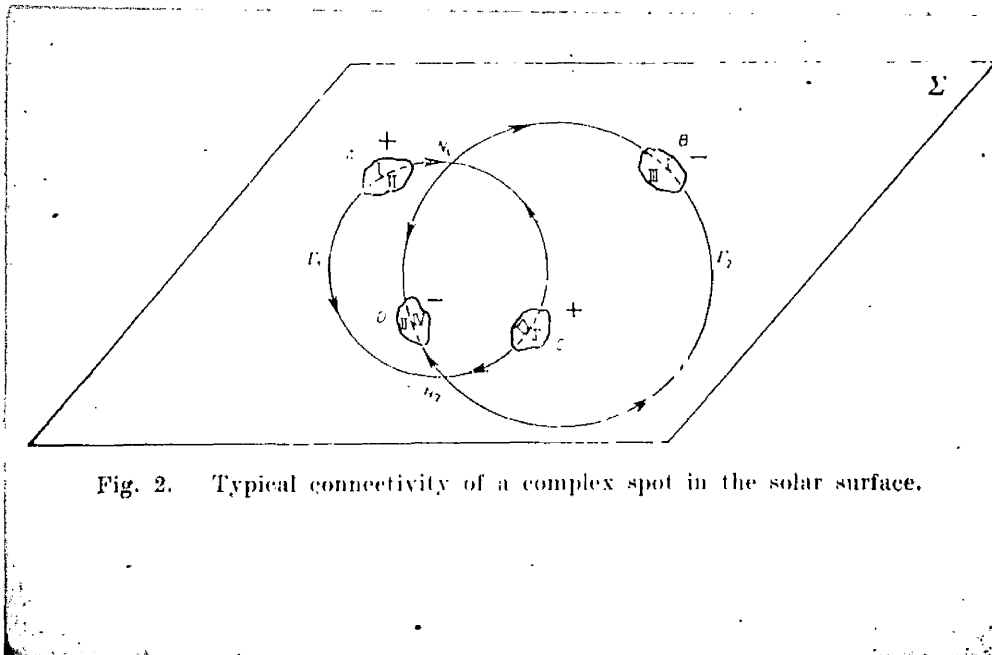


Fig. 2. Typical connectivity of a complex spot in the solar surface.

Fig (10-1). Typical connectivity of a complex spot group in the solar surface. (132)

If there is any flux sharing between the two bipolar groups, the connectivity of the field in Σ requires the existence of two neutral points N_1 and N_2 in that plane. From Figure (10-1) it is clear that the lines of force through these neutral points divide the plane Σ into four distinct areas. In fact the field above Σ can be divided into four distinct topological regions, of which the four areas in Σ are

parts of the boundaries. These four regions are referred to as I, II, III, and IV; the flux from AI recrosses Σ at EI, that entering at AII recrosses at DII, etc. The four regions above Σ are separated by four surfaces which are generated by systems of lines of force through one of the neutral points. For example, regions I and II will be separated by the lines of force that go through the boundary curve separating AI and AII; all these lines of force go to the neutral point N_2 . The four separating surfaces so defined have a common intersection above Σ , which is a line of force joining the neutral points N_1 and N_2 .

Sweet pointed out that the topology just described is relevant when any two flux tubes, or, for that matter, any two distinct sections of the same flux tube intersect.

It was assumed that the magnetic field above Σ was initially of potential form. The effect of moving the photospheric roots of the field was then considered. When this occurs without magnetic reconnection, the field can, in general, no longer be potential, and electric currents are induced. Sweet proved the important theorem that if any current flows at a deformation type neutral point that is not on a neutral line, then hydrostatic equilibrium is impossible at that

point. In the proof of the theorem the effects of gas pressure and gravity were included, assuming an isothermal atmosphere.

The theorem would imply that hydrostatic equilibrium must break down as soon as any displacement is made of the component flux systems of the model, since such displacements must induce currents. It was not proved, however, that these currents must flow at the neutral points; only a qualitative argument could be given to justify this assumption. If the interpretation is correct, then any motion of the component spots will lead to an immediate breakdown of hydrostatic equilibrium, and energy cannot be gradually stored for a sudden release, at least in this type of magnetic configuration. Interpenetration will proceed as soon as there is any relative motion of the component spots.

Sweet next showed that the voltage drop along the line of force joining the two neutral points N_1 and N_2 is equal to $-(1/c)$ times the rate of reconnection of magnetic flux. If the reconnection rate can be made sufficiently rapid to allow the field to maintain nearly potential form, then to order of magnitude the voltage, V say, will be given by

$$V \sim \frac{v L H}{c} \quad \text{e.s.u.} \quad (10-1)$$

where H and L are respectively a typical magnetic intensity and scale-length of the field, and v is the relative velocity of the sunspot components. Now this voltage will be available to accelerate particles, since it is determined from the electric field as measured by an observer moving with the fluid. From the work of Meyer, Parker, and Simpson⁽¹⁰⁰⁾, particles up to 10 BeV were accelerated in the flare of February 29, 1956.

To account for such exceptional particles, velocities of the sunspot components of the group would have to be of the order of 10^6 cm/sec on any reasonable estimate for the values of H and L . On the other hand, it must be pointed out that direct acceleration by the large scale electric field is not the only conceivable way in which particles could be accelerated. The alternative theories of Parker⁽³⁸⁾ and Severny and Shabanskii⁽¹⁰²⁾ have already been mentioned.

Velocities as large as 10 km/sec could not be expected from the generally observed motions of sunspots. Gopasuk⁽¹³³⁾ has cited an example, however, in which the displacements of the components of a spot group, as measured before and after a solar flare, required a velocity of at least 10^5 cm/sec for their explanation. On this interpretation, large voltages could result

from sunspot motions,

Parker⁽⁵⁹⁾ has argued that this induced voltage cannot accelerate cosmic ray particles, since the acceleration requires that the particles achieve runaway energies. By a crude argument, he estimates that runaway particles cannot occur, since by his computations the electrons have drift velocities that are considerably less than their thermal velocities. These computations, however, apply to Parker's compressible mode of interpenetration. This mode has been shown not to be definitive, and if the interpenetration takes place with a rate that is appropriate to Petschek's analysis, the electric field will be significantly enhanced. Further, if the two colliding fields are not exactly antiparallel, the residual field inhibits the compression, and the lower gas density in the interpenetration region reduces the critical field required for runaway electrons. If the optimum conditions of Petschek's mode are taken, not only the electrons but also the protons will be able to achieve runaway energies.

Sweet's topology of the sunspot field, and the suggestion that sunspot motions are responsible for the magnetic reconnection would seem to be unable to account for normal flares. For the conclusions about the

breakdown of hydrostatic equilibrium at the neutral point rule out a gradual storage of energy in preparation for a catastrophic release. The suddenness of flare onset cannot, therefore, be explained. However, such a model could well account without modification for the more gradual plage brightenings, of which flares are probably extreme examples distinguished by the violence of their onset.

(iii) The Gold and Hoyle Storage Mechanism.

A separate topology of a chromospheric magnetic field has been considered by Gold and Hoyle⁽⁴⁰⁾. Though it differs considerably in its external from Sweet's model, in its topological essentials it is almost identical. The Gold and Hoyle model is, however, more general in that the number of neutral points is not restricted to two.

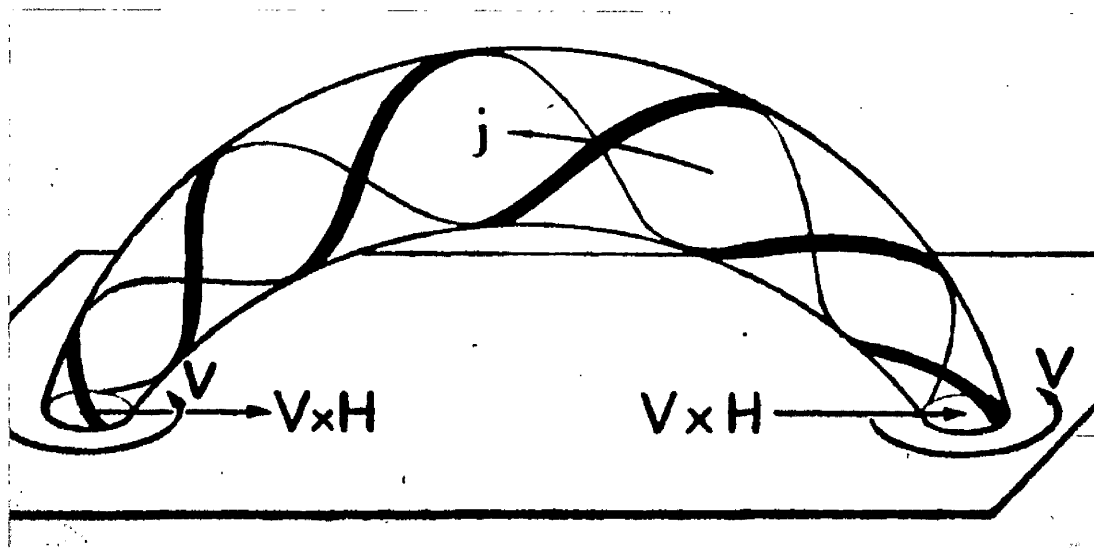


Fig (10-2). A twisted flux tube of the type considered by Gold and Hoyle.⁽⁴⁰⁾

Gold and Hoyle examined in considerable detail the field of a twisted flux tube of the kind illustrated in Figure (10-2). At chromospheric heights the field in the tube must be force-free. They identified such bundles of twisted lines of force with chromospheric filaments, claiming that flares are frequently aligned with pre-existing filamentary structures. Thus Gold and Hoyle's theory is concerned with small-scale fields rather than with the complete sunspot magnetic configuration.

The tubes of force may emerge twisted from the photosphere, or, alternatively, they may become twisted into their force-free configurations in the chromosphere due to photospheric twisting motions at their roots. In either event, such tubes of force provide isolated magnetic systems that, unlike a potential field, can store energy at chromospheric levels.

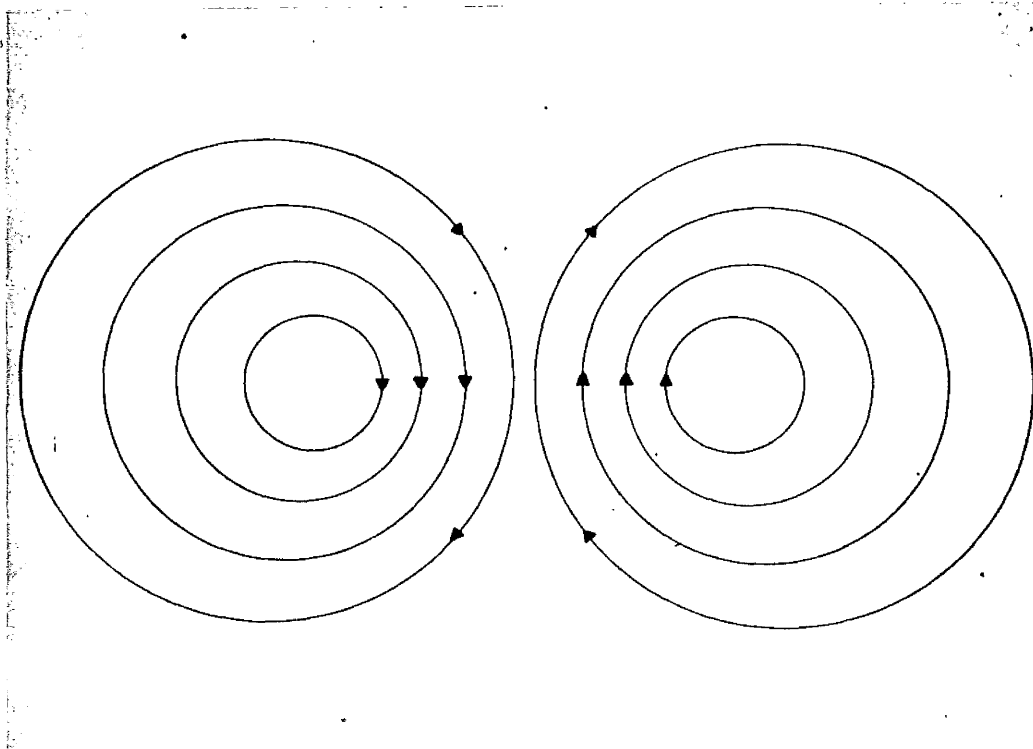


Fig (10-3). Cross-section of the colliding fields prior to any reconnection.

In their theory, Gold and Hoyle considered two such flux systems. Since the systems are isolated,

initially they will exert no forces on each other. The authors supposed that two such systems come into contact by chance along part of their length at chromospheric levels. When they first come into contact a cross-section of the colliding fields will appear as shown in Figure (10-3), and normal diffusion will take place across the boundary of contact. Due to this diffusion, the outer lines of force are reconnected and, after a short while, the cross-section of the field will appear as in Figure (10-4). Now, due to the initial reconnection, the systems are no longer isolated. The lines of force enclosing the two systems will exert forces that draw the two systems closer together. Non-singular hydrostatic equilibrium will cease to be possible and a narrow collision layer will be set up. The interpenetration will proceed at an ever increasing rate in this collision layer in which the steady conditions of the current sheet mechanism, as analysed by Parker, Petschek and others, will apply. The interpenetration rate will be determined by the velocity at which the two flux systems are being drawn together. This rate will ultimately be limited to the maximum rate of interpenetration possible in Petschek's mode.

Two important features are found, therefore, in the theory proposed by Gold and Hoyle. First they have

indicated a method by which the flare energy may be stored at chromospheric levels, and secondly they have provided a triggering mechanism. The first two of the requirements stated at the beginning of the present chapter are, therefore, successfully met in this theory. Further, in their triggering mechanism, Gold and Hoyle have indicated another type of field instability which might be appropriate in place of a dynamical instability. This will be referred to here as a macroscopic resistive instability. It may be defined as follows.

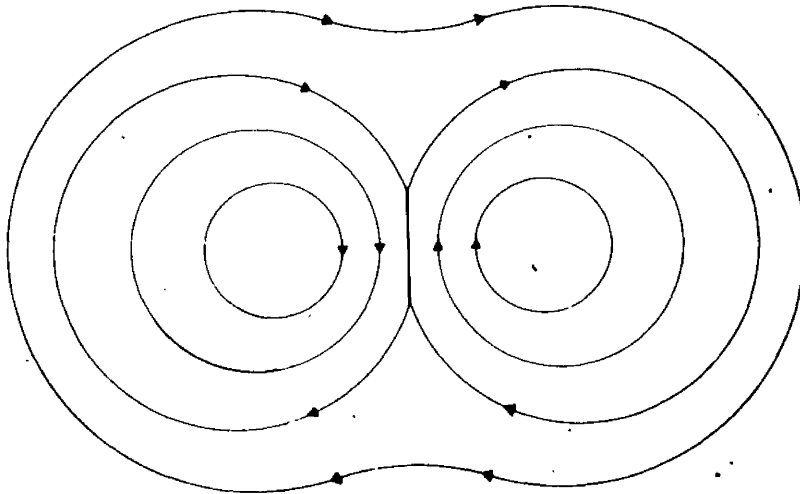


Fig (10-4). Cross-section of the colliding fields following some reconnection.

Suppose that an initially stable equilibrium configuration is gradually altered, possibly due to the gradual storage of additional magnetic energy, until a critical stage is reached, at which under a further perturbation a non-singular equilibrium configuration cannot be found without some reconnection of the lines of force. In the limit of perfect conductivity a current sheet is then induced. If finite conductivity is allowed, however, hydrostatic equilibrium breaks down, and a thin region of high current density is set up in which resistive diffusion is operative. The resulting interpenetration introduces new magnetic forces that decrease the stability of the configuration. The length of the current sheet required for equilibrium is increased, thereby increasing the extent of the diffusion. As a result, interpenetration will take place at an increasing rate until a new non-singular equilibrium configuration becomes possible. This is a slight generalization of Gold and Hoyle's type of instability; their's is the particular case where the initial configuration is not one of stable but one of neutral equilibrium.

CHAPTER 11.

SUMMARY AND CONCLUSIONS

Early magnetic theories of solar flares were criticised by Cowling⁽¹¹⁰⁾ on the grounds that if the flare heating is due to Joule dissipation of magnetic energy, then the thickness of the current cannot exceed a few metres. This conclusion follows directly from energy considerations and a simple application of Ampere's law. This criticism has been satisfactorily met in all later theories. Dungey⁽¹¹⁵⁾ pointed out that, since under solar conditions the current density is determined primarily by the magnetic field configuration, a solar discharge must be very thin in one direction.

It is possible to state this requirement of the extreme narrowness of the current region in a more elegant manner. In any flare theory, the assumed magnetic field must be capable of giving rise under displacement to singular configurations, when the resistivity of the gas is neglected. This requirement has led to the close investigation of fields with neutral points by Dungey⁽¹¹⁵⁾, Sweet⁽¹³²⁾ and others.

Given such a magnetic configuration, a complete flare theory must provide an instability to account for the sudden onset of a solar flare. The most attractive suggestion would be a dynamical instability in which an initial non-singular stable equilibrium configuration becomes unstable. If no other non-singular configuration of stable equilibrium exists into which the system can move without reconnection of the lines of force, the system must collapse to a singular equilibrium configuration. The collapse would then be accompanied by the formation of a sheet current.

Though the idea of a dynamical instability is clearly tempting, no significant work has been done to date on the existence of such an instability appropriate to the force-free conditions of chromospheric fields.

Two separate approaches are possible in the treatment of singular fields which might be caused by the collapse, and in dealing with the resulting dissipation of magnetic energy. On the one hand, Severny⁽³¹⁾ and Wentzel⁽¹²⁸⁾ have treated the problem in a time-dependent, but unidimensional, manner. They argue that a steady state is not reached as a result of the collapse. According to Severny, shock phenomena dissipate the energy of the field, leading to an impulsive heating

of the gas to a temperature of several million degrees. This provides a thermal energy store which the flare dissipates over the period of a few hours. Wentzel, however, considers that the energy of the collapse goes into turbulent motions. This turbulence then provides a store of energy that is gradually dissipated over the whole duration of the flare by Joule heating taking place at the boundaries of the turbulent eddies.

The alternative approach has been to assume that steady conditions are set up in a singular equilibrium configuration. Work along these lines has been published by Sweet⁽¹¹⁶⁾, Parker^(117,59), and Petschek⁽¹³¹⁾. When allowance is made for finite resistivity, conditions of hydrostatic equilibrium cannot hold within the current sheet, which is now replaced by a finite region of high current density. The colliding fields collapse at a rate determined by the rate of magnetic diffusion in the pinch. Four modes of interpenetration have been considered in the present treatment. In general, the interpenetration rate determined in these modes falls far short of what is required in the solar flare problem. Under optimum conditions, the 'fast' mode of chapter 6 can account, however, for the decay phase of a flare. But the rate of interpenetration derived in this mode

depends critically on some artificial features of the two-dimensional model that was assumed, since if the colliding fields are not exactly antiparallel, the interpenetration rate is much reduced.

The most relevant application of the current-sheet mechanism to the flare problem is provided by Petschek's analysis. This mode of interpenetration is sufficiently rapid to account for, not only the decay phase, but also the flash phase of a large flare under a variety of chromospheric and coronal conditions. Further, no artificial assumption about the alignment of the colliding fields is necessary, since compressibility is not an important feature of this theory. Petschek's work is, without doubt, the most successful attempt, to date, at a solar flare interpenetration mechanism. It is possible that other modes of interpenetration may have relevance in rather different solar contexts.

The current sheet mechanism could arise from a variety of causes. Firstly, it could be set off by a dynamical instability resulting from the twisting of chromospheric fields by photospheric motions. Secondly, it could arise, although not for flares, from continuous movements of the photospheric roots of the chromospheric field, as for example in the relative motions within a

complex spot group. Thirdly, and this is the least speculative alternative, the mechanism could follow from a macroscopic resistive instability of the type examined by Gold and Hoyle⁽⁴⁰⁾, and possibly of an even more general type.

In the case of the dynamical instability it is likely that, when the steady conditions arise, the interpenetration will proceed at the rate appropriate to Petschek's mode. This corresponds to a collapse of the colliding fields at near the Alfvén velocity. On the other hand, if the interpenetration is caused by continuous photospheric motions, then in the absence of a storage mechanism, the rate and mode of this interpenetration will be determined by the velocities involved in the photospheric motions themselves. Finally, if the process arises from a macroscopic resistive instability, then the rate of interpenetration will be continuously accelerated. The mode of reconnection will proceed from the slow mode, through the faster mode analysed in chapter 6, ultimately reaching the Petschek mode in which an upper limit is finally encountered.

The Petschek mode can account, therefore, for the rapidity of the solar flare flash. Further, it is likely that a wider class of plage brightenings can also

be explained by the current sheet mechanism. The criticism has been made by Wentzel⁽¹²⁸⁾, however, that such a theory is in conflict with the observation of homologous flares, since the required reconnection of the lines of force would significantly alter the magnetic configuration, and presumably, therefore, the appearance of subsequent flares of the homologous group. Models could be suggested, no doubt, in which this criticism would not apply. For example, the idea of a dynamical instability occurring in a single flux tube is tempting. A single initially untwisted flux tube could become twisted by photospheric motions as in the Gold and Hoyle model; should, then, a dynamical instability develop, the tube will buckle and the resulting interpenetration will leave the tube again in an untwisted state similar to its initial configuration. The process could, therefore, be repeated in its essentials. However, at present, such models are only speculative.

This criticism by Wentzel has usually been regarded as rather serious; but it should be pointed out that only a few cases of homologous flares have been observed, and that the interpretation of some of these is open to doubt. The most striking example of a homologous group of flares, that observed by Hansen and Gordon⁽⁵⁸⁾, may,

in fact, have been rather a homologous group of phenomena associated with a series of flares that were unobserved due to their proximity to the solar limb. For it is difficult to distinguish limb flares, such as those Hansen and Gordon were attempting to observe, from surges and other flare-like phenomena. There is no doubt, however, that homologous activity of some kind was observed in this case. But it should be pointed out that the field annihilation required for a flare will not ipso facto preclude such activity, provided the reconnection is confined to small scale features, as Gold and Hoyle have suggested. For there is then no reason to expect that the general sunspot configuration would be altered by the flare. And it is the more general features of the field that determine the form of flare-associated phenomena. Finally, if the gross features of the sunspot field are altered, this must occur in only quite exceptional 3^+ events. While such flares are known to occur in groups in particular active regions, individual flares of the groups show considerable dissimilarities, and are certainly not homologous.

Most theories of solar flares have attempted to explain the optical event. This is probably the best procedure, since the optical activity is usually the

most obvious and probably the most energetic feature. Some authors have suggested, however, that the optical flare is a secondary phenomenon. Wentzel⁽¹²⁸⁾ has put forward the interesting suggestion that the type of event consequent on the collapse of the magnetic field depends on the height of this collapse in the solar atmosphere, and on the corresponding electron density. If the collapse occurs at lower chromospheric levels, the rate of emission, which depends on the electron density, is sufficient to radiate away the energy of the Joule dissipation. If, however, the collapse occurs at higher levels and, therefore, in regions of lower electron density, the energy of the magnetic dissipation cannot be radiated off with sufficient rapidity, and heating develops. Wentzel suggests that the event does not then become visible, but that associated phenomena such as radio bursts and particle acceleration may occur.

While Wentzel's suggestion is of interest, the optical event is, nonetheless, the most frequent, generally the most conspicuous, and probably the most energetic feature of the complete solar flare event. There is no clear evidence for doubting its fundamental nature. Certainly, on occasions, associated events,

particularly Type III radio bursts, do occur without clear evidence of an optical flare, but such exceptional cases could well be due to observational selection. Radio bursts at metre wavelengths can be much more unambiguously recorded than the optical flare. Further, Type III bursts, in particular, are found to occur even with very minor flares and sub-flares. It would be rash, therefore, to conclude that such events can definitely occur without any optical counterpart. For the demarcation between small flares and unclassified minor plage brightenings is not clear. The optical counterpart could well be unidentified. In view of these remarks, the identification of the optical flare with the primary event is quite reasonable, and any suggestion that it is a secondary phenomenon is at very best conjectural.

To conclude, the observationally recorded features of solar flares provide a very detailed background for flare theories. To date, no theory has attempted to account for more than a few of these observed features. By contrast with the observational position, little progress has been made in developing a satisfactory theory of solar flares. It can be said, however, that current sheet mechanisms in the form first proposed by

Sweet can be applied, particularly in view of recent developments by Petschek, in a manner to account for some salient features, in particular, the energy supply, and the brief time-scale. Further, the mechanism can describe, though at present only qualitatively, the acceleration of cosmic-ray particles, and the production of runaway electrons, necessary for many associated radio phenomena. Finally, the mechanism may be applied in particular to systems with the Gold and Hoyle topology, which can provide a satisfactory storage mechanism and triggering device. To this extent, at least, some progress has been made.

REFERENCES

1. DODSON, H.W. and HEDEMAN, E.R., J. Geophys. Res., 65, 123 (1960).
2. Trans. I.A.U., 2, 146 (1955).
3. SMITH, H.J. and BOOTON, W.D., G.R.D. Research Notes No. 58, AFCRL 472 (1961).
4. DODSON, H.W., HEDEMAN, E.R., and McMATH, R.R., Ap. J. Supp., 2, 241 (1956).
5. ATHAY, R.G., and MORETON, G.E., Ap. J., 133, 935 (1961).
6. GIOVANELLI, R.G., Ap. J., 89, 555 (1939).
7. HOWARD, R., Ap. J., 138, 1312 (1963).
8. ELLISON, M.A., M.N., 106, 500 (1946).
9. ELLISON, M.A., Pub. Roy. Obs. Edinburgh, 1, 75 (1952).
10. SMITH, E.v.P., GRD Research Notes No. 74, AFCRL-62-226 (1962).
11. ELLISON, M.A., Q.J., 4, 62 (1963).
12. SMITH, H.J., GRD Research Notes, AFCRL-62-827 (1962).
13. SEVERNY, A.B. and SHAPOSHNIKOVA, E.F., Izvest. Krim. Ast. Obs., 12, 3 (1954).
14. WALDMEIER, M., Ergebnisse und Probleme der Sonnenforschung, 197 (1941).
15. ELLISON, M.A., M.N., 109, 3 (1949).
16. KAHN, F.D., M.N., 109, 324 (1949).
17. SVESTKA, Z., Bull. Ast. Inst. Czechoslovakia, 2, 81 (1951).
18. SVESTKA, Z., Bull. Ast. Inst. Czechoslovakia, 2, 100 (1951).

19. SVESTKA, Z., Bull. Ast. Inst, Czechoslovakia,
2, 120 (1951).
20. ELLISON, M.A., MCKENNA, S.M.P. and REID, J.H.,
Dunsink Obs. Pub., 1, 39 (1960).
21. ELLISON, M.A., and HOYLE, F., Observatory, 67,
181 (1947).
22. GOLDBERG, L., DODSON, H.W. and MÜLLER, E.A.,
Ap. J., 120, 83 (1954).
23. JEFFERIES, J.T., SMITH, E.v.P. and SMITH, H.J.,
Ap. J., 129, 146 (1959).
24. JEFFERIES, J.T., and ORRALL, F.Q., Ap. J., 127,
714 (1957).
25. KAZACHEVSKAVA, T.V. and SEVERNY, A.B., Izvest.
Krim. Ast. Obs., 19, 46 (1958).
26. SEVERNY, A.B., Proc. I.A.U. Symposium No. 6,
114 (1958).
27. McMATH, R.R., MOHLER, O.C. and DODSON, H.W.,
Proc. Nat. Acad. Sci., 46, 165
(1960).
28. ELLERMAN, F., Ap. J., 47, 298 (1917).
29. LYOT, B., Ann d'Ast., 7, 31 (1944).
30. SEVERNY, A.B., Soviet Ast., 1, 668 (1957).
31. SEVERNY, A.B., Soviet Ast., 2, 310 (1958).
32. SUEMOTO, Z., and HIEI, E., Pub. Ast. Soc. Japan,
11, 185 (1959).
33. HIRAYAMA, T., Pub. Ast. Soc. Japan, 13, 152 (1961).
34. SEVERNY, A.B., Soviet Ast., 5, 299 (1961).
35. SMITH, H.J. and SMITH, E.v.P., Solar Flares, The
Macmillan Company, N.Y., p.136
(1963).

36. BILLINGS, D.E. and ROBERTS, W.D., Ap. J., 118,
429 (1953).
37. SEVERNY, A.B., STESHENKO, N.P. and KHOKHLOVA, V.L.,
Soviet Ast., 4, 19 (1960).
38. PARKER, E.N., Phys. Rev., 107, 830 (1957).
39. NOTUKI, M., HATANAKA, T. and UNNO, W., Pub. Ast.
Soc., Japan, 8, 52 (1956).
40. GOLD, T. and HOYLE, F., M.N., 120, 89 (1960).
41. BRUZEK, A., Zs. f. Ap., 50, 110 (1960).
42. HOWARD, R. and BABCOCK, H.W., Ap. J. 132, 218, (1960)
43. MICHARD, R., MOURADAIN, Z. and SEMEL, M., Ann d'Ast.,
24, 54 (1961).
44. EVANS, J.W., Ast. J., 64, 330 (1959).
45. HOWARD, R. and SEVERNY, A.B., Ap. J., 137, 1242
(1969).
46. ELLISON, M.A., MCKENNA, S.M.P. and REID, J.H.,
Dunsink Obs. Pub., 1, 53 (1961).
47. SEVERNY, A.B., Soviet Ast., 6, 747 (1961).
48. GOPASUK, S.I., OGIR, M.B., SEVERNY, A.B.,
STESHENKO, N.V. and SHAPOSHNIKOVA,
B.F., Proc. I.A.U. Symposium No.22
(in press).
49. ZIRIN, H. and SEVERNY, A.B., Observatory, 81,
155 (1961).
50. ELLISON, M.A., MCKENNA, S.M.P. and REID, J.H.,
Observatory, 80, 149 (1960).
51. ELLISON, M.A., MCKENNA, S.M.P. and REID, J.H.,
M.N., 122, 491 (1961).
52. ELLISON, M.A., MCKENNA, S.M.P. and REID, J.H.,
M.N., 124, 263 (1962).

53. SMITH, H.J. and BOOTON, W.D., GRD Research Notes
No. 68, AFCRL-834 (1961).
54. BOISCHOT, A. and DENISSE, J.F., Compt. Rend.,
245, 2194 (1957).
55. STEPANOV, V.E., Izvest. Krim. Ast. Obs., 20,
52 (1958).
56. DODSON, H.W., and HEDEMAN, E.R., Ap. J., 110,
242 (1949).
57. ELLISON, M.A., MCKENNA, S.M.P., and REID, J.H.,
Dunsink Obs. Pub., 1, 1 (1960).
58. HANSEN, R. and GORDON, D., P.A.S.P., 72, 194 (1960).
59. PARKER, E.N., Ap. J. Supp., 8, 177 (1963).
60. WILD, J.P. and MCCREADY, L.L., Aust. J. Sci. Res.,
A3, 387 (1950).
61. WILD, J.P., SHERRIDAN, K.V. and NEYLAN, A.A.,
Aust. J. Phys., 12, 369 (1959).
62. GIOVANELLI, R.G., Aust. J. Phys., 11, 350 (1958).
63. WEISS, A.A., Aust. J. Phys., 16, 240 (1963).
64. NEWKIRK, G., Ap. J., 133, 983 (1961).
65. MAXWELL, A. and THOMPSON, A.R., Ap. J., 135,
138 (1962).
66. WILD, J.P., MURRAY, J.D. and ROWE, W.C.,
Aust. J. Phys., 7, 439 (1954).
67. BOISCHOT, A., Ann. d'Ast., 21, 273 (1958).
68. TAKAKURA, T., J. Phys. Soc. Japan, 17, Supp. A-II,
243 (1962).
69. DENISSE, J.F., Inform. Bull. S.R.O.E., No.4, 3
(1960).
70. MAXWELL, A., SWARUP, G., and THOMPSON, A.R.,
Proc. IRE, 46, 142 (1958).

71. HADDOCK, F.T., Proc. IRE, 46, 3 (1958).
72. YOUNG, C.W., SPENCER, C.L., MORETON, G.E. and ROBERTS, J.A., Ap. J., 133, 243 (1961).
73. KUNDU, M.R., ROBERTS, J.A., SPENCER, C.L. and KUIPER, J.W., Ap. J., 133, 255 (1961).
74. THOMPSON, A.R., and MAXWELL, A., Ap. J., 136, 546 (1962).
75. KUNDU, M.R. and HADDOCK, F.T., IRE Trans. Antennas Propagation AP-9, 82 (1961).
76. WILD, J.P., SMERD, S.F. and WEISS, A.A., Ann. Rev. Ast. Astrophys., 1, 291 (1963).
77. COVINGTON, A.E., J.R.A.S. Canada, 45, 49 (1951).
78. KUNDU, M.R., Ann. d'Ast., 22, 1 (1959).
79. HACHENBURG, O. and WALLIS, G., Zs. f. Ast., 52, 42 (1961).
80. TAKAKURA, T., Pub. Ast. Soc. Japan, 12, 352 (1960).
81. WILD, J.P., J. Phys. Soc. Japan, 17, Supp. A-II, 249 (1962).
82. de JAGER, C., Space Research, 628, (Edit. Kahlmann Bijl H.), North Holland, Amsterdam (1960).
83. KUNDU, M.R., J. Geophys. Res., 66, 4308 (1961).
84. ANDERSON, K.A. and WINCKLER, J.R., J. Geophys. Res., 67, 4103 (1962).
85. GINZBURG, V.L. and ZHELEZNYAKOV, V.V., Soviet Ast., 2, 653 (1958).
86. WILD, J.P., Proc. I.A.U. Symposium No.16, 115 (1963).
87. DELLINGER, J.H., J. Geophys. Res., 42, 49 (1937).

88. FRIEDMAN, H. and CHUBB, T.A., Physics of the Ionosphere, The Physical Society, London (1955).
89. BYRAM, E.T., CHUBB, T.A., and FRIEDMAN, H., J. Geophys. Res., 61, 251 (1956).
90. FRIEDMAN, H., Ann. Rev. Ast. Astrophys., 1, 59 (1963).
91. KAWABATA, K., Rept. Ion. Space Res. Japan, XIV, 405 (1960).
92. KREPLIN, R.W., CHUBB, T.A., and FRIEDMAN, H., J. Geophys. Res., 67, 2231 (1962).
93. DETWILER, C.R., GARRETT, D.L., PURCELL, J.D. and TOUSEY, R., Ann. Geophys., 17, 9 (1961).
94. McLEAN, D.T., Aust. J. Phys., 12, 404 (1959).
95. PARKER, E.N., Ap. J., 133, 1014 (1961).
96. PARKER, E.N., Space Sci. Rev., 1, 62 (1962).
97. BLACKWELL, D.E. and INGHAM, M.F., M.N., 122, 143 (1961).
98. Thompson, A.R., and MAXWELL, A., Planet. Space Sci., 2, 104 (1960).
99. THOMPSON, A.R., and MAXWELL, A., Nature, 185, 89 (1960).
100. MEYER, P., PARKER, E.N. and SIMPSON, J.A., Phys. Rev., 104, 768 (1956).
101. FERMI, E., Phys. Rev., 75, 1169 (1949).
102. SEVERNY, A.B. and SHABANSKII, V.P., Soviet Ast., 4, 583 (1960).
103. MALITSON, H.H. and WEBBER, W.R., Solar Proton Manual (edit. F.B. McDonald) (1962).

104. STEPANYAN, A.A. and VLADIMIRSKII, B.M.,
Soviet Ast., 5, 326 (1961).
105. BOISCHOT, A. and WARWICK, J.W., J. Geophys. Res.,
64, 683 (1959).
106. GOLD, T., Ap. J. Supp., 4, 406 (1960).
107. SEVERNY, A.B., Soviet Ast., 1, 324 (1957).
108. GOLDBERG, L., MOHLER, O.C. and MÜLLER, E.A.,
Ap. J., 127, 302 (1958).
109. SWEET, P.A., Proc. I.A.U. Symposium No.22 (in press)
110. COWLING, T.G., The Sun (edit. G.P. Kuiper) Univ. of
Chicago Press, p.587-590 (1953).
111. GIOVANELLI, R.G., M.N., 108, 163 (1948).
112. GIOVANELLI, R.G., Phil. Mag., 40, 206 (1949).
113. GIOVANELLI, R.G., M.N., 107, 338 (1947).
114. COWLING, T.G., M.N., 106, 218 (1946).
115. DUNGEY, J.W., Phil. Mag., 44, 725 (1953).
116. SWEET, P.A., Proc. I.A.U. Symposium No. 6, 123 (1958).
117. PARKER, E.N., J. Geophys. Res., 62, 509 (1957).
118. e.g. COPSON, E.T., Theory of Functions of a Complex
Variable, O.U.P., p.49 (1935).
119. HOYLE, F. and WICKRAMASINGHE, N.C., M.N., 123,
51 (1961).
120. ALLEN, C.W., Astrophysical Quantities, 2nd Edit.,
p. 174, Univ. of London (1963).
121. WENTZEL, D.G., Proc. NASA Symposium on Physics of
Solar Flares, Introductory Lecture,
(in press).
122. COWLING, T.G., Magnetohydrodynamics, p.105-112,
Interscience (1957).

123. ALLEN, C.W., Liège Symposium, Spectra in Far
Ultra-Violet, 241 (1961).
124. DUNGEY, J.W., Proc. I.A.U. Symposium No. 6,
135 (1958).
125. SYROVATSKII, S.I., Soviet Ast., 6, 768 (1963).
126. SEVERNY, A.B., Soviet Ast., 6, 770 (1963).
127. SHABANSKII, V.P., Soviet Ast., 5, 647 (1961).
128. WENTZEL, D.G., Proc. NASA Symposium on Physics
of Solar Flares (in press).
129. JAGGI, R.K., J. Geophys. Res., 68, 4429 (1963).
130. FURTH, H.P., KILLEEN, J. and ROSENBLUTH, M.N.,
Phys. of Fluids, 6, 459 (1963).
131. PETSCHER, H.D., Proc. NASA Symposium on Physics
of Solar Flares (in press).
132. SWEET, P.A., Nuovo Cim., Supp. 8, Ser X, 188
(1958).
133. GOPASUK, S.I., Soviet Ast., 5, 158 (1961).

APPENDIX 5-1

SOLUTION FOR $g(\xi)$.

For convenience, the differential equation (5-5) and its two boundary conditions, (5-8) and (5-9), are restated here as follows :

$$(1 - \xi^2) (g'^2 - g g'') - 2 \xi g g' = (1 - \xi^2)^2 \quad (5-1-1),$$

$$g(0) = 0 \quad (5-1-2),$$

$$g''(1) = 0 \quad (5-1-3).$$

These three equations completely define the problem, and determine a unique solution for $g(\xi)$ which must be evaluated by numerical methods.

The problem is complicated by the fact that the differential equation has two singular points, which are the points $\xi = 1$ and $\xi = 0$, the points at which the boundary conditions are imposed. In view of the difficulties of fitting numerical solutions to the series expansions that are necessary in the neighbourhood of these singular points, it was decided not to use a purely iterative method. Instead, a sequence of solutions is obtained, all of which satisfy the condition of equation (5-1-2). A single infinity of such solutions exists, each solution being specified by a value of the parameter K , to be introduced below. The numerical integration involved in determining these

solutions can then proceed on a step-by-step basis, and the Runge-Kutta method of integration is used. For each of these solutions, the value of $g''(1)$ can be obtained, and by comparing two or more such solutions, a better value of the starting parameter K can be determined. In this way, the required solution for which $g''(1) = 0$ can be successively (and rapidly) approached.

To apply the Runge-Kutta method of integration, the differential equation (5-1-1) must first be expressed as two first order ordinary differential equations. Write, therefore,

$$h(\xi) = g(\xi) g'(\xi) \quad (5-1-4).$$

Equation (5-1-1) can then be expressed as

$$g' = \frac{h}{g} \quad (5-1-5).$$

$$h' = 2 \left(\frac{h}{g} \right) - \frac{2\xi h}{1-\xi^2} - (1-\xi^2)$$

Further, it is readily seen that the boundary conditions, (5-1-2) and (5-1-3), now become

$$\begin{aligned} g(0) &= 0, \\ h'(1) &= 0, \end{aligned} \quad (5-1-6).$$

Since $\xi = 0$ is a singular point, it is

impossible to start the numerical integration from this point. A series expansion must, therefore, be obtained for $g(\xi)$ and $h(\xi)$ for a neighbourhood of this point. From equations (5-1-5), the required series expansions are found to be

$$\begin{aligned}
 g(\xi) = & \xi + \left[-\frac{1}{3} \log \xi + K \right] \xi^3 \\
 & + \left[\frac{1}{30} (\log \xi)^2 + \left(-\frac{1}{5} K + \frac{52}{225} \right) \log \xi \right. \\
 & \quad \left. + \left(\frac{3}{10} K^2 - \frac{52}{75} K - \frac{109}{375} \right) \right] \xi^5 \\
 & + \left[-\frac{1}{630} (\log \xi)^3 + \left(\frac{1}{70} K - \frac{1549}{33075} \right) (\log \xi)^2 \right. \\
 & \quad \left. + \left(-\frac{3}{70} K^2 + \frac{3048}{11025} K + \frac{65231}{2315250} \right) \log \xi \right. \\
 & \quad \left. + \left(\frac{3}{70} K^3 - \frac{1549}{3675} K^2 - \frac{65231}{771750} K + \frac{4182641}{64827000} \right) \right] \xi^7 \\
 & + o(\xi^8) \qquad (5-1-7).
 \end{aligned}$$

$$\begin{aligned}
h(\xi) = & \xi + \left[-\frac{1}{3}(4\log \xi + 1) + 4K \right] \xi^3 \\
& + \left[\frac{8}{15} (\log \xi)^2 + \left(-\frac{16}{5}K + \frac{352}{225} \right) \log \xi \right. \\
& \quad \left. + \left(\frac{24}{5}K^2 - \frac{352}{75}K - \frac{1702}{1125} \right) \right] \xi^5 \\
& + \left[-\frac{64}{630} (\log \xi)^3 + \left(\frac{64}{70}K - \frac{34036}{33075} \right) (\log \xi)^2 \right. \\
& \quad \left. + \left(-\frac{96}{35}K^2 + \frac{68072}{11025}K + \frac{871422}{1157625} \right) \log \xi \right. \\
& \quad \left. + \left(\frac{46}{35}K^3 - \frac{34036}{3675}K^2 - \frac{871422}{385875}K + \frac{10392153}{16206750} \right) \right] \xi^7 \\
& \quad + o(\xi^8) \qquad (5-1-8).
\end{aligned}$$

Here K is the parameter mentioned above.

To examine the general nature of the solutions of equations (5-1-5), several solutions were obtained using the series (5-1-7) and (5-1-8) to initiate each solution, and thus automatically satisfying the first of the boundary conditions given by equation (5-1-6). Solutions were obtained for three values of K , namely $K = -1, 0$, and $+2$, and these three solutions are illustrated in Figure (5-1-1).

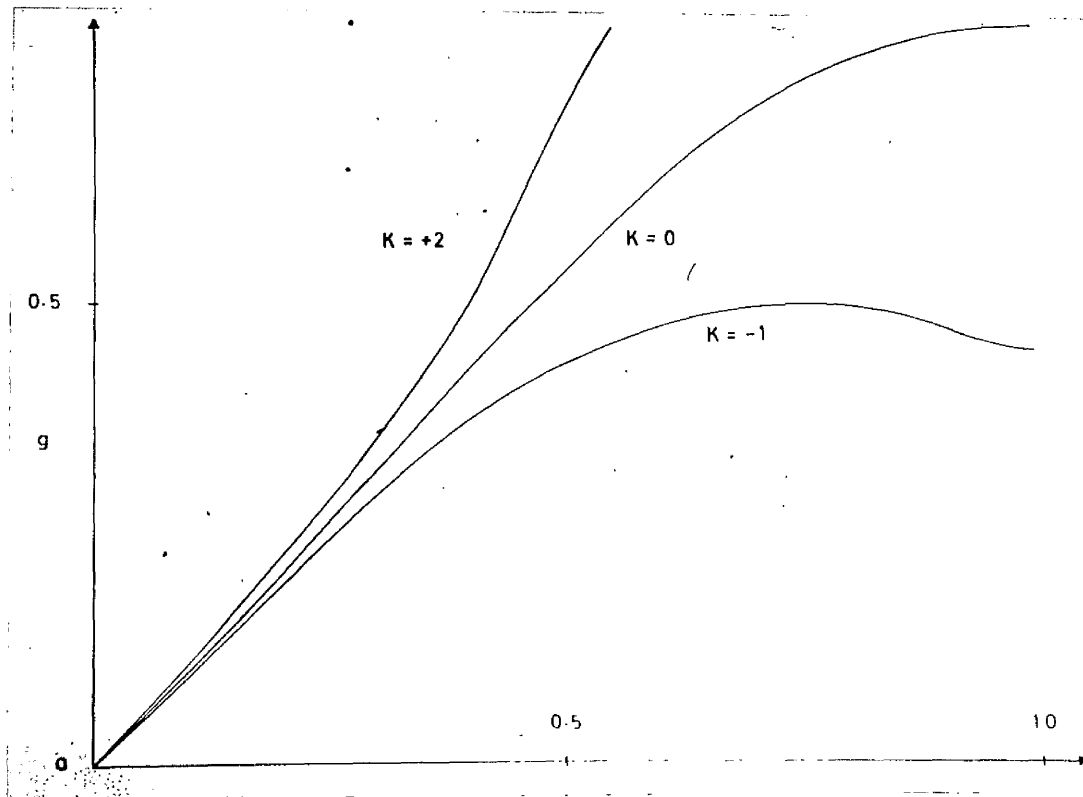


Figure (5-1-1) Graph of three solutions $g(\xi)$, satisfying the condition $g(0) = 0$.

Up to the point $\xi = 0.1$, the solutions were obtained directly from equations (5-1-7) and (5-1-8). Beyond this point the solutions were determined by numerical integration on a hand-calculator. The method used was two-stage Runge-Kutta, with an interval $\delta\xi = 0.02$. The integration formula was as follows :-
if the equations

$$\begin{aligned} g' &= p(\xi, g, h), \\ h' &= q(\xi, g, h), \end{aligned} \tag{5-1-9}$$

are used to represent the two differential equations of (5-1-5), then the two-stage integration formula is

$$\begin{aligned} g(\xi_0 + \delta\xi) &= g_0 + \delta\xi \cdot p\left(\xi + \frac{1}{2}\delta\xi, g_0 + \frac{1}{2}p_0\delta\xi, h_0 + \frac{1}{2}q_0\delta\xi\right) \\ h(\xi_0 + \delta\xi) &= h_0 + \delta\xi \cdot q\left(\xi + \frac{1}{2}\delta\xi, g_0 + \frac{1}{2}p_0\delta\xi, h_0 + \frac{1}{2}q_0\delta\xi\right) \end{aligned} \tag{5-1-10},$$

where the suffix zero has been used to indicate that the relevant function is evaluated at the point $\xi = \xi_0$.

In deriving the solutions, the effect of the singular point, $\xi = 1$, was ignored. This is a feasible approximation, since no great accuracy is required from these solutions, and the Runge-Kutta integration can be extended up to the singular point, but, of course, not beyond it. The dominant errors in the solutions are due to rounding errors which build up till the accuracy of the solution at $\xi = 1$ is only about 1 in the second decimal place. Nonetheless, the results are sufficient to indicate the general behaviour of solutions with variation in the initial parameter K (Figure (5-1-1)).

The solution of equation (5-1-5) that is ultimately required must, in addition, satisfy the condition $h'(1) = 0$. Denote by K_0 the value of K

corresponding to this required solution. Then inspection of the results of the preliminary integration indicates that, to a first crude approximation,

$$K_0 \cong - 0.75 \quad (5-1-11).$$

As the next stage of approximation, two further solutions were obtained corresponding to $K = - 0.75$, and $K = - 0.70$. These solutions were calculated on the 'Deuce' electronic computer of the Glasgow University Computing Laboratory. The method used in this computation was essentially the same as that outlined above, except that the more usual four-stage Runge-Kutta method of integration was used (A1). In this way, an accuracy of one part in 10^4 was obtained in these two machined solutions.

Due to the improved accuracy of these solutions, the difficulties involved in determining the solutions near the singular point $\xi = 1$ by the Runge-Kutta method become significant. It is necessary, therefore, to examine more closely the nature of solutions of the differential equations (5-1-5) in the neighbourhood of this point. Selecting the non-singular solution, this can be expanded in a Taylor series about the point $\xi = 1$. The expansions can be written as

$$\begin{aligned}
 g(1 + \delta\xi) = & \lambda + \frac{\mu}{2\lambda} (\delta\xi)^2 + \frac{4 + \mu}{6\lambda} (\delta\xi)^3 + \frac{2\lambda^2 + \mu^2}{8\lambda^3} (\delta\xi)^4 \\
 & + \frac{12\mu + 5\mu^2}{60\lambda^3} (\delta\xi)^5 + O((\delta\xi)^6) \quad (5-1-12),
 \end{aligned}$$

$$\begin{aligned}
 h(1 + \delta\xi) = & \mu \delta\xi + \left(2 + \frac{\mu}{2}\right) (\delta\xi)^2 + \left(1 + \frac{\mu^2}{\lambda^2}\right) (\delta\xi)^3 \\
 & + \left(\frac{8\mu}{3\lambda^2} + \frac{5\mu^2}{6\lambda^2}\right) (\delta\xi)^4 + O((\delta\xi)^5) \quad (5-1-13),
 \end{aligned}$$

$$\begin{aligned}
 \text{where} \quad \lambda & = g'(1) \\
 \mu & = h'(1)
 \end{aligned} \quad (5-1-14).$$

To use these series effectively, terms are required which are orders of magnitude higher than those included in equations (5-1-12) and (5-1-13). The complexity of the algebra involved in deriving the coefficients of these terms, however, makes their inclusion impracticable. Still their effect may be estimated as follows. It can be seen from equations (5-1-6) and (5-1-14) that for the solution ultimately required $\mu = 0$. Noting this simplification, it is possible to derive series expansions that would apply to this particular solution. Further, it is possible to obtain these series to considerably higher powers

of $\delta\xi$ than those appearing in equations (5-1-12) and (5-1-13) without recourse to excessively complicated algebra. The resulting series are

$$g(1 + \delta\xi) = \lambda + \frac{2}{3\lambda} (\delta\xi)^3 + \frac{1}{4\lambda} (\delta\xi)^4 + \frac{1}{9\lambda^3} (\delta\xi)^6 + \frac{19}{210\lambda^3} (\delta\xi)^7 + O((\delta\xi)^8) \quad (5-1-15),$$

$$h(1 + \delta\xi) = 2(\delta\xi)^2 + (\delta\xi)^3 + \frac{2}{\lambda^2} (\delta\xi)^5 + \frac{9}{5\lambda^2} (\delta\xi)^6 + \frac{2}{5\lambda^2} (\delta\xi)^7 + O((\delta\xi)^8) \quad (5-1-16).$$

The last two equations cannot be applied directly, since the solutions that have been obtained numerically are determined by their starting conditions at $\xi = 0$, (i.e. the value of K). In general, it is not expected that $h'(1)$ will be zero in these solutions. Moreover, although these solutions are good approximations to the required solution, and, therefore, μ will be small, it is, nonetheless, essential that the actual value of μ be taken into account. Still it is reasonable to neglect the effect of the non-zero value of μ in the higher order terms and to extend the series expansions of equations (5-1-12) and (5-1-13) with higher order terms derived from equations (5-1-15) and (5-1-16). In this way, composite series are derived, viz

$$\begin{aligned}
 g(1 + \delta \xi) = & \lambda + \frac{\mu}{2\lambda} (\delta \xi)^2 + \frac{4 + \mu}{6\lambda} (\delta \xi)^3 + \frac{2\lambda^2 + \mu^2}{8\lambda^3} (\delta \xi)^4 + \\
 & \frac{12\mu + 5\mu^2}{60\lambda^3} (\delta \xi)^5 + \frac{1}{9\lambda^3} (\delta \xi)^6 + \frac{19}{210\lambda^3} (\delta \xi)^7
 \end{aligned} \tag{5-1-17}$$

$$\begin{aligned}
 h(1 + \delta \xi) = & \mu \delta \xi + \left(2 + \frac{\mu}{2}\right) (\delta \xi)^2 + \left(1 + \frac{\mu^2}{\lambda^2}\right) (\delta \xi)^3 + \left(\frac{8\mu}{3\lambda^2} + \frac{5\mu^2}{6\lambda^2}\right) (\delta \xi)^4 \\
 & + \frac{2}{\lambda^2} (\delta \xi)^5 + \frac{9}{5\lambda^2} (\delta \xi)^6 + \frac{2}{5\lambda^2} (\delta \xi)^7
 \end{aligned} \tag{5-1-18).}$$

Consider again the two machined solutions obtained for $K = -0.70$, and $K = -0.75$. As already indicated, the integration near $\xi = 1$ is unsatisfactory. The Runge-Kutta solution is, therefore, rejected in the neighbourhood of $\xi = 1$, and instead, the machined solution and the series solution given in equations (5-1-17) and (5-1-18) are matched at the point $\xi = 0.90$. It is then possible to obtain the values of λ and μ by an iterative process. Clearly, for a particular solution, these values depend only on K . Write therefore,

$$\begin{aligned}
 \lambda &= \lambda(K) \\
 \mu &= \mu(K)
 \end{aligned} \tag{5-1-19).}$$

When the matching process has been carried out the following results are obtained :

$$\begin{aligned}
 \lambda(-0.70) &= 0.5640 \\
 \lambda(-0.75) &= 0.5494, \\
 \mu(-0.70) &= -0.0326, \\
 \mu(-0.75) &= +0.0427
 \end{aligned}
 \tag{5-1-20}.$$

The results of equations (5-1-20) indicate that the two solutions obtained on Deuce successfully straddle the required solution. Now let Δ_0 be the value of $g(1)$ corresponding to this required solution, then, from the definition of K_0 , it follows that

$$\begin{aligned}
 \lambda(K_0) &= \Delta_0 \\
 \mu(K_0) &= 0,
 \end{aligned}
 \tag{5-1-21)}.$$

Finally, one can obtain a more accurate approximation to K_0 by an inverse linear interpolation for $\mu(K)$ based on the results of equations (5-1-20); in this way a second approximation is obtained, viz

$$K_0 \approx -0.7214 \tag{5-1-22)}.$$

A final approximation to the required solution was obtained using more elaborate programme techniques. This solution was obtained on the IBM 'Stretch' electronic computer of the U.K.A.E.A. at Aldermaston. The essence of the programme is as follows : using the result of

equation (5-1-22), it was decided to determine two solutions of equations (5-1-5) based on the values $K = -0.720$, $K = -0.723$. The method of integration was once again four-stage Runge-Kutta, but this time with an interval of 0.005. These two solutions were matched to the series solutions of equations (5-1-17) and (5-1-18) at the point $\xi = 0.90$, thus providing two new values of $\mu(K)$. Then an inverse interpolation for μ yields a fresh value K_0 , which was printed out, and found to be

$$K_0 = -0.721032 \quad (5-1-23).$$

This value of K_0 is sufficiently exact to make further approximations unnecessary. A final solution was, therefore, computed for this value of K . The complete solution for both $g(\xi)$ and $h(\xi)$ is given in tabular form in Appendix (5-2), for $\xi = 0$ up to $\xi = 1.1$. In the interval $\xi = 0$ to 0.1, the solution is obtained from the series in equations (5-1-7) and (5-1-8); for the intervals $\xi = 0.1$ to 0.9 the solutions were determined by the Runge-Kutta process; and for the interval $\xi = 0.9$ to 1.1, the series solutions in equations (5-1-17) and (5-1-18) were used, the values of λ and μ being obtained from the matching process. A check on the precision of the value of K_0 chosen is

provided by the value of μ determined in this way; it is found that $\mu = 0(5 \cdot 10^{-6})$, indicating a very high degree of precision.

From this last result it is possible to estimate the accuracy of this final approximation as of the order of 1 in the sixth decimal place. Such an accuracy is more than sufficient for the immediate purpose of determining a lower bound for Λ_0 . The solutions of $g(\xi)$ and $h(\xi)$ must, however, be the basis of any attempt at a complete solution of the partial differential equation (5-1), and for this purpose the additional accuracy could be useful. For the present, the complete solution of $g(\xi)$ and $h(\xi)$ is not required, only the value of $g(1)$, which has been represented by the symbol Λ_0 . From the solutions in Appendix (5-2) one obtains the important numerical result that

$$\Lambda_0 = 0.557753 \quad (5-1-24).$$

Reference

- A1. e.g. Modern Computing Methods, edit. E.T. Goodwin, National Physical Laboratory, Notes on Applied Science No 16, 2nd edit., HMSO (1961).

APPENDIX 5-2. THE NUMERICAL SOLUTION OF
EQUATIONS (5-1-5) AND (5-1-6).

| ξ | $g(\xi)$ | $h(\xi)$ | ξ | $g(\xi)$ | $h(\xi)$ |
|-------|----------|----------|-------|----------|----------|
| 0.00 | 0.000000 | 0.000000 | | | |
| 0.01 | 0.010001 | 0.010003 | 0.16 | 0.159527 | 0.156733 |
| 0.02 | 0.020005 | 0.020016 | 0.17 | 0.169332 | 0.165687 |
| 0.03 | 0.030012 | 0.030039 | 0.18 | 0.179095 | 0.174442 |
| 0.04 | 0.040022 | 0.040068 | 0.19 | 0.188811 | 0.182979 |
| 0.05 | 0.050035 | 0.050096 | 0.20 | 0.198476 | 0.191282 |
| 0.06 | 0.060046 | 0.060113 | 0.21 | 0.208085 | 0.199333 |
| 0.07 | 0.070056 | 0.070109 | 0.22 | 0.217633 | 0.207113 |
| 0.08 | 0.080061 | 0.080070 | 0.23 | 0.227116 | 0.214606 |
| 0.09 | 0.090057 | 0.089984 | 0.24 | 0.236530 | 0.221796 |
| 0.10 | 0.100043 | 0.099835 | 0.25 | 0.245869 | 0.228665 |
| 0.11 | 0.110015 | 0.109609 | 0.26 | 0.255129 | 0.235200 |
| 0.12 | 0.119968 | 0.119290 | 0.27 | 0.264305 | 0.241384 |
| 0.13 | 0.129900 | 0.128859 | 0.28 | 0.273393 | 0.247204 |
| 0.14 | 0.139807 | 0.138302 | 0.29 | 0.282388 | 0.252647 |
| 0.15 | 0.149684 | 0.147599 | 0.30 | 0.291285 | 0.257701 |

| ξ | $g(\xi)$ | $h(\xi)$ | ξ | $g(\xi)$ | $h(\xi)$ |
|-------|----------|----------|-------|----------|----------|
| 0.31 | 0.300080 | 0.262353 | 0.51 | 0.448497 | 0.264076 |
| 0.32 | 0.308769 | 0.266595 | 0.52 | 0.454301 | 0.259793 |
| 0.33 | 0.317347 | 0.270416 | 0.53 | 0.459934 | 0.255163 |
| 0.34 | 0.325810 | 0.273809 | 0.54 | 0.465396 | 0.250205 |
| 0.35 | 0.334153 | 0.276766 | 0.55 | 0.470686 | 0.244933 |
| 0.36 | 0.342374 | 0.279282 | 0.56 | 0.475803 | 0.239367 |
| 0.37 | 0.350467 | 0.281352 | 0.57 | 0.480748 | 0.233524 |
| 0.38 | 0.358428 | 0.282974 | 0.58 | 0.485518 | 0.227423 |
| 0.39 | 0.366255 | 0.284144 | 0.59 | 0.490116 | 0.221084 |
| 0.40 | 0.373943 | 0.284863 | 0.60 | 0.494540 | 0.214527 |
| 0.41 | 0.381490 | 0.285131 | 0.61 | 0.498792 | 0.207773 |
| 0.42 | 0.388891 | 0.284950 | 0.62 | 0.502871 | 0.200843 |
| 0.43 | 0.396143 | 0.284323 | 0.63 | 0.506780 | 0.193758 |
| 0.44 | 0.403244 | 0.283255 | 0.64 | 0.510518 | 0.186539 |
| 0.45 | 0.410191 | 0.281752 | 0.65 | 0.514088 | 0.179209 |
| 0.46 | 0.416981 | 0.279821 | 0.66 | 0.517491 | 0.171789 |
| 0.47 | 0.423611 | 0.277470 | 0.67 | 0.520728 | 0.164301 |
| 0.48 | 0.430080 | 0.274708 | 0.68 | 0.523802 | 0.156766 |
| 0.49 | 0.436386 | 0.271548 | 0.69 | 0.526715 | 0.149207 |
| 0.50 | 0.442525 | 0.267999 | 0.70 | 0.529468 | 0.141645 |

| ξ | $g(\xi)$ | $h(\xi)$ | ξ | $g(\xi)$ | $h(\xi)$ |
|-------|----------|----------|-------|----------|----------|
| 0.71 | 0.532066 | 0.134100 | 0.91 | 0.556911 | 0.015436 |
| 0.72 | 0.534510 | 0.126595 | 0.92 | 0.557159 | 0.012268 |
| 0.73 | 0.536804 | 0.119148 | 0.93 | 0.557354 | 0.009447 |
| 0.74 | 0.538950 | 0.111782 | 0.94 | 0.557500 | 0.006979 |
| 0.75 | 0.540953 | 0.104514 | 0.95 | 0.557606 | 0.004873 |
| 0.76 | 0.542816 | 0.097364 | 0.96 | 0.557677 | 0.003135 |
| 0.77 | 0.544542 | 0.090352 | 0.97 | 0.557721 | 0.001773 |
| 0.78 | 0.546136 | 0.083494 | 0.98 | 0.557743 | 0.000792 |
| 0.79 | 0.547601 | 0.076808 | 0.99 | 0.557751 | 0.000199 |
| 0.80 | 0.548942 | 0.070311 | 1.00 | 0.557753 | 0.000000 |
| 0.81 | 0.550164 | 0.064020 | 1.01 | 0.557754 | 0.000201 |
| 0.82 | 0.551271 | 0.057948 | 1.02 | 0.557762 | 0.000808 |
| 0.83 | 0.552268 | 0.052112 | 1.03 | 0.557785 | 0.001827 |
| 0.84 | 0.553160 | 0.046526 | 1.04 | 0.557830 | 0.003265 |
| 0.85 | 0.553952 | 0.041202 | 1.05 | 0.557905 | 0.005127 |
| 0.86 | 0.554649 | 0.036153 | 1.06 | 0.558017 | 0.007421 |
| 0.87 | 0.555257 | 0.031392 | 1.07 | 0.558174 | 0.010155 |
| 0.88 | 0.555782 | 0.026929 | 1.08 | 0.558383 | 0.013335 |
| 0.89 | 0.556228 | 0.022775 | 1.09 | 0.558654 | 0.016970 |
| 0.90 | 0.556603 | 0.018941 | 1.10 | 0.558993 | 0.021070 |

APPENDIX 7-1. DATA FOR FIGURE (7-1).

| $h(10^3 \text{ km})$ | $\log T$ | $\log N$ | $\log \tau_1$ | $\log \tau_2$ | $\log \tau_3$ |
|----------------------|----------|----------|---------------|---------------|---------------|
| 0 | 3.65 | 15.9 | 6.80 | 6.73 | 6.65 |
| 0.2 | 3.67 | 15.3 | 6.67 | 6.45 | 6.22 |
| 0.5 | 3.69 | 14.5 | 6.48 | 6.07 | 5.65 |
| 1 | 3.72 | 13.6 | 6.28 | 5.65 | 5.01 |
| 2 | 3.77 | 12.6 | 6.08 | 5.20 | 4.32 |
| 3 | 3.80 | 11.9 | 5.92 | 4.88 | 3.84 |
| 4 | 3.87 | 11.3 | 5.82 | 4.65 | 3.47 |
| 5 | 4.10 | 10.7 | 5.84 | 4.58 | 3.31 |
| 6 | 4.48 | 10.2 | 6.00 | 4.71 | 3.41 |
| 7 | 4.88 | 9.8 | 6.20 | 4.91 | 3.61 |
| 8 | 5.20 | 9.4 | 6.34 | 5.03 | 3.71 |
| 10 | 5.60 | 8.9 | 6.52 | 5.18 | 3.84 |
| 15 | 6.00 | 8.5 | 6.72 | 5.38 | 4.04 |
| 20 | 6.00 | 8.4 | 6.69 | 5.33 | 3.96 |

APPENDIX 9-1. DATA FOR FIGURE (9-3).

| $h(10^3 \text{ km})$ | $\log T$ | $\log N$ | K | $\log K$ | $\log \tau$ |
|----------------------|----------|----------|-------|----------|-------------|
| 0 | 3.65 | 15.9 | 7.79 | 0.89 | 4.16 |
| 0.2 | 3.67 | 15.3 | 8.12 | 0.91 | 3.88 |
| 0.5 | 3.69 | 14.5 | 8.55 | 0.93 | 3.50 |
| 1 | 3.72 | 13.6 | 9.04 | 0.96 | 3.08 |
| 2 | 3.77 | 12.6 | 9.62 | 0.98 | 2.60 |
| 3 | 3.80 | 11.9 | 10.01 | 1.00 | 2.27 |
| 4 | 3.87 | 11.3 | 10.42 | 1.02 | 1.99 |
| 5 | 4.10 | 10.7 | 11.06 | 1.04 | 1.71 |
| 6 | 4.48 | 10.2 | 11.88 | 1.07 | 1.49 |
| 7 | 4.88 | 9.8 | 12.68 | 1.10 | 1.32 |
| 8 | 5.20 | 9.4 | 13.36 | 1.13 | 1.15 |
| 10 | 5.60 | 8.9 | 14.21 | 1.15 | 0.92 |
| 15 | 6.00 | 8.5 | 15.01 | 1.18 | 0.75 |